Universidade Federal do Rio Grande – FURG

Instituto de Oceanografia

Programa de Pós-Graduação em Oceanologia

SISTEMA CARBONATO E FLUXOS DE DIÓXIDO DE CARBONO NO ESTUÁRIO DA LAGOA DOS PATOS

CÍNTIA DE ALBUQUERQUE WANDERLEY COELHO

Tese apresentada ao Programa de Pós-Graduação em Oceanologia, como parte dos requisitos para a obtenção do título de Doutor.

Orientador: *Prof. Dr.* RODRIGO KERR Duarte Pereira
Universidade Federal do Rio Grande (FURG), Brasil.

Rio Grande, RS, Brasil

Março 2022

SISTEMA CARBONATO E FLUXOS DE DIÓXIDO DE CARBONO NO ESTUÁRIO DA LAGOA DOS PATOS

Tese apresentada ao Programa de Pós-Graduação em Oceanologia,
como parte dos requisitos para a obtenção do Título de Doutor

por

CÍNTIA DE ALBUQUERQUE WANDERLEY COELHO

Rio Grande, RS, Brasil

Março 2022

COELHO, CÍNTIA DE ALBUQUERQUE WANDERLEY
Sistema Carbonato e fluxos de dióxido de carbono no estuário da Lagos dos Patos / Cíntia de Albuquerque Wanderley Coelho. – Rio Grande: FURG, 2022.
137p.
Tese (Doutorado) – Universidade Federal do Rio Grande. Doutorado em Oceanologia. Área de Concentração: Oceanografia Química.
1. Estuário. 2. Sistema Carbonato. 3. Dióxido de Carbono.

Av. Itália, km 8, Bairro Carreiros, Rio Grande - RS, CEP: 96.203-900 - Fone (53)3233.6715 -
http://www.pogo.furg.br

ATA ESPECIAL DE DEFESA DE TESE DE DOUTORADO – 01/2022

Às 08h do dia 18 de março do ano de dois mil e vinte e dois, por videoconferência, reuniu-se a Comissão Examinadora da Tese de **DOUTORADO** intitulada: "**Sistema carbonato marinho e fluxos líquido de dióxido de carbono no estuário da Lagoa dos Patos, RS**", da **Acad. Cintia de Albuquerque Wanderley Coelho**. A Comissão Examinadora foi composta pelos seguintes membros: Prof. Dr. Rodrigo Kerr – Orientador (IO/FURG), Prof. Dr. Osmar O. Möller Jr. (IO/FURG), Profa. Dra. Eunice da Costa Machado (IO/FURG), Profa. Dra. Letícia Cotrim da Cunha (UERJ), Prof. Dr. Carlos Rafael Borges Mendes (IO/FURG). Dando início à reunião, o Orientador e Presidente da sessão, Prof. Dr. Rodrigo Kerr, agradeceu a presença de todos e fez a apresentação da Comissão Examinadora. Logo após esclareceu que a Candidata teria um tempo de 45 a 60 min para explanação do tema, e cada membro da Comissão Examinadora, um tempo máximo de 30 min para perguntas e considerações. A seguir, passou a palavra à Candidata, que apresentou o tema e respondeu às perguntas formuladas. Após ampla explanação, a Comissão Examinadora reuniu-se em reservado para discussão do conceito a ser atribuído a Candidata. Foi estabelecido que as sugestões de todos os membros da Comissão Examinadora, que seguem em pareceres em anexo, foram aceitas pelo Orientador/Candidata para incorporação na versão final da Tese. Finalmente, a Comissão Examinadora considerou a candidata **APROVADA**, por unanimidade. Nada mais havendo a tratar, foi lavrada a presente ATA que, após lida e aprovada, será assinada pela Comissão Examinadora, pela Candidata e pelo Coordenador do Programa de Pós-Graduação em Oceanologia.

Prof. Dr. Rodrigo Kerr
Presidente

Prof. Dr. Osmar Möller Jr.

Profa. Eunice da Costa Machado

Profa. Dra. Letícia Cotrim da Cunha

Prof. Dr. Carlos Rafael Borges Mendes

Cintia de Albuquerque Wanderley Coelho
Acad. Cintia de Albuquerque W. Coelho

Prof. Dr. Rodrigo Kerr
Coordenador PPGO

"É preciso força pra sonhar e perceber que

a estrada vai além do que se vê"

Marcelo Camelo

Índice

Agradecimentos

Primeiramente, agradeço a Deus por me iluminar, abrir todas as portas que precisei para chegar onde cheguei e por me sustentar nos momentos mais nebulosos e de incertezas.

Em todos os passos que dou, quatro pessoas estão sempre comigo e, certamente, essa conquista também é deles. Obrigada pelas inúmeras ligações, por todos os "quer vir pra casa? A gente dá um jeito", todas as conversas que tivemos e os muitos mimos pra esquentar o coração. Em todas as minhas decisões, mesmo sem eu saber se eu estava certa ou errada ou se daria certo ou não, vocês me apoiaram, deram força e, se eu estava errada, deram colo. E deram muito. Obrigada por tudo, pai, mãe, Marcelo e Henrique. Espero que continuemos sempre assim, do nosso jeito de amar único e singular, mas que faz da nossa casa um verdadeiro lar.

Morar em tão tão distante foi um desafio pessoal e tanto durante todo o Doutorado. Como diria Tom Jobim "Fundamental é mesmo o amor, é impossível ser feliz sozinho" e ao longo desses cinco anos são muitas as pessoas que eu preciso agradecer por todos os abraços, choros, sorrisos, cervejas geladas e docinhos . Alguns somente passaram, outros ficaram, mas como cada um que passa deixa um pouco de si conosco, todos foram importantes para a construção da Cíntia de hoje e da realização desse momento. Obrigada a todos! Obrigada, meus amigos do Rio e de Rio Grande! Vocês são especiais demais e ocupam um espaço enorme nesse pequeno coração.

Muito do que aprendi vem do legado construído no CEOCEAN e, especialmente, desse grupo querido que é o *Carbon Team*. Obrigada pela paciência, por compartilharem os ensinamentos e as experiências e me acolherem tão bem desde o ínicio. Deixo aqui meu muito obrigada a toda essa equipe sensacional!

A minha banca de acompanhamento foi essencial para o andamento de todo o Doutorado. Obrigada, Eunice, Elisa e Osmar! Sem as revisões cuidadosas, a presença nos seminários e todas as valiosas considerações essa Tese não seria a mesma.

Obrigada a FURG e ao Programa de Pós-Graduação em Oceanologia por proporcionarem o melhor para os seus alunos e estarem sempre dispostos a fazer de tudo não só pelo universo acadêmico como também para a sociedade. Precisamos de mais universidades públicas e Programas de Pós-Graduação assim.

Agradeço a CAPES pelo fomento através da bolsa de doutorado durante todo o período.

Por último e da maneira mais especial que consigo agradecer, deixo aqui meu muito obrigada ao meu orientador Rodrigo. Por muitas vezes eu pensei em desistir, e mesmo assim em nenhum momento você me deixou abandonar o barco. Mesmo quando eu não acreditava mais que daria certo ou que eu conseguiria, os recados no final de cada email ou no WhatsaAp foram o gás que eu precisava pra continuar. Obrigada por toda confiança depositada em mim e no meu trabalho, e todo o apoio direcionado para a minha formação acadêmica!

Muito obrigada a todos que estiveram comigo nessa caminhada!

Lista de Figuras

Lista de Tabelas

Lista de Acrônimos e Abreviações

A

A_T – Alcalinidade Total

B

BrOA – Brasileira de Pesquisa em Acidificação dos Oceanos

BR-LTER – *Brazilian Long Term Ecological Research*

C

CO_2 – Dióxido de carbono

C_T – Carbono Inorgânico dissolvido total

CO_3^{2-} – Carbonato

Chl-a – Clorofila-a

$CaCO_3$ – Carbonato de cálcio

C_{Tmr} – Carbono Inorgânico dissolvido total quando a entrada ribeirinha é alta

C_{Toc} – Carbono Inorgânico dissolvido total do oceano

C_{Tr} – Carbono Inorgânico dissolvido total do rio

C_{Tmix} – Carbono Inorgânico dissolvido total quando ocorre a mistura com a água do oceano

C_{Tmo} – Carbono Inorgânico dissolvido total quando não tem influência do rio

C_T^{est} – Carbono Inorgânico dissolvido total do estuário

C_{Ti} – Carbono Inorgânico dissolvido total da estação i

$[CO_2]_m$ – Concentração de CO_2 da mistura das águas

$[CO_2]_{oceano}$ – Concentração de CO_2 da mistura das águas

$[CO_2]_{rio}$ – Concentração de CO_2 da mistura das águas

$[CO_2]_{est}$ – Concentração de CO_2 do estuário

D

DISME – Distrito de Meteorologia

E

ELP – Estuário da Lagoa dos Patos

ENSO – El Niño-Oscilação Sul

ESRL – *Earth System Research Laboratories*

F

FCO_2 – Fluxos líquidos de CO_2

G

Gt – Gigatoneladas (10^9 Toneladas)

GML – *Global Monitoring Laboratory*

H

H_2CO_3 – Ácido carbônico

HCO_3^- – Bicarbonato

H^+ – Hidrogênio

HCl – Ácido clorídrico

I

IBGE – Instituto Brasileiro de Geografia e Estatística

IPCC – *Intergovernmental Panel on Climate Change*

INMET – Instituto Nacional de Meteorologia

INPE – Instituto Nacional de Pesquisas Espaciais

K

k_t – Coeficiente de transferência da velocidade do gás

K_S – Coeficiente de solubilidade do gás

N

NaCl – Cloreto de sódio

NOAA – *National Oceanic and Atmospheric Administration*

NT – Não-termal

O

OH^- – Hidroxila

P

***p*CO_2** – Pressão parcial do CO_2

***p*CO_2 T** – Pressão parcial do CO_2 termal

***p*CO_2 NonT** – Pressão parcial do CO_2 não termal

PELD – Pesquisa Ecológica de Longa Duração

***p*Ar** – Pressão barométrica

***p*H_2O** – Pressão de vapor d'água

***p*CO_2^{drv}** – Drivers da pressão parcial do CO_2

***p*CO_2^{atm}** – Pressão parcial do CO_2 atmosférica

PLE – Patos Lagoon Estuary

S

Sal – Salinidade

Sc – Schmidt

S_i – Salinidade da estação i

S_{oc} – Salinidade do oceano

S_r – Salinidade do rio

T

T – Termal

Temp – Temperatura

U

U_{10} – Velocidade do vento a 10 m

X

xCO_2^{ar} – Fração molar de CO_2

Ω

ΩCa – Estado de saturação da calcita

ΩAr – Estado de saturação da aragonita

Δ

ΔpCO_2 – Diferença entre a pressão parcial de CO_2 na água e na atmosfera

ΔTemp – Diferença entre as médias de temperatura sazonal e total

ΔSal – Diferença entre as médias de salinidade sazonal e total

ΔA_T – Diferença entre as médias de alcalinidade total sazonal e total

ΔC_T – Diferença entre as médias de carbono inorgânico dissolvido total sazonal e total

Resumo

Os estuários são considerados grandes fontes de dióxido de carbono (CO_2) para a atmosfera, mesmo ocupando apenas 4% da plataforma continental global. Entretanto, a variação de desempenho que pode ocorrer entre a condição de sumidouro e fonte de CO_2 nestes ambientes não está somente ligada a relação de sub ou supersaturação de CO_2 dissolvido na água, mas também fortemente condicionada por fatores bióticos e abióticos. Desta forma, este estudo faz uma investigação inédita apresentando a primeira caracterização geral dos parâmetros do sistema carbonato, a determinação dos fluxos líquidos de CO_2 na interface água-ar e a estimativa da origem das principais fontes de carbono no estuário da maior lagoa costeira estrangulada do mundo, a Lagos dos Patos. As águas superficiais da zona inferior do estuário da Lagoa dos Patos (ELP) foram consideradas alcalinas e supersaturadas em relação tanto à calcita quanto à aragonita. Os processos estuarinos predominantes que regeram as mudanças no sistema carbonato no baixo estuário foram a diluição e a concentração de sais, que são dependentes do complexo equilíbrio entre os fluxos de água doce e água salgada que alteram a salinidade da superfície, produzindo condições favoráveis para o desenvolvimento do fitoplanctôn e para a entrada de carbono continental. Os baixos valores encontrados da pressão parcial de CO_2 na água (pCO_2) refletiram nas condições de absorção de CO_2 (verão/outono austral) e na emissão de CO_2 (inverno/primavera austral) para a atmosfera. Esse balanço entre sumidouro e fonte foi modulado pela combinação da velocidade do vento, vazão de água doce, temperatura da água e correntes de saída/entrada, sendo a proliferação de fitoplâncton e a forte mistura vertical induzida pelo vento forçantes pontuais no ELP que resultaram nas trocas de CO_2 altamente variáveis nas diferentes regiões. Ao contrário da maioria dos sistemas estuarinos, o ELP atuou, no geral, como um sumidouro líquido de –2 mmol m^{-2} d^{-1} de CO_2 de durante o período investigado entre 2017 e 2021. A maior concentração estuarina de CO_2, devido a produção autóctone, indicou a heterotrofia em águas estuarinas e concluiu-se que parte desse carbono produzido no estuário é exportado para o litoral, sendo evidenciado pela alta concentração de CO_2 na foz do estuário. A variabilidade temporal dos parâmetros do sistema carbonato

e dos fluxos líquidos de CO_2 revelaram a complexidade da biogeoquímica na região de estudo e os desafios a serem enfrentados em futuras pesquisas, para se obter uma melhor compreensão da variabilidade do sistema carbonato e do entendimento das trocas regionais de CO_2, elucidando o papel de grandes estuários e baías costeiras no balanço global de carbono.

Palavras-Chave: estuários, biogeoquímica, ciclo do carbono, sistema carbonato, fluxo líquido de CO_2.

Abstract

Estuaries are considered large sources of carbon dioxide (CO_2) to the atmosphere, even occupying only 4% of the global continental shelf. However, the performance variation observed that can occur between the sink and source condition of CO_2 in these environments is not only linked to the sub- or supersaturation of CO_2 dissolved in the water, but also strongly conditioned by biotic and abiotic factors. In this way, this study makes an unprecedented investigation presenting the first general characterization of the parameters of the carbonate system, the determination of the water-air CO_2 net fluxes and the estimation of the origin of the main sources of carbon in the estuary of the largest chocked coastal lagoon in the world, the Patos Lagoon. The surface waters of the lower zone of the Lagoa dos Patos estuary (ELP) were considered alkaline and supersaturated in relation to calcite and aragonite. The predominant estuarine processes that govern changes in the carbonate system in the lower estuary were the dilution and concentration of salts, which are dependent on the complex balance between freshwater and seawater fluxes that alter surface salinity and produce favorable conditions for the development of phytoplankton and for the continental carbon input. The low values found for the partial pressure of CO_2 in the water (pCO_2) reflected in the conditions CO_2 absorption (austral summer/autumn) and emission (austral winter/spring) of CO_2 to the atmosphere. This balance between sink and source was modulated by the combination of wind speed, freshwater discharge, water temperature and inflow/outflow currents, with phytoplankton and strong wind-induced vertical mixing as punctual forcing in the ELP, which led to highly variable CO_2 exchanges in different regions. Unlike most estuarine systems, the ELP generally acted as a net CO_2 sink of –2 mmol m^{-2} d^{-1} during the investigated period between 2017 and 2021. The highest estuarine CO_2 concentration, due to production autochthonous, indicated heterotrophy in estuarine waters and it was concluded that part of this carbon produced in the estuary is exported to the coast, evidenced by the high CO_2 concentration at the mouth of the estuary. The temporal variability of the parameters of the carbonate system and the CO_2 net fluxes revealed the complexity of biogeochemistry in the

study region and the challenges to be faced in future research, to obtain a better understanding of the variability of the carbonate system and the understanding of regional exchanges of CO_2, elucidating the role of large estuaries and coastal bays in the global carbon budget.

Keywords: estuaries, biogeochemistry, carbon cycle, carbonate system, water–air CO_2 net flux.

Prefácio

A evolução da relação homem e natureza provocou abundantes benefícios para a sociedade, entretanto esse estreito laço originou inúmeros impactos negativos simultaneamente, principalmente para o meio ambiente. Com o passar dos anos, a utilização excessiva dos recursos naturais promoveu desde a acentuação da eutrofização em corpos d'água até o esgotamento de elementos marinhos, como o desaparecimento de determinadas espécies.

Os oceanos possuem um importante papel na regulação climática da Terra através da circulação superficial que armazena uma elevada quantidade de calor no equador e o distribui até os polos. Por sua alta capacidade térmica, a água precisa receber grande quantidade de calor para alterar a sua temperatura e por isso não se acreditava que um dia sofreríamos com o aquecimento global. Entretanto, com o aumento das emissões antrópicas de dióxido de carbono (CO_2) e a ampliação do efeito estufa, hoje, este fenômeno é real e propicia uma série de consequências para os sistemas naturais marinhos

e, consequentemente, para a vida humana.

A partir dessa motivação, questões relacionadas aos oceanos e ao clima foram começando a ser amplamente estudadas em conjunto, enquanto as zonas costeiras continuavam em segundo plano. Contudo, essas áreas mais próximas da costa abrigam a maior parte da população, inclusive no Brasil, onde estima-se que suas margens acomodem mais de 50,7 milhões de habitantes [IBGE 2022].

Ao iniciar os estudos na oceanografia eu me encantei por todo um mundo oceanográfico. Entre descobrir o porquê da água ser salgada, conhecer espécies de peixes e mergulhar no universo das placas tectônicas, a acidificação e todas as suas vertentes sempre me chamaram mais atenção. Por tentar fazer meu papel na sociedade aliando um amor antigo, surgiu a oportunidade de entender mais sobre o ciclo do carbono e seus parâmetros em uma região de extrema importância, que além de ser uma via navegável de escoamento de diversos produtos, também é configurada como a área mais relevante do Rio Grande do Sul para o crescimento de diversas espécies de peixes e do camarão rosa.

Portanto, esta tese segue o modelo de artigos científicos proposto pelo Programa de Pós-Graduação em Oceanologia (PPGO) e apresenta a primeira visão geral de parte do ciclo do carbono nas águas superficiais na zona estuarina da Lagoa dos Patos. Este é o primeiro passo de uma longa jornada. A partir deste trabalho, espera-se incentivar e contribuir para novos estudos nesta linha de pesquisa na região, afomentando a compreensão da variabilidade natural e dos impactos antropogênicos e climáticos que podem afetar a dinâmica do carbono na região.

Hipótese

O estuário da Lagoa dos Patos é uma fonte de CO_2 para a atmosfera durante todas as estações do ano e contribui com emissões significativas para as estimativas do balanço global de carbono.

Capítulo I: Introdução

O início da Era Industrial, no século XVIII, foi um marco para história mundial tanto no desenvolvimento de novas tecnologias como também pelos impactos ambientais gerados por essa inovação. A partir dessa época, as emissões antrópicas aumentaram a concentração de dióxido de carbono (CO_2) na atmosfera em quase 40%, principalmente através da queima de combustíveis fósseis e das mudanças no uso do solo (Fig. 1) [Zeebe 2012].

O CO_2 é um dos gases mais importantes do efeito estufa [Zeebe e Wolf-Gladrow 2007] e seu aumento tem contribuído para intensificar este fenômeno, retendo mais calor e causando o aquecimento global. Enquanto em 1750 os valores de CO_2 na atmosfera eram de 247 ppm [Joos e Spahni 2008], em 2013 já foram verificados valores acima de 400 ppm, mesmo com a criação de políticas públicas, como o Protocolo de Montreal. Seis anos depois, a concentração média do CO_2 atmosférico para o mês de maio foi de aproximadamente 415 ppm, indicando a continuação da tendência de aumento para a próxima década (Fig. 2). Atualmente, a concentração de CO_2 atmosférico é de cerca de 419 ppm

(média de fevereiro de 2022), conforme registrado pela mais longa série contínua de medição em Mauna Loa [GML 2022].

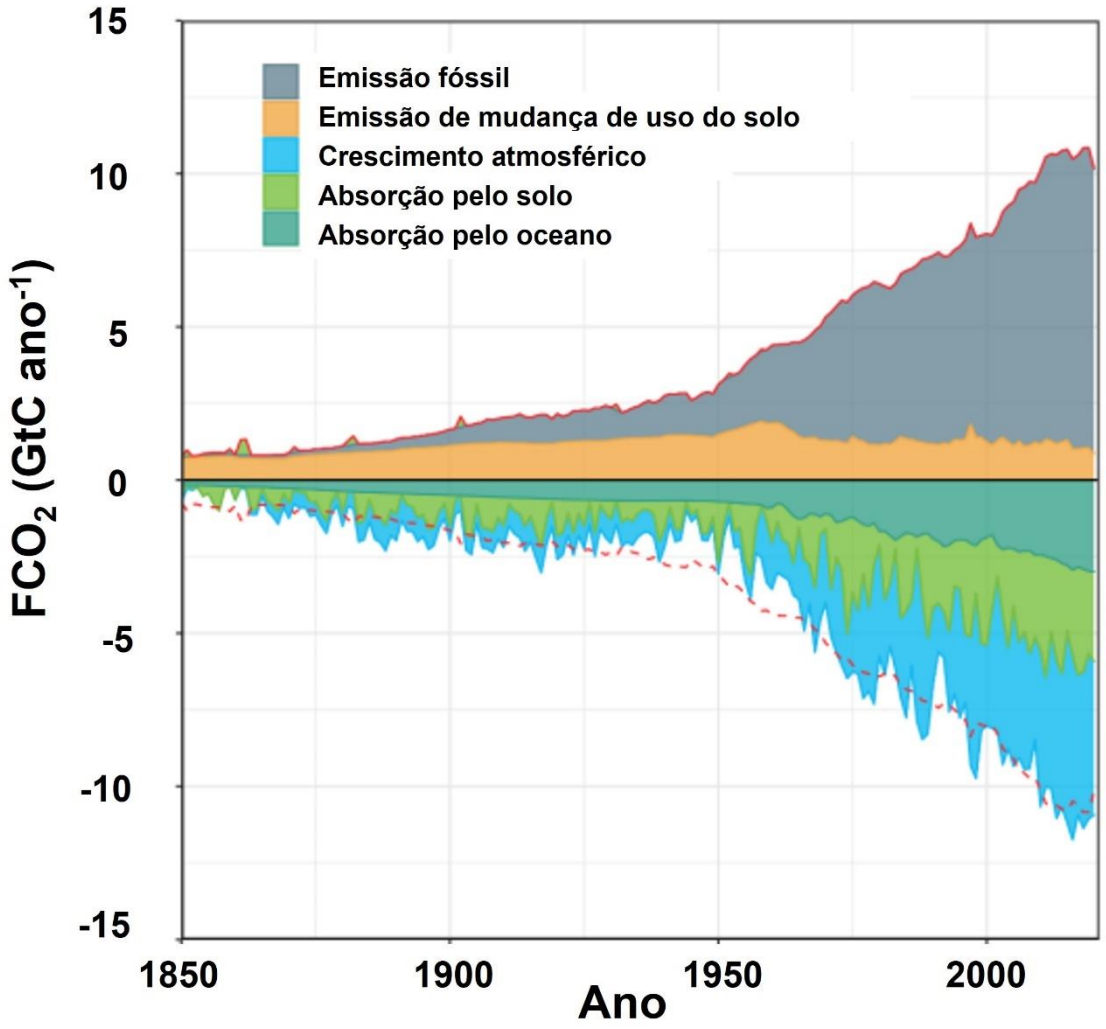

Figura 1. Estimativa anual das emissões de carbono (GtC ano^{-1}) a partir da Revolução Industrial dos combustíveis fósseis (em cinza), da mudança no uso do solo (em laranja) e dos reservatórios do oceano (em verde), do solo (em verde claro e da atmosfera (em azul). O particionamento é baseado em estimativas quase independentes de observações e do modelo de processo conjuntos limitados por dados e não somam exatamente a soma das emissões, resultando em um desequilíbrio orçamentário que é representado pela diferença entre a linha vermelha inferior e a soma dos fluxos de carbono nos reservatórios do oceano, da terra e da atmosfera. Adaptado de Friedlingstein et al. 2021.

O aumento exponencial de CO_2 ao longo de aproximadamente 200 anos tem causado a dissolução significativa desse gás em corpos d'água [Cai 2011], gerando mudanças na química da superfície da água, além de impactos na biota

e nos ecossistemas marinhos [e.g. Cai 2011, Salt et al. 2016, Kerr et al. 2016]. Como consequência, ocorre a diminuição da capacidade de tamponamento das águas, o que levará a uma redução da absorção oceânica de CO_2 no futuro [Gallego et al. 2018].

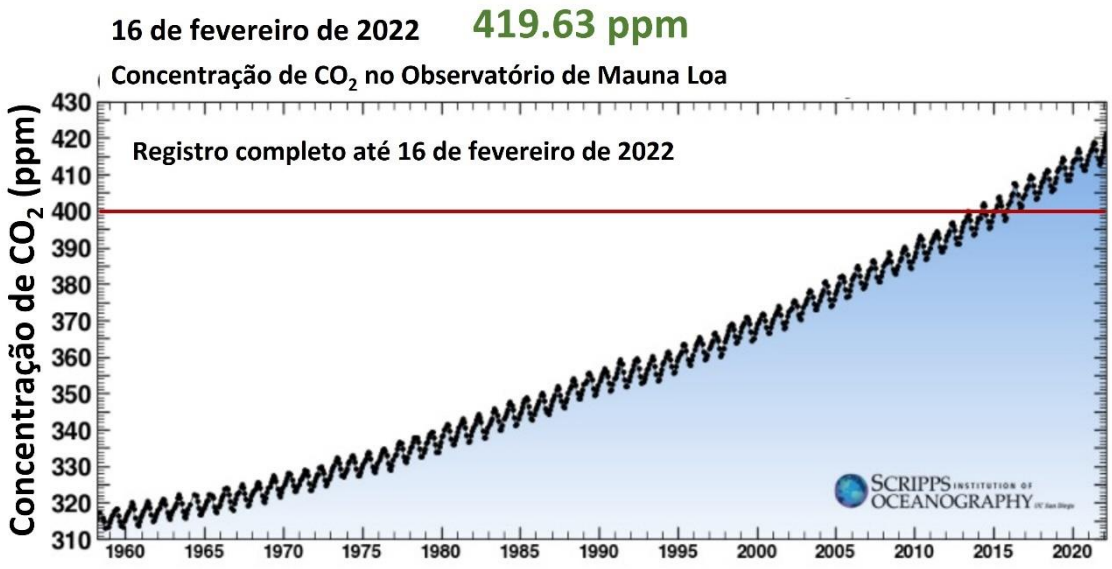

Figura 2. Registro completo das concentrações de dióxido de carbono (CO_2) na atmosfera no observatório de Mauna Loa (curva de Keeling). A linha vermelha contínua indica o patamar alcançado de 400 ppm. Adaptado de https://scripps.ucsd.edu/programs/keelingcurve/.

Ao ser absorvido na água, o CO_2 sofre hidrólise e forma o ácido carbônico ($H_2CO_{3(aq)}$). Essa absorção do CO_2 no meio marinho propicia a dissociação iônica do $H_2CO_{3(aq)}$ que tem como produtos os íons hidrogênio (H^+), íons bicarbonato (HCO_3^-) e íons carbonato (CO_3^{2-}; Eqs. 1-3). A maior absorção do CO_2 suscita o aumento da reação entre o CO_2 e os íons CO_3^{2-}, formando mais HCO_3^- e reduzindo a disponibilidade de CO_3^{2-} no ambiente. Simultaneamente a esses processos, o HCO_3^- e o CO_3^{2-} também reagem com as moléculas de água, liberando íons hidroxila (OH^-) e $H_2CO_{3(aq)}$. Parte dessas OH^- reagem com os íons H^+ produzidos nas dissociações de $H_2CO_{3(aq)}$ e HCO_3^-, e parte fica livre, sendo responsáveis pelo efeito tampão da água do mar. Portanto, o aumento da

concentração dos íons H^+ e a redução dos íons OH^- na água reduzem o pH e, consequentemente, a capacidade de tamponamento das águas.

$$CO_2\,(g) \leftrightarrow CO_2\,(aq) \quad (1)$$

$$CO_2\,(aq) + H_2O\,(aq) \leftrightarrow H^+(aq) + HCO_3^-(aq) \quad (2)$$

$$HCO_3^-(aq) \leftrightarrow H^+(aq) + CO_3^{2-}(aq) \quad (3)$$

O CO_2 pode ser absorvido na água por dois mecanismos diferentes: pela bomba biológica e pela bomba física (Fig. 3). A bomba biológica começa quando se inicia o processo de fotossíntese com a produção de carbono orgânico pelos organismos fitoplanctônicos na zona eufótica. Parte do carbono orgânico produzido através da remineralização do carbono inorgânico na coluna d'água é transportado para o interior dos oceanos até chegar aos sedimentos. A outra fase da bomba biológica está relacionada com a formação biogênica de carbonato de cálcio ($CaCO_3$) que também é um processo importante e caracteriza a bomba contrária de carbonato [Ciais et al. 2013]. Muitos organismos utilizam o $CaCO_3$ para a construção de suas carapaças calcárias e o resultado final da formação de $CaCO_3$ é a liberação de CO_2 para o meio. Já através da bomba física, o CO_2 é absorvido pela superfície da água por difusão e transportado para o oceano profundo movido pelo afundamento de águas com baixa temperatura e maior conteúdo de sal, resultando na formação de massas de água por subsidência ou convecção [e.g. Touratier et al. 2016]. Em ambos os processos, ao chegar no sedimento e quando não consumido por organismos decompositores, o carbono é armazenado por um longo período de anos ou

séculos nas águas mais profundas do oceano, o que é importante para o ciclo do carbono, pois ajuda a regular os níveis de CO_2 atmosférico.

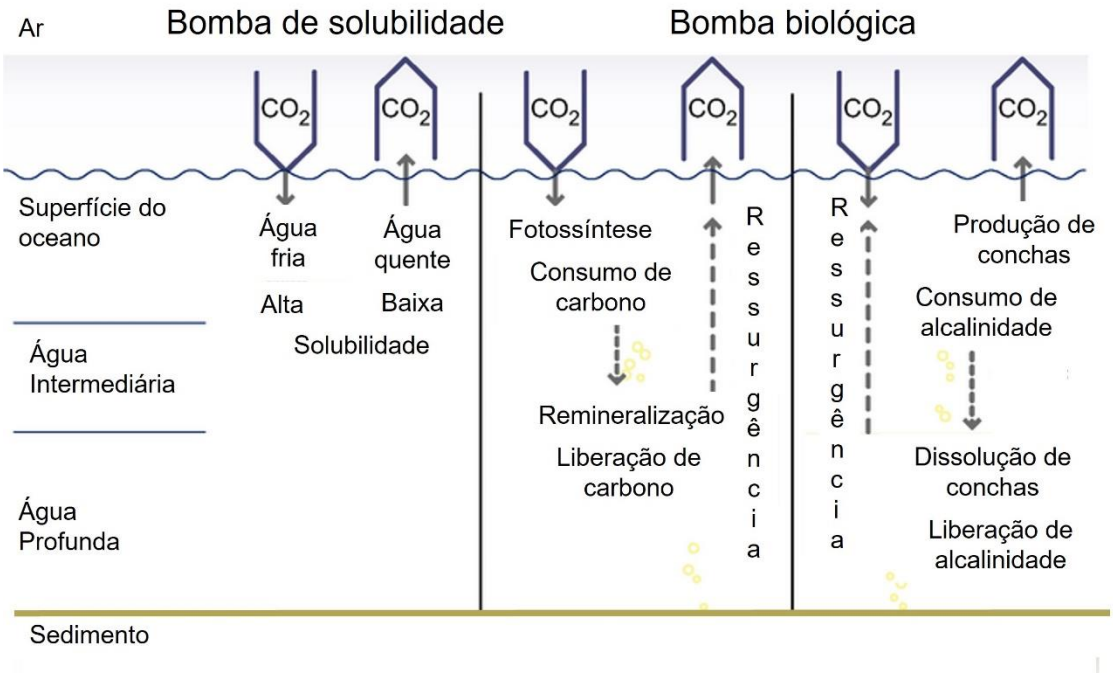

Figura 3. Figura esquemática dos processos de bomba biológica (dividida em bomba de carbono orgânico e bomba contrária de carbonato) e de bomba de solubilidade (parte da bomba física). Adaptado de IPCC 2007.

As alterações causadas pelo excesso de CO_2 no meio marinho resultam no desequilíbrio do sistema carbonato. Sistema esse que, em condições normais, controla a acidez da água do mar, funcionando como um tampão natural para o pH da própria da água do mar. Quatro parâmetros principais compõe o sistema carbonato: a alcalinidade total (A_T), o carbono inorgânico dissolvido total (C_T), a pressão parcial do CO_2 (pCO_2) da água e o pH, sendo estas variáveis associadas à temperatura, salinidade e pressão [Dickson 2010]. Cada componente desse sistema tem um papel importante no tamponamento da água e por isso se faz necessário entender a função de cada uma no meio aquoso.

A A_T é a capacidade natural da água em neutralizar os ácidos e pode ser definida como o número de moles do íon H^+ equivalente ao excesso de prótons aceptores mais prótons doadores, o que está diretamente relacionado a quantidade de CO_2 dissolvido neste meio [Dickson 1981, Carter et al. 2016]. Este parâmetro engloba os principais prótons inorgânicos conhecidos na água do mar, sendo os íons CO_3^{2-} e borato os principais integrantes da A_T [Emerson e Hedges 2008], e por isso é comumente observada sua relação linear com a salinidade. Já o C_T pode ser definido como a soma das quatro formas de carbono inorgânico dissolvido na água: CO_2, $H_2CO_{3(aq)}$, HCO_3^- e CO_3^{2-}, sendo HCO_3^- a forma predominante compondo 90% do total [Libes 2009]. A pCO_2 é a fração molar do CO_2 em equilíbrio na fração total da amostra, ou seja, é a medida do grau de saturação da amostra de água com o CO_2 gasoso [Dickson 2010]. Por último, o pH expressa o grau de acidez ou alcalinidade de uma solução e é definido como o logaritmo negativo da concentração molar de íons H^+ (Eq. 4) [Zeebe e Wolf-Gladrow 2007]. Esta variável é importante em soluções aquosas, já que afeta diretamente propriedades químicas e bioquímicas. O equilíbrio entre os quatro parâmetros do sistema carbonato em cada região é o responsável pela variação do funcionamento do mesmo e por isso a química desse sistema funciona de formas distintas para os diversos tipos de ambientes aquáticos [Borges e Gypens 2011].

$$pH = -\log[H^+] \quad (4)$$

Os oceanos são considerados grandes sumidouros do CO_2 atmosférico

junto com a plataforma continental [Cai 2011]. Em ecossistemas costeiros não há um padrão exato de comportamento como fonte ou sumidouro de CO_2, devido ao seu estado metabólico de ecossistema heterotrófico [Borges et al. 2005, Cai 2011]. As regiões de plataforma continental externa são conhecidas por absorver CO_2 da atmosfera. Entretanto, os estuários, que ocupam uma área de superfície de apenas 4% da plataforma continental global, geralmente, exibem fluxos líquidos de CO_2 (FCO_2) na interface ar-água mais elevados do que aqueles observados na superfície do oceano (Fig. 4) [Borges et al. 2004]. Os valores observados de FCO_2 nos estuários do globo variam de –5 a 80 mol C m^{-2} ano^{-1} [Cai 2011], onde valores negativos indicam absorção de carbono pela água e valores positivos a liberação para a atmosfera.

Os estuários são ecossistemas aquáticos caracterizados pela mistura de águas fluviais e marinhas, abrigando uma diversidade de interfaces e gradientes, com características físicas, geomorfológicas e biológicas distintas [Borges e Abril 2011, Cai 2011]. A variação de desempenho observada que pode ocorrer entre a condição de sumidouro e fonte de CO_2 nestes ambientes não está somente ligada a relação de sub ou supersaturação da água em CO_2 dissolvido na água, mas também fortemente condicionada por fatores biológicos (e.g. produtividade primária e mineralização da matéria orgânica), climáticos (e.g. ventos), físicos (e.g. estratificação/mistura no estuário e intensidade e amplitude das marés) e químicos (e.g. temperatura, fluxos de nutrientes e carbono e fontes de material provenientes do continente). Os estuários, em especial, transformam profundamente o material trazido pelos rios, antes de exportá-lo para a zona costeira adjacente. Como resultado dos processos biogeoquímicos estuarinos nos sedimentos e na coluna d'água, observa-se comumente a emissão do CO_2

para a atmosfera [Sunda e Cai 2012].

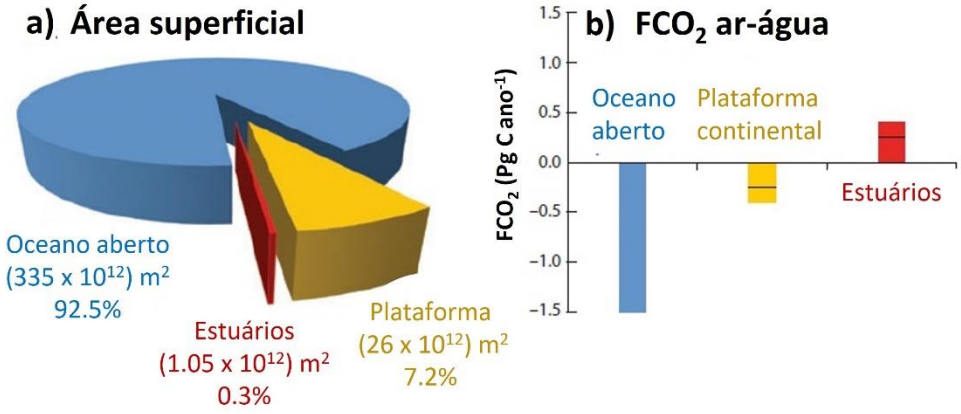

Figura 4. (a) Área superficial do oceano aberto, das plataformas continentais e dos estuários e (b) seus fluxos estimados de CO_2 (FCO_2; Pg C ano^{-1}) ar-água. O FCO_2 do oceano aberto está representado pela cor azul, das plataformas continentais em amarelo e dos estuários pela cor vermelha. Adaptado de Cai (2011).

A supersaturação generalizada de CO_2 eleva os níveis de pCO_2 e mantém a heterotrofia proeminente [e.g., Feely et al. 2010, Borges e Abril 2011, Cloern et al. 2014]. As mudanças na pCO_2 regulam os gradientes de CO_2 entre o ar e a água, determinando a direção das trocas de CO_2 [Sarma et al. 2001], já que esta ocorre com fluxo do meio mais concentrado para o menos concentrado. Em geral, os valores de pCO_2 e as emissões de CO_2 são muito maiores em estuários dominados por rios do que em estuários dominados pela água do mar [Jiang et al. 2008]. Já em sistemas estuarinos de micromarés localizados em regiões temperadas, tropicais ou de altas latitudes apresentam menor emissão ou são caracterizados como sumidouros de CO_2 para atmosfera quando comparados aos estuários de macromaré [Koné et al. 2009, Crosswell et al. 2012].

Além de toda complexidade e variabilidade, os estuários alojam uma grande parcela da população humana, criando modificações induzidas pelo

homem no metabolismo dos ecossistemas aquáticos associadas ao enriquecimento de nutrientes e eutrofização que alteram os parâmetros da água [Zhai et al. 2007, Cotovicz Jr. et al. 2015]. Ao reduzir o pH, a água se torna mais ácida ocasionando o processo de acidificação [Doney et al. 2009] ao reduzir os íons CO_3^{2-} do ambiente. Como esses íons são componentes chave de muitos organismos que os usam como material para seus esqueletos e suas conchas [Doney et al. 2020], a sua redução pode afetar desde a fisiologia e a reprodução até a distribuição geográfica destes seres [Zeebe 2012, Hatje et al. 2013].

Embora os organismos estuarinos possam tolerar alta variabilidade nas propriedades biogeoquímicas e se aclimatar às rápidas mudanças impostas naturalmente pelo ambiente [Bible e Sandford 2016], muitas espécies podem ser afetadas, particularmente os juvenis que usam os estuários como berçários temporários e habitats de alimentação. Nessa fase, esses organismos são mais sensíveis, o que acarreta possíveis alterações não só na diversidade de espécies, mas também em todo o ecossistema do estuário.

Estudos têm demonstrado que as emissões de CO_2 por sistemas estuarinos e águas costeiras são globalmente significativas [Chen e Borges 2009]. No entanto, enquanto o sumidouro de carbono no oceano está atualmente estimado em 2,5 ± 0,5 GtC ano^{-1} [Le Quéré et al. 2018], com um grau de confiança relativamente alto, as trocas de CO_2 na interface ar-água e seus processos controladores permanecem incertos em todo o litoral. Estudos estuarinos do sistema carbonato e do FCO_2 estão localizados, principalmente, ao longo das costas da Europa, Ásia, Índia e leste da América do Norte [e.g. Bauer et al. 2013, Evans et al. 2013]. Apesar da acidificação dos oceanos ser um tema atual na literatura, poucos trabalhos abordaram os sistemas de trocas

de CO_2 na interface água-ar que margeiam a costa brasileira [e.g. Noriega et al. 2013, Noriega e Araujo 2014, Cotovicz et al. 2015, Cotovicz et al. 2020, Abril et al. 2021] devido a desproporcional e insuficiente amostragem tanto no espaço quanto no tempo [Borges e Abril 2011, Cai 2011]. Até o presente momento, o que foi encontrado são ambientes altamente diversificados em relação à saturação de CO_2. O conhecimento aprofundado do ciclo do carbono em escalas regionais é considerado um elemento-chave para diminuir as incertezas do balanço global do carbono [Cotovicz et al. 2020] já que os oceanos funcionam como termorreguladores do clima em nosso planeta em longas escalas de tempo.

Como grande corpo d'água do Hemisfério Sul, um melhor entendimento da biogeoquímica do carbono estuarino e do comportamento regional dos fluxos de CO_2 no Estuário da Lagoa dos Patos (ELP) é fundamental para que possa ser inserido em um contexto global. Apesar de sua importância socioeconômica e ambiental [Odebrecht et al. 2017], poucos estudos avaliam as alterações químicas das águas estuarinas neste ambiente complexo [e.g., Niencheski et al. 2006, Baumgarten e Niencheski 2010, Wallner-Kersanach et al. 2016]. A maior parte dos trabalhos tem como foco principal o conhecimento da hidrodinâmica estuarina, da biologia e da fisiologia de espécies estuarinas dominantes e da ecologia do ecossistema [e.g. Möller et al. 2001, Möller e Fernandes 2010, Haraguchi et al. 2015, Abreu e Odebrecht 2016, Mendes et al. 2016, Islabão et al. 2017, Odebrecht et al. 2017].

Dentro deste contexto e de forma inédita, esta Tese de Doutorado avalia e apresenta o primeiro panorama do comportamento dos processos biogeoquímicos e das trocas de CO_2 na interface água-ar na zona estuarina

inferior da Lagoa dos Patos através da investigação dos parâmetros do sistema carbonato e dos condutores de pCO_2, da estimativa das fontes de CO_2 na região, e da variabilidade temporal tanto dos parâmetros do sistema carbonato quanto dos fluxos líquidos de CO_2 neste ambiente. Assim, conhecer a variabilidade intrínseca do sistema de CO_2-carbonato no ELP torna-se o primeiro passo para avaliar e compreender a variabilidade natural do sistema, bem como os impactos antropogênicos e climáticos que podem afetar a dinâmica do carbono numa região tão importante para toda a sociedade gaúcha.

Objetivos

O objetivo geral desse estudo é compreender a variabilidade do sistema CO_2-carbonato no ELP. Assim, os seguintes objetivos específicos foram definidos:

(i) investigar a variabilidade sazonal e interanual dos parâmetros do sistema carbonato (e.g., A_T, C_T, pH e pCO_2) na região de estudo;

(ii) determinar e investigar o comportamento do FCO_2 nas diferentes estações do ano; e

(iii) inferir sobre os processos controladores da pCO_2 e o papel emissor ou absorvedor da região de estudo.

Capítulo II: Estuário da Lagoa dos Patos

A Lagoa dos Patos está localizada na planície costeira do Rio Grande do Sul e é a maior lagoa estrangulada do mundo [Kjerfve 1986], sendo conectada ao mar por um canal estreito (~ 1 km de largura) [Castelão e Möller 2003, Marques e Möller 2008, Marques et al. 2009]. A área de superfície da Lagoa dos Patos é de aproximadamente 10.360 km^2, e a bacia de drenagem de 200.000 km^2, com profundidade média de 5 m [Möller 1996, Seeliger 2001]. A lagoa compreende regiões de clima subtropical e temperado quente com uma temperatura média do ar de 18 °C e precipitação média anual variando entre 1.200 mm e 1.500 mm [Abreu et al. 2016]. A dinâmica do sistema lagunar é dominada pela ação dos ventos em escalas de tempo associados a passagem de sistema frontais e pela descarga fluvial. Isso se dá devido à dimensão da bacia de drenagem e às dimensões e orientação do eixo longitudinal do corpo lagunar [Möller e Fernandes 2010, Vaz et al. 2006]. A lagoa pode ser dividida geomorfologicamente em três partes: zona estuarina, lagoa central e lagoa

superior (Fig. 5) [Delaney 1965].

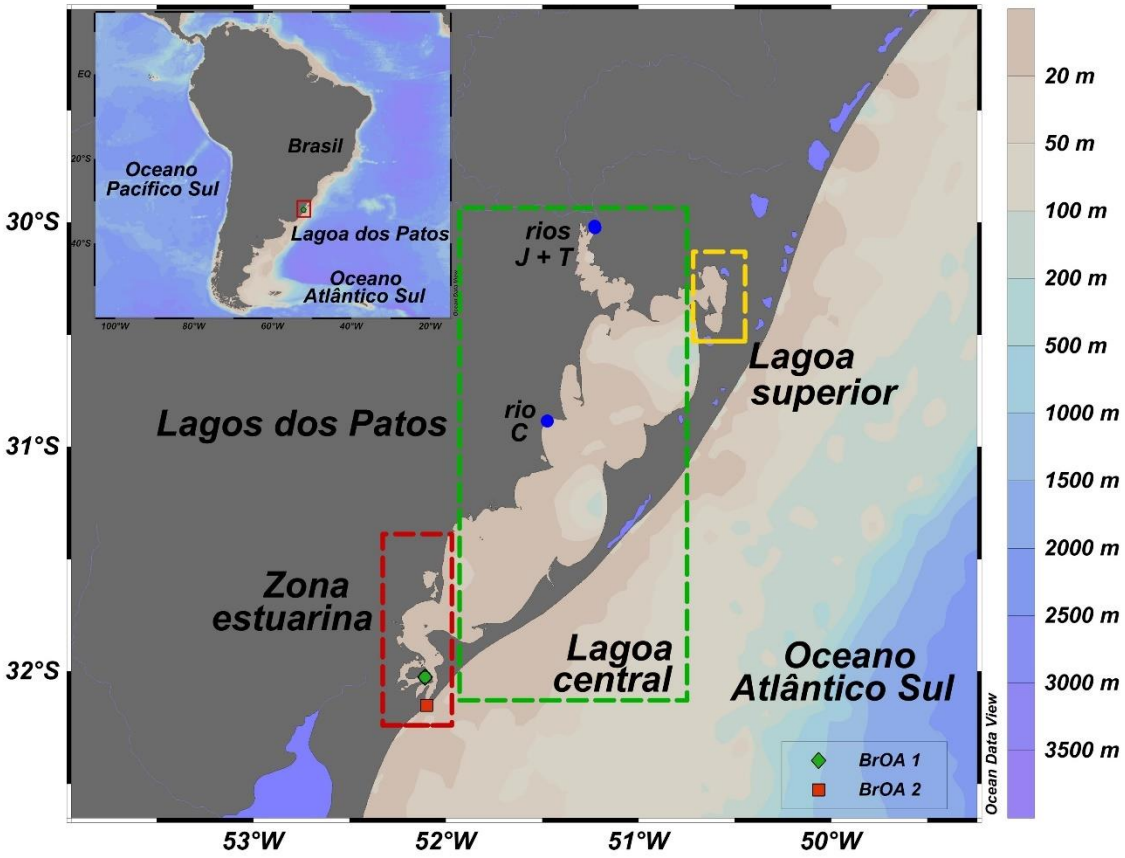

Figura 5. Mapa da região de estudo: Lagoa dos Patos. Localização da Lagoa dos Patos e divisões geomorfológicas para a zona estuarina (retângulo vermelho), lagoa central (retângulo verde) e lagoa superior (retângulo amarelo). O destaque superio a esquerda mostra um mapa da América do Sul com a localização da Lagoa dos Patos (retângulo vermelho). Pontos azuis indicam as regiões de descarga dos rios Jacuí e Taquari (J + T) e Camaquã (C).

A zona estuarina, também chamada de lagoa inferior, é delimitada pela embocadura da lagoa e pela Ponta da Feitoria. A entrada de água salgada, geralmente, se restringe a essa porção que ocupa cerca de 10% da área total da lagoa. As trocas entre a lagoa e o oceano adjacente ocorrem por gradiente de pressão, resultado da combinação do efeito das forças locais e não locais com ventos direcionados tanto para a lagoa quanto para o oceano, respectivamente. Assim como em toda a lagoa, a hidrodinâmica do ELP é controlada, principalmente, pela ação dos ventos e pela força da descarga fluvial [Möller et al. 2001]. O afunilamento natural característico do estuário intensifica as

correntes de vazante e atua como um filtro para os movimentos de maré que apresentam uma importância secundária na região [Möller et al. 2007]. Além da direção do vento e da descarga de água doce, a hidrologia no estuário é controlada também pelo equilíbrio entre os níveis de precipitação e evaporação [Castelão e Möller 2003, Möller e Fernandes 2010, Abreu et al. 2016].

Quando os ventos sopram de nordeste simultaneamente ao período de alta descarga fluvial, no final do inverno e na primavera, há o favorecimento das correntes de vazante. Durante o verão e a primavera, há a presença bem-marcada de ventos de leste, indicando a influência do sinal da brisa marítima. No outono, a intrusão de água salgada é maior do que nas outras estações devido à passagem frequente de sistemas frontais com ventos de sul combinados com baixa entrada de água doce, resultando em inundações e salinização do ELP. Portanto, os ventos dos quadrantes norte e sul formam estruturas verticais de salinidade que podem variar de uma cunha de sal a um gradiente bem misturado [Möller et al. 2001, Möller e Fernandes 2010].

Os níveis de salinidade no estuário variam de 0 a 35, sendo as menores salinidades encontradas nos períodos de primavera e as maiores observadas no verão [Vaz et al. 2006]. Devido a sua morfologia, o estuário apresenta diferentes áreas. As regiões mais abrigadas, em geral, são mais rasas (com profundidade de até 2 m) e possuem maior tempo de residência da água, enquanto o oposto é observado nas áreas mais expostas. O canal de ligação com o mar apresenta 12 m de profundidade e é uma zona altamente dinâmica devido a proximidade do oceano adjacente e ao fluxo de água salgada [Möller et al. 2001].

O ELP é um berçário para várias espécies de peixes e crustáceos, devido

aos seus diferentes habitas temperados [e.g. marismas e gramas marinhas; Tagliani et al. 2003]. Os altos níveis de produção primária garantem o fornecimento de alimentos para diversas espécies de organismos que apresentam importância econômica na região [Abreu et al. 2016]. A alta concentração de nutrientes no ELP [Niencheski e Windom 1994, Niencheski et al. 2006] favorece principalmente o crescimento de diatomáceas, que constituem o grupo fitoplanctônico dominante (mais de 50%), seguido por cianobactérias, flagelados, dinoflagelados e clorófitas [Islabão et al. 2017]. No entanto, estudos recentes relatam tendências no crescimento de dinoflagelados e cianobactérias devido às mudanças na salinidade [e.g. Haraguchi et al. 2015, Islabão et al. 2017]. Além disso, o crescimento do fitoplâncton é amplamente limitado pela luz e afetado pelo tempo de residência das águas no ELP [Odebrecht et al., 2015].

Desde a década de 1980, nota-se um aumento nas concentrações de nutrientes no ELP [Wallner- Kersanach et al. 2016] e que atualmente tem apresentado sinais de eutrofização em pontos específicos [e.g., Abreu et al. 2010, Marreto et al. 2017]. A dinâmica dos nutrientes mudou ao longo do tempo por causa da hidrodinâmica local e da rápida renovação de água [e.g., Möller et al. 2001, Wallner-Kersanach et al. 2016]. Os aumentos na concentração de nutrientes foram seguidos por mudanças na comunidade de produtores primários, como um aumento na frequência de florações oportunistas de macroalgas e mudanças na composição do fitoplâncton [Wallner-Kersanach et al. 2016, Marreto et al. 2017, Lanari e Copertino 2017

Capítulo III: Dados e métodos

Neste trabalho, as amostras de água de superfície foram coletadas mensalmente usando uma garrafa van Dorn de 5 L em duas estações fixas estuarinas fixas em píeres da lagoa para medir os dados hidrográficos, biológicos e químicos. Essas estações estão localizadas na zona inferior do ELP, sendo uma na região mesomixohalina de entrada interna (a uma profundidade inferior a 2 m) e a outra em uma região euhalina inferior (com grande variação de salinidade a uma profundidade de ~12 m próxima a desembocadura do ELP; Fig. 6) [Abreu et al. 2016]. Os parâmetros físicos, biológicos e químicos foram amostrados pelo programa de monitoramento ecológico chamado Pesquisa Ecológica de Longa Duração (PELD) do Estuário da Lagoa dos Patos e Costa Marinha Adjacente, em funcionamento desde 1999 (www.peld.furg.br) [Odebrecht e Abreu 2019]. O banco de dados inclui temperatura da água de superfície, salinidade, nutrientes dissolvidos (ou seja, nitrato, nitrito, ácido silícico e fosfato) e clorofila-a (Chl-a) [Lemos et al. 2021]. Já os parâmetros do sistema carbonato medidos diretamente, ou seja, a A_T e o pH, foram amostrados pela

Rede Brasileira de Pesquisa em Acidificação dos Oceanos (rede BrOA; www.broa.furg.br) [Kerr et al. 2016]. As duas estações são aqui referidas como BrOA #1 (região mesomixohalina numa área abrigada da zona inferior do estuário) e BrOA #2 (região euhalina numa área mais exposta ao oceano na desembocadura da lagoa). O programa de monitoramento mensal dos parâmetros do sistema carbonato, executado pela rede BrOA, começou em outubro de 2015 e continua até o presente momento. A exceção é para o monitoramento do pH que se iniciou em maio de 2017. Neste estudo, o conjunto de dados utilizado abrange o período entre maio de 2017 e junho de 2021. Isso se deve ao fato de que a utilização de pH e A_T gerarem parâmetros estimados com melhor precisão [Millero et al. 2006] e uma possível superestimação do C_T medido diretamente antes de 2017.

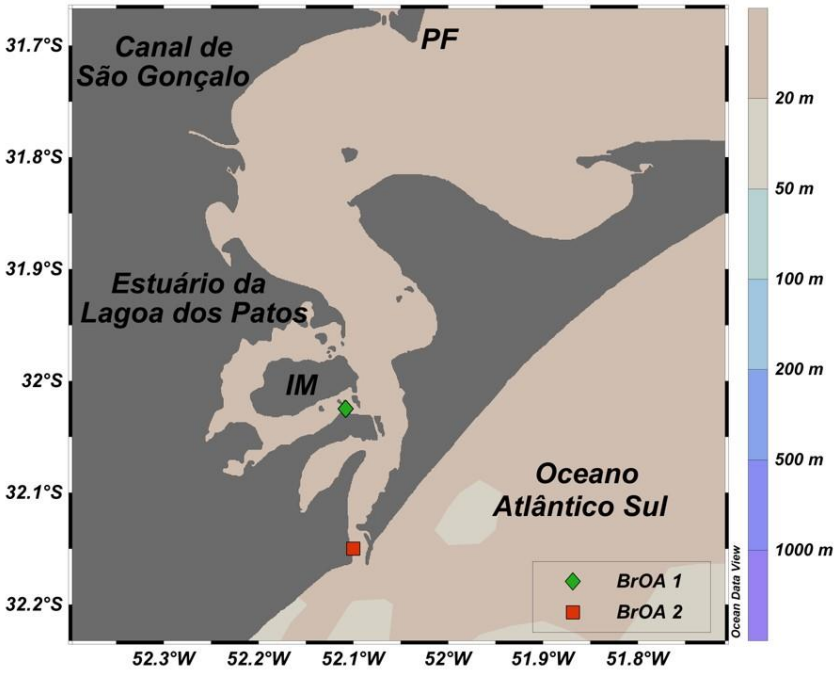

Figura 6. Localização das estações BrOA # 1 (diamante verde) e # 2 (quadrado vermelho) do monitoramento fixo no píer na zona inferior do Estuário da Lagoa dos Patos. A Ilha dos Marinheiros (IM) e a Ponta da Feitoria (PF) são indicados.

As metodologias trabalhadas nessa tese envolvem a determinação de

parâmetros do sistema carbonato para cálculo do FCO_2 e da composição do CO_2 presente no estuário. Neste capítulo, estas análises serão descritas de forma separada a fim de melhor detalhar cada etapa.

3.1 Determinação da temperatura, salinidade, nutrientes dissolvidos e clorofila-a (Chl-a)

A temperatura e a salinidade da água superficial foram medidas *in situ* por termômetro digital e condutivímetro, respectivamente. A salinidade foi aferida em laboratório. Os nutrientes dissolvidos foram medidos em água filtrada e suas concentrações determinadas de acordo com o método de Strickland e Parsons [1972]. As concentrações de nutrientes foram usadas apenas para estimar os parâmetros derivados do sistema carbonato.

Amostras discretas de água de superfície de 50-250 mL (dependendo da concentração de material) foram filtradas em luz fraca através de filtros Whatman GF / F (tamanho de poro nominal de 0,7 µm e 25 mm de diâmetro) usando uma pressão de vácuo de <5 em mercúrio e imediatamente congeladas (–80 ° C) para determinações posteriores da concentração de Chl-a total pelo método fluorimétrico. No laboratório, o pigmento foi extraído em acetona 90%, e a fluorescência determinada em fluorímetro Turner Designs TD-700 (previamente calibrado com padrão Sigma® de clorofila-a), seguindo o método de não acidificação de Welschmeyer [1994], usado em outros trabalhos na literatura onde a metodologia está melhor detalhada [e.g. Murrell & Lores 2004, Giannini et al. 2021]

3.2 Análise dos parâmetros do sistema carbonato

Com um par de parâmetros do sistema carbonato (i.e., A_T, C_T, pH e pCO_2) é possível calcular os demais com certo erro associado [Millero et al. 2006]. Dessa maneira, a partir da determinação da A_T e do pH foram calculados os outros parâmetros do sistema carbonato.

3.2.1 Alcalinidade total (A_T)

As amostras de água da superfície para análise de A_T foram coletadas sem que houvesse a formação de bolhas em frascos de vidro de borosilicato de 500 mL e fixadas com 100 µL de uma solução supersaturada de cloreto de mercúrio para prevenir a atividade biológica seguindo o procedimento descrito por Dickson et al. [2007]. As amostras foram refrigeradas para evitar evaporação e posteriormente analisadas em laboratório. A A_T foi determinada em laboratório por titulação potenciométrica em uma cela fechada [Dickson et al. 2007] com um titulador automático (Metrohm® Titrando 808) e um eletrodo de referência de vidro combinado (Metrohm® 6.0262.100) a uma temperatura controlada de 25 ± 0,1°C sustentado por um banho termostático (Tamson® TLC 15). Com o volume da cela fechada previamente calibrado, foi efetuada a titulação de uma quantidade conhecida de água do mar. A titulação foi feita com solução de ácido clorídrico (HCl) adicionado de cloreto de sódio (NaCl) com a finalidade de simular a força iônica da água do mar, mantendo os coeficientes de atividade aproximadamente constantes durante a titulação. O progresso da titulação é monitorado usando um eletrodo de pH e um termômetro. Inicialmente é adicionada uma quantidade maior de ácido (~3 mL), seguida de pequenos

incrementos de ácido (0,1 a 0,2 mL). Ao final de cada adição, o volume de ácido e a força eletromotriz são monitorados para determinar o ponto de inflexão da curva de titulação. Assim, a A_T é calculada a partir desses dados usando um método de mínimos quadrados com base em um ajuste de curva não linear [Dickson et al. 2007]. Devido à alta faixa de variabilidade da salinidade no estuário (de 0 a ~32), uma adaptação do método de célula fechada [Dickson et al. 2007] foi adotada, dividindo-se as amostras em dois grupos de acordo com a faixa de salinidade (0 a 19 e > 19). Soluções de HCl (0,1 M) com bases de NaCl com diferentes salinidades foram usadas como titulantes para aproximar a salinidade real das amostras. A precisão para as medições de A_T foi determinada usando material de referência certificado (lotes nos. 96, 149, 162 e 177, adquiridos do *Scripps Institution of Oceanography*) [Dickson et al. 2003]. Análises de controle foram realizadas regularmente (diariamente) durante todo o período do estudo para garantir a qualidade dos resultados. Um fator de correção foi aplicado aos valores medidos com base nas leituras dos valores do material de referência certificado e na diluição da amostra pela solução de cloreto de mercúrio [Dickson et al. 2007]. A precisão analítica das análises de A_T foi de ± 4,0 µmol kg^{-1} (variando de 2,3 a 5,0 µmol kg^{-1} considerando os lotes de amostra analisados). A consistência dessas medições foi avaliada diariamente durante todo o período de análise, com análises replicadas de uma única água padrão.

3.2.2 pH

Amostras para análise de pH foram coletadas em frascos âmbar de borosilicato de 125 mL. O pH foi determinado potenciometricamente dentro de

um período máximo de duas horas após a amostragem. Para realizar essas medições, usamos um medidor de pH Metrohm® 913 ou 914 acoplado a um eletrodo de referência de vidro e um sensor de temperatura. Soluções tampão padrão Fluka® Sigma-Aldrich® (com fungicida) com valores de pH iguais a 4,008 (hidrogenoftalato de potássio + cloreto de fenilmercúrio) e 7,413 (hidrogenofosfato dissódico + di-hidrogenofosfato de potássio) ou padrão Certipur® Merck com valores de pH iguais a 4,00 (ácido cítrico + hidróxido de sódio + cloreto de hidrogênio), 7,00 (hidrogenofosfato dissódico + di-hidrogenofosfato dipotássico) e 9,00 (ácido bórico + sódio hidróxido + cloreto de potássio), todos a 25°C, foram usados para calibrar o eletrodo de pH antes que as amostras de cada perfil fossem medidas. Aplicamos a equação desenvolvida por Gieskes [1969] para corrigir as medidas de pH para as temperaturas *in situ*. Por fim, os valores de pH foram convertidos e relatados na escala total. A precisão e exatidão das medições de pH foram avaliadas por análises repetidas de amostras em duplicado coletadas da mesma garrafa van Dorn e por medições regulares da solução tampão com pH = 7,413 durante as análises. A incerteza das medições foi ≤ 0,05 unidades de pH NBS.

3.2.3 Outros parâmetros do sistema carbonato

O C_T, a pCO_2 e o estado de saturação (Ω) de calcita (ΩCa) e aragonita (ΩAr) foram estimados através do software CO2Sys v.2.1 desenvolvido por Lewis et al. [1998] e modificado por Pierrot et al. [2006]. Os dados de temperatura da superfície da água, salinidade, A_T, pH, ácido silícico e concentrações de fosfato foram usados como parâmetros de entrada. A escala total foi escolhida para o pH *in situ*. Como o estudo foi realizado em um ambiente estuarino com

ampla faixa de salinidade, aplicamos o seguinte conjunto de constantes: as constantes de dissociação K_1 e K_2 de Millero et al. [2006], também utilizados por Liu et al. [2017], Carstensen et al. [2018] e Chen et al. [2020] em ambientes estuarinos e costeiros, e as constantes de sulfato e borato de Dickson [1990] e Uppström [1974], respectivamente.

As incertezas dos parâmetros do sistema carbonato foram determinadas de acordo com Orr et al. [2018]. Os erros de temperatura e salinidade foram menores que 0,1°C ou 0,1 unidades de salinidade (valores pequenos dada a amplitude de variação dos parâmetros no ambiente), respectivamente, e não foram considerados neste cálculo. Portanto, as incertezas propagadas nos parâmetros do sistema carbonato representam fundamentalmente os erros associados aos valores estimados de A_T e pH. As incertezas médias dos valores calculados do C_T, da pCO_2, do ΩCa e do ΩAr foram ± 13 µmol kg^{-1}, ± 46 µatm, ± 0,02 e ± 0,01, respectivamente. Além disso, revisamos o software CO_2Sys v.2.1 para verificar a sensibilidade dos parâmetros do sistema de carbonato com base no conjunto de constantes usadas. Mudamos o conjunto de constantes para as constantes de dissociação K_1 e K_2 de Cai e Wang [1998], as constantes de sulfato de Khoo et al. [1977] e as constantes de borato de Lee et al. [2010]. As diferenças médias entre as estimativas derivadas da aplicação original e os novos valores foram consideradas variados para águas estuarinas: 55 µmol kg^{-1}, 80 µatm, 0,01 e 0,007 para C_T, pCO_2, ΩCa e ΩAr, respectivamente.

3.3 Efeitos termais e não-termais da pressão parcial do CO_2 da superfície da água (pCO_2)

A relação termodinâmica entre pCO_2 e temperatura é de 4,23% $°C^{-1}$ [Takahashi et al. 1993], e variações sazonais na pCO_2 superficial podem ser dissociadas em efeitos térmicos e não-térmicos. A abordagem relatada por Takahashi et al. [2002] foi usada para avaliar esses efeitos nas mudanças sazonais na pCO_2 nas estações BrOA #1 e #2. O efeito térmico está relacionado principalmente a processos termodinâmicos que afetam a solubilidade do CO_2 em água, já os efeitos não-térmicos representam a variabilidade da pCO_2 devido a mudanças na concentração de C_T e/ou A_T, que inclui a mistura vertical e a utilização biológica do CO_2 [Körtzinger et al. 2008]. Primeiro, os dados de pCO_2 foram calculados para uma temperatura média mensal e sazonal a fim de excluir o efeito da temperatura (Eq. 5):

$$pCO_2\ \text{NonT} = (pCO_2)\ \ \text{Exp}\ [0.0433\ (T_m - T) \qquad (5)$$

onde T_m é a média mensal da temperatura da superfície da água e T é a temperatura observada. Então, a pCO_2 foi calculada para a temperatura in situ para se obter o sinal da temperatura (Eq.6):

$$pCO_2\ T = (pCO_{2\,m})\ \ \text{Exp}\ [0.0433\ (T - T_m) \qquad (6)$$

onde pCO_{2m} é a média mensal e sazonal da pCO_2 superficial. Para cada estação, tanto a pCO_2 sazonal termal quanto a não-termal foram calculadas usando a diferença entre os valores máximo (máx) e mínimo (min; Eqs. 7 e 8):

$$\Delta pCO_2\ T = (pCO_2\ T)_{máx} - (pCO_2\ T)_{min} \quad (7)$$

$$\Delta pCO_2\ NonT = (pCO_2\ NonT)_{máx} - (pCO_2\ NonT)_{min} \quad (8)$$

A razão (T:NT) entre as duas condições foi aplicada para comparar a influência relativa dos efeitos termais (T) e não-termais (NT; Eq. 9):

$$T{:}NT = \Delta pCO_2\ T / \Delta pCO_2\ NonT \quad (9)$$

onde T:NT < 1 indica que o efeito não-termal tem maior magnitude e varibilidade, enquanto T:NT > 1 indica que o efeito não-termal é fraco ou raramente constante.

3.4 Cáculo dos drivers da pressão parcial do CO_2 da superfície da água (pCO_2)

Os drivers da pCO_2 foram calculados com base na diferença sazonal na zona inferior do ELP (Fig. 6) e nas derivadas parciais correspondentes associadas aos parâmetros associados seguindo a Eq.10. As diferenças na pCO_2 foram separadas em contribuições que representam os papéis das diferenças na temperatura, salinidade, A_T e C_T. As contribuições relativas de cada driver foram avaliadas convertendo suas mudanças relativas em unidades de pCO_2 (µatm) seguindo Lenton et al. [2012]:

$$\Delta pCO_2^{drv} = (\partial pCO_2/\partial Temp)\ \Delta Temp + (\partial pCO_2/\partial Sal)\ \Delta Sal + (\partial pCO_2/\partial A_T)\ \Delta A_T +$$

$(\partial pCO_2/\partial C_T)\ \Delta C_T$ (10)

onde ΔTemp, ΔSal, ΔA_T e ΔC_T são as diferenças entre as médias de cada estação e a estação anterior da superfície da água na zona inferior do ELP de cada parâmetro de maio de 2017 a junho de 2021. As derivadas parciais foram calculadas usando as Eqs. 11-13 e o termo envolvendo temperatura usando a Eq. 14 [Takahashi et al. 2014].

$\partial pCO_2/\partial C_T = (pCO_2/\partial C_T)$ Fator Revelle (11)

$\partial pCO_2/\partial A_T = (pCO_2/\partial A_T)$ Fator de Alcalinidade (12)

$\partial pCO_2/\partial Sal \approx (pCO_2/\partial Sal)$ (13)

$\partial pCO_2/\partial Temp\ \Delta Temp \approx 2pCO_2\ \{Exp\ [0.0423\ (\Delta Temp/2)] - 1\}$ (14)

onde ΔTemp é a diferença entre as médias de cada estação e estação anterior da superfície da água na zona inferior do ELP da temperatura para o período de maio de 2017 a junho de 2021, o Fator Revelle é 14,2 e o Fator de Alcalinidade é – 26,5.

3.5 Cálculos dos fluxos líquidos de CO_2 (FCO_2)

O FCO_2 foi calculado a partir do produto da diferença da pCO_2 entre a superfície da água e a atmosfera ($\Delta pCO_2 = pCO_2 - pCO_2^{atm}$) e os coeficientes de transferência gasosa (k_t) e de solubilidade do CO_2 na água do mar (K_s) (Eq. 15)

[e.g. Jiang et al. 2008]. Portanto, valores negativos de ΔpCO_2 são indicativos de uma absorção de CO_2 da atmosfera pela superfície da água e, inversamente, valores positivos são indicativos de liberação de CO_2 para a atmosfera.

$$FCO_2 = k_t K_s (\Delta pCO_2) \quad (15)$$

A pCO_2^{atm} foi calculada a partir da Eq. 16:

$$pCO_2^{atm} = xCO_2^{ar} [pAr - (1.5/101.325) - pH_2O) \quad (16)$$

A fração molar de CO_2 atmosférico (xCO_2^{ar}) em ar seco foi obtida do Observatório Mauna Loa (NOAA ESRL *Global Monitoring Laboratory*) [Thoning et al. 2021] com dados defasados em 6 meses antes do período correspondente devido à resposta atmosférica entre os hemisférios norte e sul [Millero 2013], uma vez que não havia dados de fração molar para a região de estudo. O *p*Ar é a pressão barométrica da estação meteorológica da cidade de Rio Grande (Brasil; https://portal.inmet.gov.br/) e pH_2O (atm) é a pressão de vapor d'água calculada usando salinidade e temperatura [Weiss e Price 1980].

A maior problemática no cálculo do FCO_2 em águas estuarinas ocorre por causa do k_t, devido ao fato desse ecossistema ter sua hidrodinâmica complexa e geomorfologia variada [e.g. Dinauer e Mucci 2017, Yao et al. 2020]. Várias relações diferentes entre a velocidade do vento e a velocidade de transferência do CO_2 foram propostas com base em estudos de laboratório e de campo. Neste estudo, o k_t foi parametrizado usando a velocidade do vento e a

equação de Jiang et al. [2008] (Eq. 17), derivado de Raymond e Cole [2001] e o K_s de Weiss [1974], calculado usando a temperatura em Kelvin (T) (Eq. 18). A parametrização de Jiang et al. [2008] é usada principalmente no ambiente estuarino [e.g. Evans et al. 2013, Van Dam et al. 2018, Yao et al. 2020].

$$k = [(0{,}314\ U_{10}^2) - (0{,}436\ U_{10} + 3{,}99)]\ (Sc/600)^{-0{,}5} \quad (17)$$

$$K_0 = \text{Exp}\ (-58{,}0931 + 90{,}5069 * (100/Temp) + 22{,}2940*\ln(T/100)\ Sal*(0{,}027766 - 0{,}025888 * (Temp/100) + 0{,}0050578 * (Temp/100)^2 \quad (18)$$

Os dados mensais de velocidade do vento a 10 m (U_{10}) foram obtidos através do 8º Distrito de Meteorologia do Instituto Nacional de Meteorologia (8º DISME / INMET; https://portal.inmet.gov.br/) para o Estado do Rio Grande do Sul. O número de Schimidt (Sc) que aparece na Eq.17 foi calculado (Eq.19), usando-se a temperatura (Temp) em graus Celsius (°C). Para água estuarina, os coeficientes adotados foram: A= 1742; B=91,24; C= 2,208 e D=0,0219.

$$Sc = A - Bt + Ct^2 - Dt^3 \quad (19)$$

A partir da equação de Raymond e Cole [2001] (Eq. 20), foi recalculado o k_t a fim de verificar a sensibilidade do FCO_2 com base nas equações utilizadas. As diferenças médias entre as estimativas derivadas da aplicação original e os novos valores foram de –0,3 ± 0,8 mmol m^{-2} d^{-1} entre as abordagens de Jiang et al. [2008] e Raymond e Cole [2001] (Fig. 7).

$$k = 1{,}91 \text{ Exp } (0{,}35\ U_{10})\ (Sc/600)^{-0{,}5} \quad (20)$$

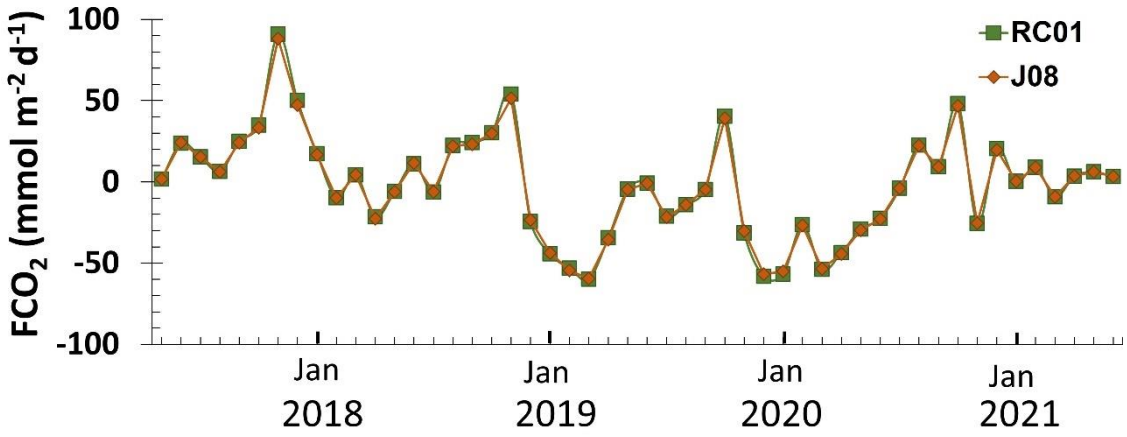

Figure 7. Comparação da média da variabilidade mensal dos fluxos líquidos água-ar de CO_2 (FCO_2) de maio de 2017 a junho de 2021 com a velocidade de transferência do gás calculada a partir da metodologia de Jiang et al. [2008] (J08; losangos laranjas) e da metodologia de Raymond & Cole [2001] (RC01; quadrados verdes).

3.6 CO_2 estuarino

Para calcular a concentração de CO_2 na água, primeiro foram calculadas as concentrações de C_T e A_T do rio, da água do mar e do estuário seguindo a metodologia de Jiang et al. [2008]. A mudança do C_T devido à mistura rio-oceano que ocorre em águas estuarinas é calculada de duas formas: uma quando a entrada de água ribeirinha é alta (C_{Tmr}; Eq. 21) e outra é devido à mistura do oceano em determinada estação (denominada estação *i*; C_{Tmix}; Eq. 22):

$$C_{Tmr} = (S_i/S_{oc})\ C_{Toc} + [(1 - S_i)/S_{oc}]\ C_{Tr} \quad (21)$$

$$C_{Tmix} = [(S_{oc} - S_i)\ C_{Tr} + (S_i - S_r)\ C_{Toc}]/S_{oc} - S_r \quad (22)$$

Como não houve amostragem contínua durante o período estudado na foz do rio ou em um ponto fixo no oceano, as concentrações médias de C_T e salinidade do rio (C_{Tr} e S_r, respectivamente) foram determinadas da estação mais próxima do deságue do rio (BrOA #1) e as concentrações médias de C_T e salinidade do oceano (C_{Toc} e S_{oc}, respectivamente) da estação mais próxima do oceano (BrOA #2). Foi feita a média dos valores encontrados para a salinidade entre 0 e 5 da estação BrOA #1 (representando a salinidade do rio) e acima de 30 da estação BrOA #2 (caracterizando a salinidade do oceano), quanto a média dos valores de C_T correspondentes de cada salinidade dos pontos amostrados (Tabela 1).

Quando não há influência do rio, o C_T na estação *i* (C_{Tmo}) pode ser calculado a parti da Eq. 23:

$$C_{Tmo} = (S_i/S_{oc})\, C_{Toc} \qquad (23)$$

Tabela 1. Valores da salinidade, do carbono inorgânico dissolvido total (C_T em µmol kg^{-1}) e da alcalinidade total (A_T em µmol kg^{-1}) representando as situações de água do rio e do oceano, a partir dos cálculo das médias das estações BrOA #1 e #2.

	Salinidade	**C_T (µmol kg^{-1})**	**A_T (µmol kg^{-1})**
Rio	2,57	703,30	699,47
Oceano	31,36	1648,38	2087,04

Dessa forma, O C_T produzido/consumido devido aos processos biogeoquímicos estuarinos (C_T^{est}) pode ser calculado pela Eq. 24:

$$C_T^{est} = C_{Ti} - C_{Tm} \quad (24)$$

onde o C_{Ti} é o C_T na estação *i* e o C_{Tm} é o C_T devido a mistura de dois membros finais e pode ser calculado pelas Eqs. 21-23. Seguindo a mesma explicação, a A_{Tm} e A_T^{est} podem ser estimados simplesmente substituindo o C_T por A_T nas Eqs. 21-23. Para os membros finais da A_T, as médias também foram definidas (Tabela 1).

Por fim, a concentração estuarina de CO_2 foi calculada por meio do software CO_2Sys v.2.1 desenvolvido por Lewis et al. [1998] e modificado por Pierrot et al. [2006] usando as variáveis C_T, A_T, salinidade e temperatura como parâmetros de entrada. Usamos $[CO_2]_{oceano}$, $[CO_2]_{rio}$ e $[CO_2]_{est}$ para representar a concentração de CO_2 derivada do oceano, do rio e do estuário, respectivamente. O CO_2 aquoso não se mistura de forma conservativa, então, a $[CO_2]_{oceano}$ é a concentração de CO_2 aquoso do oceano se este for diluído por uma água doce com zero C_T, calculado por C_{Tmo} e A_{Tmo} (Eq. 23). A $[CO_2]_{rio}$ é a diferença entre a $[CO_2]$ devido à mistura e a $[CO_2]_{oceano}$ (Eq. 25) [Jiang et al. 2008].

$$[CO_2]_{rio} = [CO_2]_m - [CO_2]_{oceano} \quad (25)$$

Logo, a $[CO_2]$ do estuário ($[CO_2]_{est}$) é calculada pela diferença entre a $[CO_2]$ na estação *i* ($[CO_2]_i$) e a $[CO_2]$ da mistura das águas entre o rio e o oceano ($[CO_2]_m$; Eq.26):

$$[CO_2]_{est} = [CO_2]_i - [CO_2]_m \quad (26)$$

A $[CO_2]_{est}$ negativa indica que é o CO_2 está sendo consumido, enquanto valores positivos representam que o CO_2 está sendo produzido no estuário por processos biogeoquímicos. Quando o $[CO_2]$ foi calculado a partir do C_T e da A_T, foi utilizada a temperatura média anual de 21,03 °C, uma vez que o $[CO_2]$ dissolvido está sujeito às variações da temperatura da água.

3.7 Outras análises: Estatística e Ondeletas

As análises de correlação entre os parâmetros abióticos (variáveis ambientais) foram realizadas no Software Statistica. Matrizes de correlação e coeficiente de correlação de Pearson (*r*) foram calculados entre as variáveis.

A análise da transformada Wavelet foi usada para avaliar o padrão de variabilidade nas séries temporais dos parâmetros do sistema carbonato e do FCO_2. A ondeleta mãe usada foi a função Morlet. A escala usada para a transformada de ondeleta foi de 12 meses porque havia uma amostra por mês, e o comprimento (ou seja, espaçamento entre escalas discretas) foi de 0,125. O comprimento da função Morlet deve ser menor que 0,5 para identificar a variabilidade na escala anual, com valores menores proporcionando melhores resoluções [Torrence e Compo 1998]. O cone de influência foi determinado com base no processo de ruído vermelho com um coeficiente de defasagem de 0,72 [Gilman et al. 1963]. Os resultados da análise de ondeleta forneceram valores

de energia na forma logarítmica de base 2 em meses, onde os valores positivos indicam alta energia (maior variabilidade) e os valores negativos apontam baixa energia (menor variabilidade).

Capítulo IV: O sistema carbonato no Estuário da Lagoa dos Patos

O primeiro manuscrito, em síntese, apresenta a primeira caracterização do sistema carbonato na zona inferior do ELP, cujo objetivo foi a investigação da variabilidade temporal da distribuição dos parâmetros do sistema carbonato na região de estudo. Este trabalho possibilitou observar a variabilidade sazonal e interanual das principais variáveis que compõe o sistema carbonato e, ainda, contribuiu para um melhor entendimento da biogeoquímica na área estudada. De autoria de Cíntia Albuquerque, Rodrigo Kerr, Thiago Monteiro, Iole Beatriz Marques Orselli, Mariah de Carvalho-Borges, Andréa da Consolação de Oliveira Carvalho, Eunice da Costa Machado, Júlia Kalid Mansur, Margareth Copertino e Carlos Rafael Borges Mendes, intitulado "***Seasonal variability of carbonate chemistry and its controls in the subtropical estuary***", foi submetido no periódico *"**Estuarine, Coastal and Shelf Science**"* em outubro de 2021 e encontra-se em revisão. A

análise dos dados, as principais interpretações e a redação deste manuscrito foram feitas por mim, como parte da minha tese de doutorado. Rodrigo Kerr liderou as atividades da rede BrOA na Lagoa dos Patos, propôs o estudo e fez toda a supervisão para que chegássemos à conclusão desse estudo. Todos os autores tiveram participação significativa na redação final do texto submetido ao periódico e importantes contribuições ao longo desse trabalho. Cíntía Coelho, Rodrigo Kerr, Thiago Monteiro, Iole Orselli, Mariah de Carvalho-Borges, Andréa Carvalho, Carlos Rafael Mendes e Júlia Mansur contribuíram nas coletas de campo e/ou análises químicas de laboratório. Eunice Machado contribuiu como especialista em biogequímica de estuários. Margareth Copertino e Carlos Rafael Mendes contribuíram como especialistas em ecologia de produtores primários.

Abstract

We performed an unprecedented investigation of the seasonal variability in carbonate system parameters (the total alkalinity – A_T, the total dissolved inorganic carbon – C_T, the pH, and the partial pressure of carbon dioxide – pCO_2) in the lower zone of the Patos Lagoon Estuary (PLE), the largest choked lagoon in the world. Sampling was conducted monthly from May 2017 to June 2021. A_T and pH were measured during the study period, while other carbonate system parameters were estimated using CO_2Sys software. The pH distribution reflected the average natural alkaline conditions throughout the year, with an average of 8.0 pH units. The surface waters in the lower zone of the PLE are generally characterized by a supersaturated calcium carbonate environment. However, a susceptibility to undersaturation conditions was observed during winter (calcite

and aragonite) and spring (aragonite). Furthermore, the average surface water pCO_2 was 394 μatm during the analyzed period, with the highest values recorded in winter and early spring. The predominant estuarine processes governing changes in the carbonate system in the PLE were the dilution and concentration of salts. These processes depend on the complex balance between freshwater outflows and oceanic inflows that change the surface salinity and produce favorable conditions for primary producer development and the input of continental carbon. However, the remineralization of organic matter and CO_2 ingassing likely contribute to the deviations in the theoretical mixing line, causing the increased C_T in the region. In addition, the nonthermal effects on seasonal changes in the pCO_2 prevail over thermal effects, and the region presents an ocean-dominated (riverine-dominated) condition during summer and autumn (winter and spring). The novel results described here reveal the complexity and challenges that still exist to a better comprehension of how carbonate system parameters evolve temporally and spatially in the PLE, especially considering the climate- and anthropogenic-driven stressors. Finally, this study contributes to the understanding of carbonate system variability in coastal ecosystems and highlights the need for more intense and continuous biogeochemical monitoring of Southern Hemisphere estuaries.

4.1 Introduction

Estuaries occupy a surface area of only 4% of the global continental shelf and generally exhibit higher water-air carbon dioxide (CO_2) net fluxes than those observed over the ocean surface [Borges et al. 2004]. In addition, estuarine

systems are characterized by intense carbon fixation and respiration due to high primary production and decomposition rates of organic matter. The river inputs and rapid cycling of autochthonous and allochthonous organic matter, which are degraded by microbial action, cause supersaturation of CO_2 in estuarine waters [Sunda and Cai 2012]. This behavior results in variability in the water-air CO_2 net fluxes in these ecosystems, along with variations in biological, physical, and chemical parameters of estuarine surface waters [e.g., Maher and Eyre 2012, Evans et al. 2013, Cotovicz et al. 2020]. Moreover, changes in the distribution of carbonate system parameters are associated with an increase in atmospheric CO_2 levels, changes in hydrological properties and estuarine dynamics, enhanced estuarine biogeochemical processes (e.g., respiration, production, carbonate dissolution, and precipitation), and changes in atmospheric conditions (e.g., wind speed and rainfall). These processes may shift the role of estuarine waters between net CO_2 sinks and sources [e.g., Cai 2011, Salt et al. 2016, Cotovicz et al. 2020]. The hydrodynamics and climatic conditions in each estuary vary according to local processes [Borges and Abril 2011], strongly influencing the seasonal and spatial heterogeneity in water mixing between riverine-oceanic waters [e.g., Bauer et al. 2013, Carstensen et al. 2018].

Changes in water chemistry can affect estuarine and marine organisms directly and/or indirectly. For instance, the acidification process leads to a decrease in carbonate ions (CO_3^{2-}), a key component for many organisms that use them to build their shells and skeleton material. This change may impair the calcification rates of these organisms and possibly affect their physiology, reproduction, and even geographical distributions [Zeebe 2012, Hatje et al. 2013, Doney et al. 2020]. Although estuarine organisms can tolerate the high variability

in biogeochemical properties and acclimate to the rapid changes imposed by estuaries [Bible and Sandford 2016], many marine species might be affected, particularly juveniles that use estuaries as temporary nurseries and feeding habitats [Vinagre et al. 2013]. Furthermore, studies on carbonate system variables in tropical and subtropical environments are relatively limited, and the effect of CO_2 system variability on marine organisms are not well studied in these ecosystems, specifically in the transitional coastal environments between the continent and ocean of the Southern Hemisphere [e.g., Vieillard et al. 2020, Vargas et al. 2016]. This limitation hampers the general comprehension of the behavior and variability of carbonate system parameters at a global scale in these ecosystems [Ciais et al. 2013, Roobaert et al. 2019].

Despite the available knowledge and information provided by long-term monitoring and research programs [Seeliger et al. 1998, Seeliger et al. 2004, Seeliger and Odebrecht 2010, Odebrecht et al. 2017] about the internal variability of biological parameters and estuarine hydrodynamics in the Patos Lagoon Estuary (PLE; Fig. 8b) [Castelão and Möller 2003, Vaz et al. 2006, Möller et al. 2007, Möller and Fernandes 2010, Haraguchi et al. 2015, Lisboa 2015, Lanari and Copertino 2017, Lanari et al. 2018], information about the carbonate system in this area is scarce. Thus, investigating the biogeochemistry of the Patos Lagoon zones (Fig. 8a), which are located in extreme southern Brazil (~32°S), may provide considerable information to fill the knowledge gap in carbonate system variability in estuarine areas of the Southern Hemisphere. Thus, the present study aims to provide the first overview of the seasonal variability and estuarine processes driving the changes in the carbonate system parameters of the surface waters in the lower estuarine zone of the PLE (Fig. 8b).

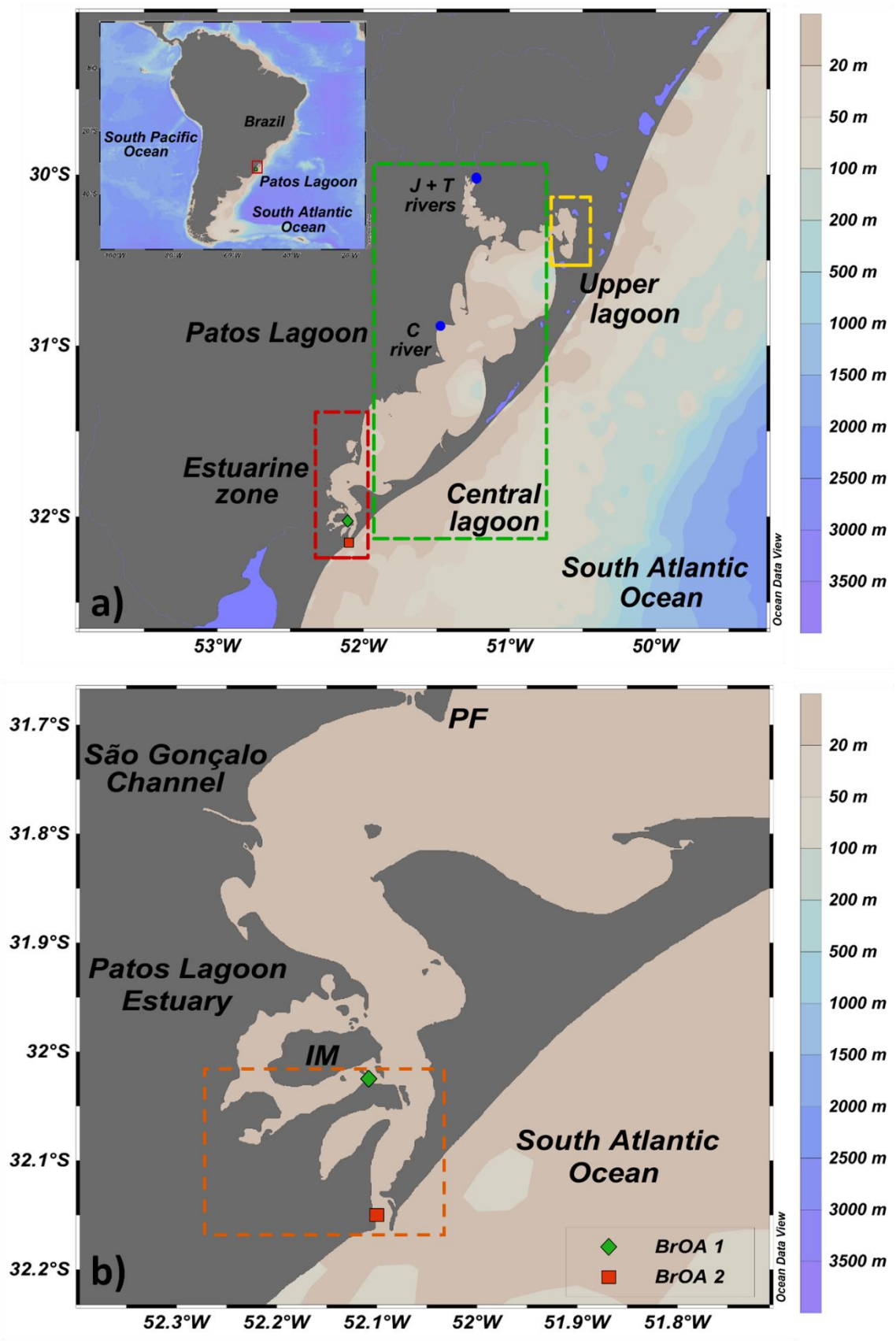

Figure 8. Map of the study region: Patos Lagoon. **(a)** Location of the Patos Lagoon and its geomorphological divisions: the estuarine zone (red rectangle), the central lagoon (green rectangle) and the upper lagoon (yellow rectangle). Blue dots indicate regions of freshwater discharge from the Jacuí and Taquari (J + T) and Camaquã (C) Rivers. The inset in (a) shows a

map of South America with the location of the Patos Lagoon (red rectangle).. **(b)** Location of the pier-fixed monitoring BrOA #1 (green diamond) and #2 (red square) stations in the Patos Lagoon Estuary with the southern region highlighted (orange rectangle). Marinheiros Island (IM) and Ponta da Feitoria (PF) are indicated.

4.2 Patos Lagoon features

Patos Lagoon is the largest choked lagoon in the world [Kjerfve 1986] and is connected to the South Atlantic Ocean by a narrow channel (~1 km wide) [Castelão and Möller 2003, Marques and Möller 2008, Marques et al. 2009]. The surface area of Patos Lagoon is approximately 10,360 km^2, and the drainage basin is approximately 200,000 km^2, with an average depth of 5 m; 85% of the estuarine area has a depth of less than 2 m [Möller 1996, Seeliger 2001]. The lagoon comprises subtropical and warm temperate climate regions with an annual average air temperature of 18°C and annual average precipitation ranging between 1,200 mm and 1,500 mm, with the highest rainfall occurring during the summer [Abreu et al. 2016]. In general, the input of saline water is restricted to the lower estuary, which covers approximately 10% (~1,000 km^2) of the total area of the lagoon [Seeliger 2001], resulting in a pronounced range of salinity from 0 to 35 [Vaz et al. 2006]. In addition, the lower estuarine zone of the PLE has a water residence time of approximately two days, considering the water exchanges up to the region near the Ponta da Feitoria (Osmar O. Möller Jr. personal communication). Thus, although the mouth of the estuary (an euhaline zone) has strong and energetic currents, the residence time is relatively short. On the other hand, the shallow and embayment mesohaline zones of the PLE experience a water residence time that is slightly higher. Moreover, strong hydrodynamic events spread the PLE freshwater plume, reducing salinity near the coast [Zavialov et al. 2018].

In this sense, the hydrodynamics of Patos Lagoon are dominated by wind at time scales associated with the passage of frontal systems and the strength of freshwater discharge in the microtidal region [Möller et al. 2001]. Therefore, wind and freshwater discharge are the main drivers of PLE hydrodynamics. Notably, the hydrodynamic processes are related to the size of the drainage basin and the dimensions and orientation of the longitudinal axis of the lagoon [Vaz et al. 2006, Möller and Fernandes 2010]. The natural bottleneck characteristic of the estuary intensifies the ebb currents and acts as a filter for the already nonimportant tidal movements [Möller et al. 2007]. In addition to wind direction and freshwater discharge, the hydrology in the estuary is controlled by the balance between precipitation and evaporation levels [Castelão and Möller 2003, Möller and Fernandes 2010, Abreu et al. 2016]. Thus, seawater intrusion in autumn is greater than in other seasons due to the frequent passage of frontal systems with southerly winds combined with low freshwater inputs, resulting in flooding and salinization of the PLE. When winds blow from the northeast at the end of winter and spring, periods of high freshwater discharge favor ebb currents. During summer and spring, a well-marked presence of east winds occurs, indicating an influence of sea breezes signal. The north and south quadrant winds form vertical salinity structures that can range from a salt wedge to a well-mixed gradient [Möller et al. 2001, Möller and Fernandes 2010]. Therefore, during the months of flooding and higher wind speed, the estuary tends to present a well-mixed gradient; while during the months of higher freshwater discharge, salt wedge conditions are more frequently observed [Möller et al. 2001]. Furthermore, the PLE is directly affect by the variability in El Niño-Southern Oscillation (ENSO) events, which affect the regional temperature, precipitation, wind patterns, and

freshwater discharge (Seeliger and Odebrecht 2010]. During the warm phase of ENSO under El Niño conditions, southern Brazil is characterized by higher precipitation and warm air temperatures, while relatively dry and cold atmospheric conditions prevail during La Niña (Grimm and Ferraz 1998]. Consequently, those changes alter the magnitude of freshwater discharge into the PLE (Möller et al. 2001) because, freshwater discharge is above the average level (~1770 m^3 s^{-1}) under El Niño conditions, and the opposite is true under La Niña conditions [Vaz et al. 2006; Seeliger and Odebrecht 2010].

Considering the complex hydrodynamics of the PLE waters, the mixing between riverine-oceanic water dynamics prompts questions about its effect on the seasonal cycle of the carbonate parameters. Despite the knowledge of the effect of freshwater and seawater mixing on the PLE, carbonate system parameters have not been measured over the seasons to provide proper quantification and an understanding of carbonate seasonal variability and its implications in the face of anthropogenic changes is lacking. Regarding the chemical changes in the PLE waters, some inner areas of the PLE have presented signals of eutrophication [e.g., Abreu et al. 2010, Marreto et al. 2017], as was noted by a study conducted the 1980s that showed an increase in nutrient concentrations [Wallner-Kersanach et al. 2016]. Moreover, nutrient dynamics have changed slightly over time because of the relatively fast estuarine water renewal [e.g., Möller et al. 2001, Wallner-Kersanach et al. 2016] that may be faster if the freshwater discharge is higher [Odebrecht et al. 2015]. The increases in the nutrient concentrations were followed by changes in the primary producer community, such as an increase in the frequency of opportunistic macroalgal blooms (causing green tides) or changes in the phytoplankton composition

[Wallner-Kersanach et al. 2016, Marreto et al. 2017, Lanari and Copertino 2017]. Following nutrient pulses, the equilibrium of the community of the primary producers is normally restored. Thus, although human-induced impacts may influence the structure and dynamics of this environment [Odebrecht et al. 2017], the eutrophication already reported in the PLE is likely offset by estuarine water dynamics, which prevents the accumulation of nutrients in surface waters [Abreu et al. 2010]. These biogeochemical changes reported in previous studies may also affect the seasonal variability of the carbonate system.

4.3 Data and Methods

4.3.1 Database from the Brazilian monitoring programs

The physical, biological, and chemical parameters are sampled by the Brazilian Long Term Ecological Research (BR-LTER) of PLE and Adjacent Marine Coast, an ecological monitoring program since 1999 (www.peld.furg.br) [Odebrecht and Abreu 2019]. The database includes surface water temperature, salinity, contents of dissolved nutrients (i.e., nitrate, nitrite, silicic acid, and phosphate), and chlorophyll-a (Chl-*a*) content. The total alkalinity (A_T) and pH are sampled by the Brazilian Ocean Acidification Network (BrOA Network; www.broa.furg.br) [Kerr et al. 2016] together with the sampling performed by the BR-LTER since 2015.

Surface water samples (1 m below the surface) were collected monthly using a 5 L van Dorn bottle in two estuarine regions at pier-fixed stations in the southern part of the PLE. These stations are located (i) in an inner inlet

mesohaline region (at a depth of less than 2 m) and in a (ii) lower euhaline region (at a depth of ~12 m near the mouth of the PLE) in the lower zone of the PLE (Fig. 8b) [Abreu et al. 2016]. Both regions are located in the southern part of the PLE and may represent the lower estuarine area characterized by a wide salinity variation (0 to > 35) and hydrodynamic differences. The mesohaline region is shallow and is more substantially affected by the influence of winds promoting water column mixture and exchanges with the bottom, while the station located at the euhaline region is more sea-exposed and is characterized by a greater effect of water intrusions from the South Atlantic Ocean. In addition, while the mesohaline regions may experience longer periods of relatively calm conditions of water, the lower euhaline region is affected by the water inflow/outflow, depending on the strengthening of the estuarine dynamics. The two stations are hereafter referred to as BrOA #1 (mesohaline region) and BrOA #2 (euhaline region). The sampling procedure always begins at BrOA #1 followed by BrOA #2 sampling in the early morning. The interval between sampling at the stations is approximately 20-30 min. Here, the dataset used from the monthly monitoring programs spans from May 2017 until June 2021.

4.3.2 Determination of temperature, salinity, dissolved nutrients, and chlorophyll-a

Surface water temperature and salinity were measured *in situ* using a digital thermometer and portable refractometer, respectively. The salinity was further verified at laboratory with a conductivity meter. Dissolved nutrients were measured in filtered water, and their concentrations were determined using the method reported by Strickland and Parsons [1972]. The nutrient concentrations

were used only to estimate the derived parameters of the carbonate system. Discrete surface water samples of 50–250 mL (depending on material concentration) were filtered through Whatman GF/F filters (nominal pore size 0.7 µm and 25 mm diameter) under dim light using a vacuum pressure of < 5 in mercury and immediately frozen (–80°C) for subsequent determination of the total Chl-*a* concentration using a fluorometric method. In the laboratory, the pigment was extracted in 90% acetone, and fluorescence was determined in a Turner Designs TD-700 fluorometer (previously calibrated with a Sigma® chlorophyll-a standard) using the non-acidification method described by Welschmeyer [1994].

4.3.3 Determination of total alkalinity and pH

Water samples for the total alkalinity (A_T) analysis were collected at the same depth as other parameters (1 m below the surface) in 500 mL borosilicate glass bottles and fixed with 100 µL of a supersaturated mercury chloride solution to prevent biological activity following the procedure described by Dickson et al. [2007]. The samples were refrigerated to prevent evaporation and were analyzed in the laboratory. A_T was measured in the laboratory by potentiometric titration in a closed cell [Dickson et al. 2007] with an automated titrator (Metrohm® Titrando 808) and a combined glass-reference electrode (Metrohm® 6.0262.100) at a controlled temperature of 25 ± 0.1°C sustained by a thermostatic bath (Tamson® TLC 15). Due to the high salinity range in the estuary (from 0 to ~32), an adaptation of the closed cell method [Dickson et al. 2007] was adopted. Solutions of HCl (0.1 M) with NaCl backgrounds for different salinities were used as titrants to approximate the actual salinity of the samples. The precision of both A_T

measurements was determined using a certified reference material (batches nos. 96, 149, 162 and 177, acquired from Scripps Institution of Oceanography) [Dickson et al. 2003]; control analyses were performed regularly (weekly) throughout the study period to ensure the quality of the results. A correction factor was applied to the measured values based on the certified reference material values and the dilution of the sample with the mercury chloride solution [Dickson et al. 2007]. The average analytical precision of the A_T analyses was ± 4.0 µmol kg^{-1} (range of 2.3 < A_T < 5.0 µmol kg^{-1} considering the analyzed sample batches). The consistency of these measurements was evaluated daily throughout the analysis period with replicate analysis of a single sample.

Surface samples for the pH analysis were collected in 125 mL borosilicate amber flasks. The pH was potentiometrically determined within a maximum period of two hours after sampling. We used a Metrohm® 913 or 914 pH meter coupled with a glass-reference electrode cell and a temperature sensor to perform these measurements. Fluka® Sigma-Aldrich® buffer solutions with pH values equal to 4.008 (potassium hydrogen phthalate + phenylmercury chloride) and 7.413 (disodium hydrogen phosphate + potassium dihydrogen phosphate (KH_2PO_4)), both at 25°C, were used to standardize the pH electrode before the samples from each profile were measured. We applied the equation developed by Gieskes [1969] to correct the pH measurements for the *in situ* temperatures. The pH values were reported in the total scale. The precision and accuracy of the pH measurements were evaluated by performing repeated analyses of duplicate samples collected from the same van Dorn bottle and by performing regular measurements of the buffer solution at pH = 7.413 during the analyses. The uncertainty of the measurements was ≤ 0.05 pH NBS units.

4.3.4 Determination and sensitivity of other carbonate system parameters

Total dissolved inorganic carbon (C_T), partial pressure of CO_2 (pCO_2) and calcium carbonate ($CaCO_3$) saturation state (Ω) of calcite (ΩCa) and aragonite (ΩAr) were estimated using CO_2Sys v.2.1 software developed by Lewis et al. [1998] and modified by Pierrot et al. [2006]. Surface water temperature, salinity, A_T, pH, silicic acid, and phosphate concentrations were used as input parameters. The total scale was chosen for pH at *in situ* temperature. Since the study was performed in an estuarine environment with a broad salinity range, we applied the following set of constants: the K_1 and K_2 dissociation constants reported by Millero et al. [2006], such as those used by Liu et al. [2017], Carstensen et al. [2018] and Chen et al. [2020] in estuary and coastal environments, and the sulfate and borate constants reported by Dickson [1990] and Uppström [1974], respectively.

The carbonate system parameter uncertainties were determined using the method reported by Orr et al. [2018]. The temperature and salinity errors were lower than 0.1°C or 0.1 salinity units, respectively, and were not considered in this calculation. Hence, the propagated uncertainties in carbonate system parameters fundamentally represent the errors associated with the estimated A_T and pH values. The average uncertainties of the calculated C_T, pCO_2, ΩCa and ΩAr values were ±13 µmol kg^{-1}, ±46 µatm, ±0.02 and ±0.01, respectively. Additionally, we reran CO_2Sys v.2.1 software to verify the sensitivity of the carbonate system parameters based on the set of constants used. We changed the set of constants to the K_1 and K_2 dissociation constants of Cai and Wang

(1998), the sulfate constants described by Khoo et al. [1977] and the borate constants of Lee et al. [2010]. Afterward, the average differences between the estimates derived from the original application and the new values were considered relatively low for estuarine waters, which were 55 µmol kg^{-1}, 80 µatm, 0.01 and 0.007 for C_T, pCO_2, ΩCa and ΩAr, respectively.

4.3.5 Controls of pCO_2: thermal vs.nonthermal effects

The thermodynamic relation between pCO_2 and temperature is 4.23% $°C^{-1}$ [Takahashi et al. 1993], and seasonal variations in surface pCO_2 can be decoupled into thermal and nonthermal effects. We used the approach reported by Takahashi et al. [2002] to evaluate those effects on seasonal changes in pCO_2 at the BrOA #1 and #2 stations. The thermal effect is mainly related to thermodynamic processes affecting CO_2 solubility in water. The nonthermal effects represent the pCO_2 variability due to changes in the concentration of C_T and/or A_T, which includes vertical mixing and the biological utilization of CO_2 [Körtzinger et al. 2008]. First, pCO_2 data were calculated for a monthly and seasonal average temperature to exclude the temperature effect (Eq. 27):

$$pCO_2\ \text{NonT} = (pCO_2)\ \ \text{Exp}\ [0.0433\ (T_m - T) \qquad (27)$$

where T_m is the monthly mean surface water temperature and T is the observed temperature. Then, pCO_2 was calculated for a particular *in situ* temperature to obtain the temperature signal (Eq. 28):

$$pCO_2\ T = (pCO_{2\ m})\ \ Exp\ [0.0433\ (T - T_m) \quad (28)$$

where $pCO_{2\ m}$ is the monthly and seasonal average surface pCO_2. For each station, both the thermal (ΔpCO_2 T) and nonthermal (ΔpCO_2 NonT) seasonal changes were calculated using the difference between maximum (max) and minimum (min) values for pCO_2 at surface temperature for the thermal effect and pCO_2 at surface temperature for the nonthermal effect (Eqs. 29 and 30):

$$\Delta pCO_2\ T = (pCO_2\ T)_{máx} - (pCO_2\ T)_{min} \quad (29)$$

$$\Delta pCO_2\ NonT = (pCO_2\ NonT)_{máx} - (pCO_2\ NonT)_{min} \quad (30)$$

The ratio (T:NT) between the two conditions was applied to compare the relative effect of both thermal (T) and nonthermal effects (NT) (Eq. 31):

$$T{:}NT = \Delta pCO_2\ T/\Delta pCO_2\ NonT \quad (31)$$

Thus, T:NT < 1 indicates that the nonthermal effect has greater magnitude and variability, while T:NT > 1 indicates that the nonthermal effects are weaker or rather constant.

4.3.6 Dispersion diagrams and riverine and ocean properties endmembers

The river (freshwater) and ocean (seawater) physical and biogeochemical endmembers were determined to verify the deviations from the theoretical conservative mixture lines. As continuous sampling was not performed during the study period at the mouth of the rivers (for which inflow is located further north in the central lagoon, Figure 1a) or at a fixed point in the ocean, the most pure conditions of riverine and ocean water were determined from the station closest to the river outlet (BrOA #1; salinity < 3) and from samples of opportunity in the near coastal shelf (salinity > 31), respectively. Thus, the riverine biogeochemical endmembers were A_T = 664 µmol kg^{-1}, C_T = 675 µmol kg^{-1}, pH = 7.9 and pCO_2 = 565 µatm, while the ocean endmembers were A_T = 2,107 µmol kg^{-1}, C_T = 1,738 µmol kg^{-1}, pH = 8.3 and pCO_2 = 251 µatm.

In addition, the main physical-biogeochemical processes controlling the equilibrium of the carbonate system can be recognized from A_T-C_T diagrams. The processes characterized by the A_T:C_T ratio are photosynthesis and respiration, $CaCO_3$ calcification and dissolution, CO_2 outgassing and ingassing as proposed by Zeebe and Wolf Gladrow [2007]. The former (second) processes are responsible for the decrease (increase) in the pCO_2 in the water. The dilution and salt concentration processes presented in this diagram are based on the theoretical conservative mixture line determined from the calculated endmembers.

4.3.7 Wavelet analysis

Wavelet transform analysis was used to evaluate the pattern of variability in the carbonate system parameters over the time series. The mother wavelet

used was the Morlet function. The scale used for the wavelet transform was 12 months because one sample was collected per month, and the length (i.e., spacing between discrete scales) was 0.125. The length of the Morlet function must be smaller than 0.5 to identify variability at the annual scale, with smaller values providing better resolution [Torrence and Compo 1998]. The cone of influence was determined based on the red noise process with a lag coefficient of 0.72 [Gilman et al. 1963]. The results of wavelet analysis provided energy values in base-2 logarithmic form and revealed the period (months) with the highest intensity in the variability. Additionally, we determined whether the periods of variability changed throughout the years investigated in this study.

4.4 Results

4.4.1 Seasonal variability of the hydrographic and carbonate system properties

The seasonal cycle of the surface water temperature displayed a similar pattern at both stations BrOA #1 and #2, with amplitude values greater than 10°C (Figs. 9a and S1a). The annual average surface water temperature was 21 ± 4.4°C from 2017 to 2021 (Fig. S1a). The seasonal cycle of the surface salinity also displayed a similar pattern of variability at stations BrOA #1 and #2 (Figs. 9b and S1b). The surface salinity ranged from freshwater to seawater values (i.e., 0 to 35) in the PLE, with the highest salinity occurring during the end of summer and early autumn and the lowest salinity occurring during spring, following the changes in freshwater discharge (Fig. 2b). The monthly average freshwater discharge was calculated from the available dataset from 2015 to 2017 of the three largest rivers that flow into the PLE (i.e., Jacuí, Taquari and Camaquã

Rivers); unfortunately, more recent data are not available yet. However, this ancillary dataset was used here only qualitatively to mark periods of high (June-November) and low (December-May) freshwater discharge.

The Chl-*a* concentrations ranged from 0 to ~24 µg L^{-1} and exhibited a marked seasonal cycle, with the highest values observed during spring and summer months and the lowest values observed in autumn and winter (Fig. 9c). The highest Chl-*a* concentration of ~23 µg L^{-1} was observed in January 2019 at BrOA #2 and ~24 µg L^{-1} in October 2019 at BrOA #1 (Fig. S1c).

The A_T seasonal cycle showed irregular behavior with high concentrations in late autumn (April to June) and low concentrations in early spring (October and November), with a seasonal range of 900 µmol kg^{-1} at BrOA #1 and 800 µmol kg^{-1} at BrOA #2 (Fig. 9d). On average, the highest values of C_T occurred during late autumn (May and June) and the lowest values occurred during spring (October), with a seasonal range of up to 700 µmol kg^{-1} at BrOA #1 and 600 µmol kg^{-1} at BrOA #2 (Fig. 9e). Notable A_T and C_T variability evolved in cycles of periods of 2, 5 and 11 months (Figs. 12a and S3a), which were most visible at BrOA #1 (Figs. 12b and S3b). The highest A_T concentration of 2,245 µmol kg^{-1} was observed in March 2018, and the lowest concentration of 412 µmol kg^{-1} was observed in October 2020 (Fig. S2a). The highest C_T of 2,041 µmol kg^{-1} was observed in March 2018, and the lowest concentration of 435 µmol kg^{-1} was observed in October 2020 (Figure S2b).

The seasonal variation in pH was marked by maximum pH values in late spring (November and December; Fig. 9f), with more alkaline pH conditions prevailing during spring and summer. The average pH at the two monitoring sites

in the PLE was estimated to be 8.0 between 2017 and 2021, with the pH remaining above 7.0 during the entire sampling period (Fig. S3c). In contrast to A_T and C_T, the pH changes only occurred at periods of 5 months at BrOA #1 (Fig. 12c). The highest pH (8.8) was observed in December 2019, and the lowest pH (7.3) was observed in October 2018 (Fig. S2c).

The seasonal cycle of surface water pCO_2 nearly mirrors the pH cycle (see Fig. 9f and 9g).The highest pCO_2 values occurred in October (early spring) for both BrOA#1 and BrOA#2, followed by a decrease in pCO_2 in November and December (late spring), and the lowest value was reached during summer (March; Figure 9g). The nonthermal pCO_2 showed higher values than the thermal pCO_2, mainly at the BrOA #1 station (Fig. 11b and 11c). For the entire study region, the T:NT ratio was < 1 during all months (Fig. 10), indicating that the nonthermal effect prevailed over the thermal effect on pCO_2. However, changes in the main effect controlling the pCO_2 in the PLE likely occurred mainly during winter, because it is the season in which the T:NT ratio oscillates from the average value observed in other seasons. A delay of ~2-3 months was observed in the monthly variability periods of the pCO_2 at BrOA #1 compared with changes in A_T and C_T. The water pCO_2 evolved at periods of 7 and 14 months; however, interannual oscillations were marked with higher energy (Fig. 12d). In addition, the interannual variability in pCO_2 had a higher frequency at BrOA #1 than #2, with maximum energy detected in approximately 2018 and 2019. The highest pCO_2 (1,306 µatm) was observed in November 2018, whereas the lowest annual pCO_2 value (99µatm) was detected in December 2018 (Fig. 11a). In general, the water pCO_2 was lower than ~350 µatm since 2019.

The ΩCa and ΩAr seasonal cycles were similar and attained their

maximum values in late spring (December) and minimum values in early spring (October and November; Fig. 9h). The highest ΩCa (9.5) was observed in May 2020, and the lowest value (0.0) was observed in spring months (Fig. S2d). Both ΩCa and ΩAr were supersaturated (i.e., Ω > 1) during most of the studied period (Fig. S2d and S2e) and BrOA #2 generally presented higher values for both ΩCa and ΩAr than the mesohaline zone (BrOA #1; Fig. 9h). Despite this supersaturation condition, the waters of PLE were susceptible to $CaCO_3$ undersaturation conditions during winter and spring (Table 2).

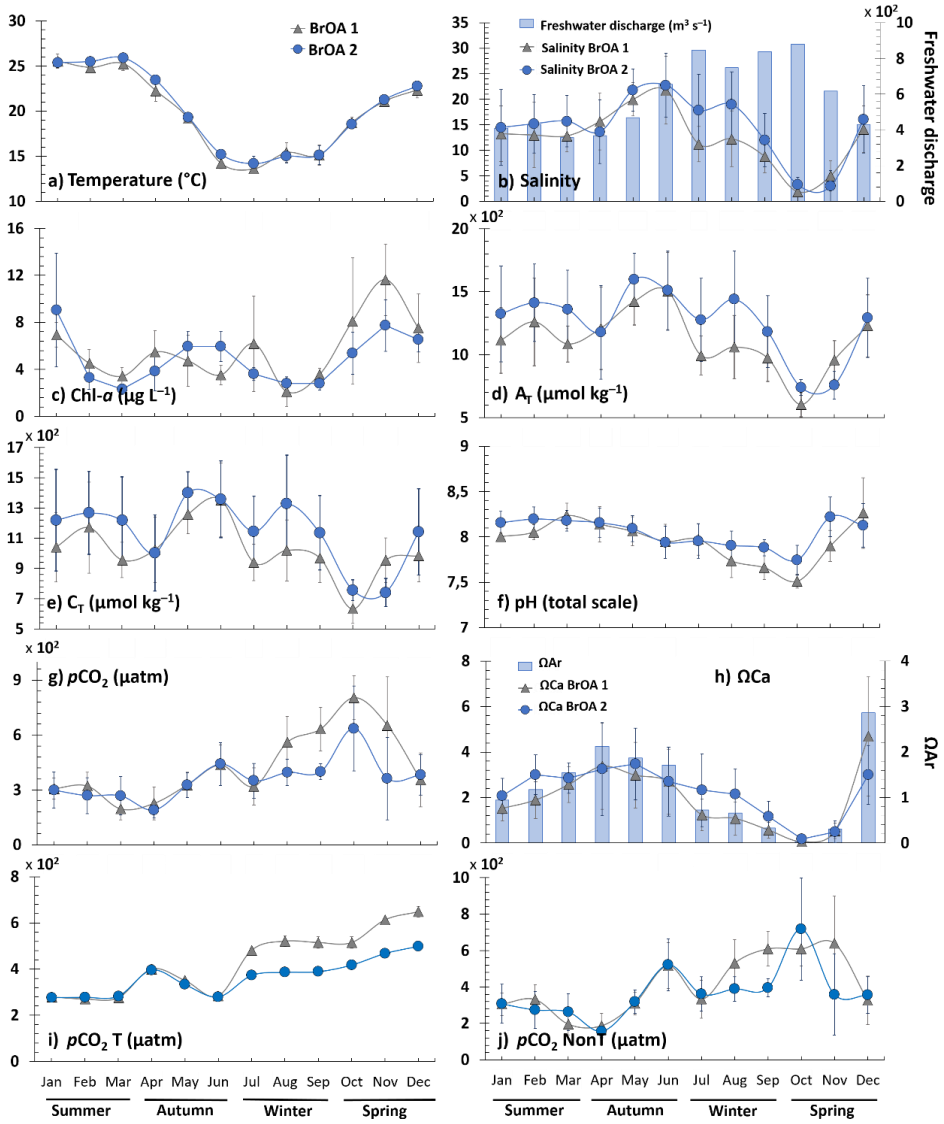

Figure 9. Seasonal cycle of surface water properties at BrOA #1 (gray line and triangles) and

BrOA #2 (blue line and dots) stations in the Patos Lagoon Estuary from May 2017 to June 2021: **(a)** temperature (°C), **(b)** salinity and riverine freshwater discharge (m^3 s^{-1}; blue bars), **(c)** chlorophyll-*a* (Chl-*a*; μg L^{-1}), **(d)** total alkalinity (A_T; μmol kg^{-1}), **(e)** total dissolved inorganic carbon (C_T; μmol kg^{-1}), **(f)** pH at the total scale, **(g)** partial pressure of CO_2 (pCO_2; μatm), **(h)** saturation state of calcite (ΩCa, left axis) and aragonite (ΩAr; blue bars, right axis), **(i)** partial pressure of CO_2 thermal (pCO_2 T; μatm) and **(j)** partial pressure of CO_2 nonthermal (pCO_2 NonT; μatm). The ΩAr values in (h) depict the average at BrOA #1 and BrOA #2. The error bars indicate the standard errors in each month.

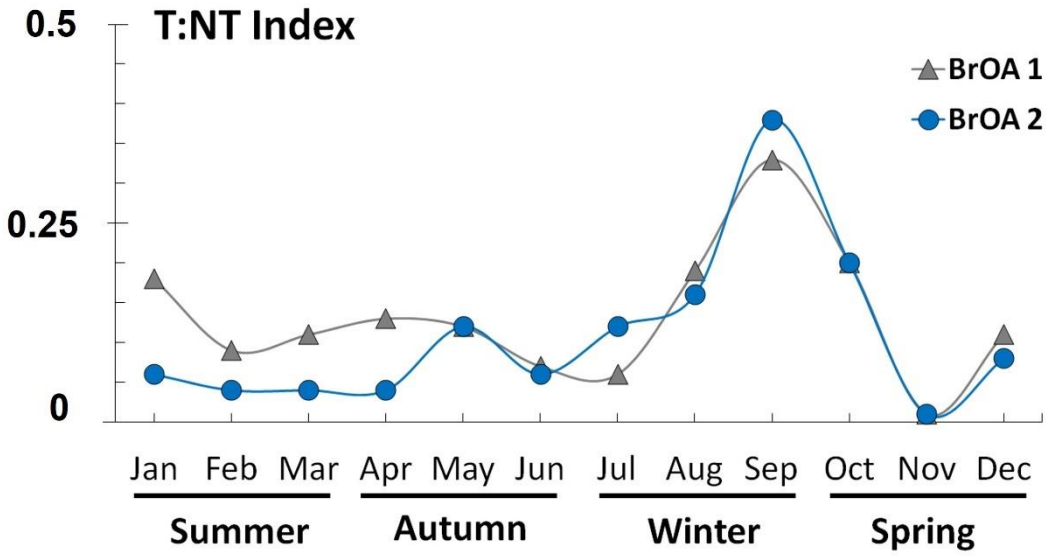

Figure 10. Seasonal cycle of the T:NT ratio at the BrOA #1 (gray line and triangles) and BrOA #2 (blue line and dots) stations in the Patos Lagoon Estuary from May 2017 to June 2021. Acronyms; Thermal (T) and nonthermal effects (NT).

Table 2. Seasonal averages and standard deviation of surface water temperature (°C), salinity, chlorophyll-*a* (Chl-*a*; μg L^{-1}), total alkalinity (A_T; μmol kg^{-1}), total dissolved inorganic carbon (C_T; μmol kg^{-1}), pH at the total scale, $CaCO_3$ saturation state of calcite (ΩCa) and aragonite (ΩAr), partial pressure of CO_2 (pCO_2; μatm), thermal partial pressure of CO_2 (pCO_2 thermal; μatm), nonthermal partial pressure of CO_2 (pCO_2 nonthermal; μatm) and T:NT index in the BrOA #1 (first line) and BrOA #2 (second line) stations. The bold values refer to a seasonal average of Ω < 1.

Parameters	Season			
	Summer	**Autumn**	**Winter**	**Spring**
Temperature (°C)	25.19 ± 1.31	18.29 ± 3.70	14.71 ± 1.90	20.71 ± 1.90
	25.60 ± 0.79	19.03 ± 3.53	14.75 ± 1.65	20.87 ± 1.99
Salinity	13.02 ± 9.37	19.39 ± 10.93	10.73 ± 7.67	6.98 ± 7.87
	15.13 ± 11.19	19.81 ± 11.73	16.29 ± 11.74	7.45 ± 10.03
Chl-a (μg L^{-1})	4.96 ± 2.37	4.50 ± 3.46	3.95 ± 4.80	9.08 ± 7.40
	4.88 ± 6.04	5.47 ± 3.31	3.59 ± 1.83	6.55 ± 3.33
A_T (μmol kg^{-1})	1,153 ± 485	1,391 ± 558	1,009 ± 367	931 ± 416
	1,364 ± 607	1,446 ± 615	1,300 ± 618	931 ± 444
C_T (μmol kg^{-1})	1,056 ± 426	1,225 ± 421	977 ± 300	857 ± 306
	1,234 ± 544	1,271 ± 467	1,202 ± 498	880 ± 375
pH (total scale)	8.09 ± 0.20	8.04 ± 0.36	7.79 ± 0.32	7.90 ± 0.55
	8.17 ± 0.22	8.05 ± 0.33	7.91 ± 0.27	8.03 ± 0.43
ΩCa	1.99 ± 1.38	2.99 ± 3.11	**0.96 ± 1.15**	1.76 ± 3.50
	2.64 ± 1.47	3.13 ± 3.35	1.87 ± 2.20	1.22 ± 1.95
ΩAr	1.22 ± 0.89	1.88 ± 2.01	**0.57 ± 0.70**	1.06 ± 2.13
	1.63 ± 0.94	1.98 ± 2.18	1.17 ± 1.42	**0.73 ± 1.17**
***p*CO_2 (μatm)**	275 ± 130	337 ± 203	504 ± 262	603 ± 392
	279 ± 182	328 ± 200	381 ± 133	460 ± 379
***p*CO_2 thermal (μatm)**	275 ± 15	341 ± 53	505 ± 41	605 ± 49
	279 ± 9	332 ± 50	383 ± 27	462 ± 38
***p*CO_2 nonthermal (μatm)**	277 ± 136	248 ± 232	492 ± 233	611 ± 400
	282 ± 188	346 ± 249	382 ± 132	478 ± 428
T:NT	0.11	0.20	0.19	0.14
	0.06	0.15	0.21	0.09

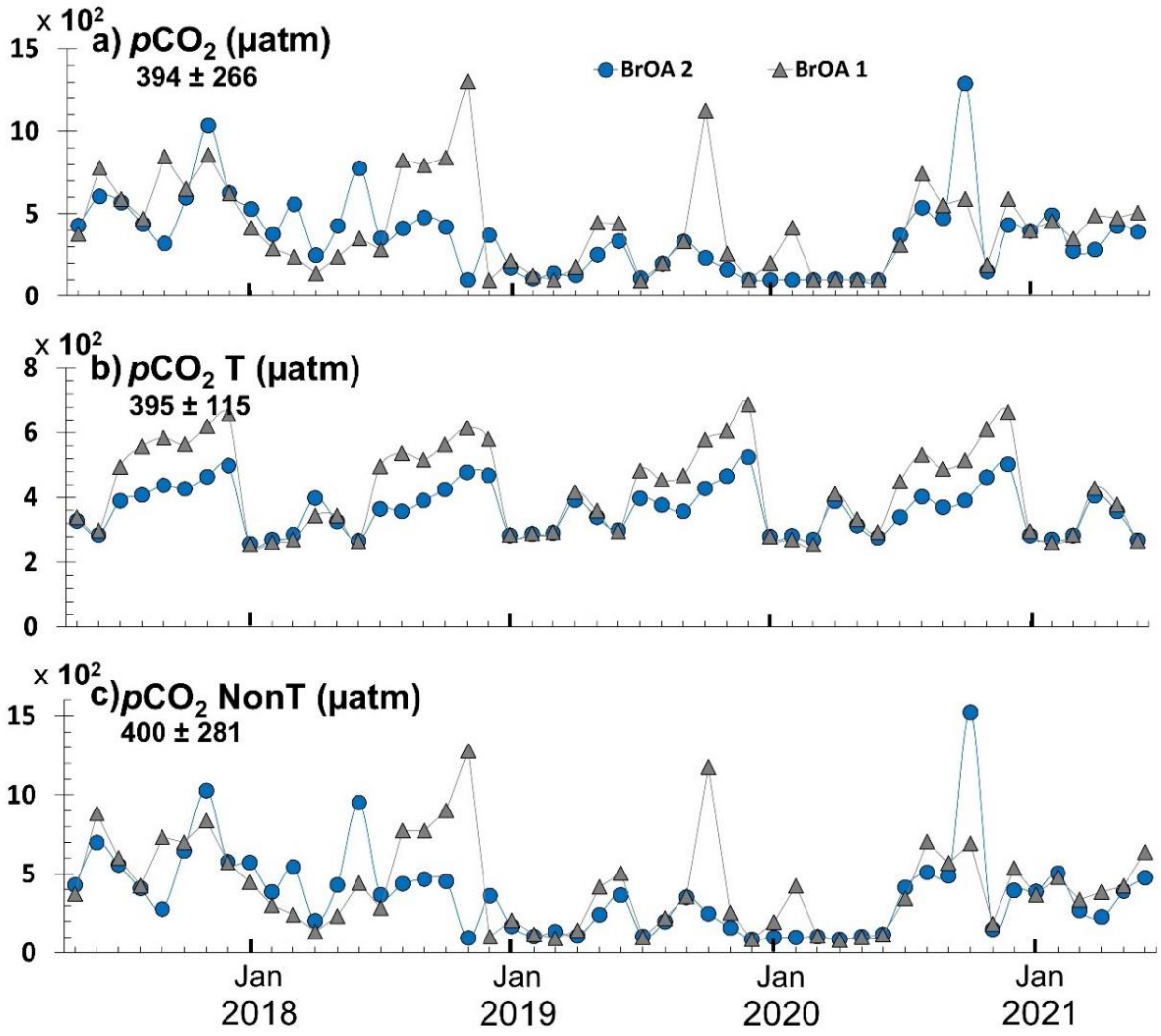

Figure 11. Monthly variability of surface water properties for the stations located in the BrOA #1 (gray line and dots) and BrOA #2 (blue line and dots) Patos Lagoon Estuary regions from May 2017 to June 2021. The annual average and standard deviation are indicated in the top left panels for water surface **(a)** partial pressure of CO_2 thermal (pCO_2 T; µatm), **(b)** partial pressure of CO_2 thermal (pCO_2 T; µatm) and **(c)** partial pressure of CO_2 nonthermal (pCO_2 NonT; µatm).

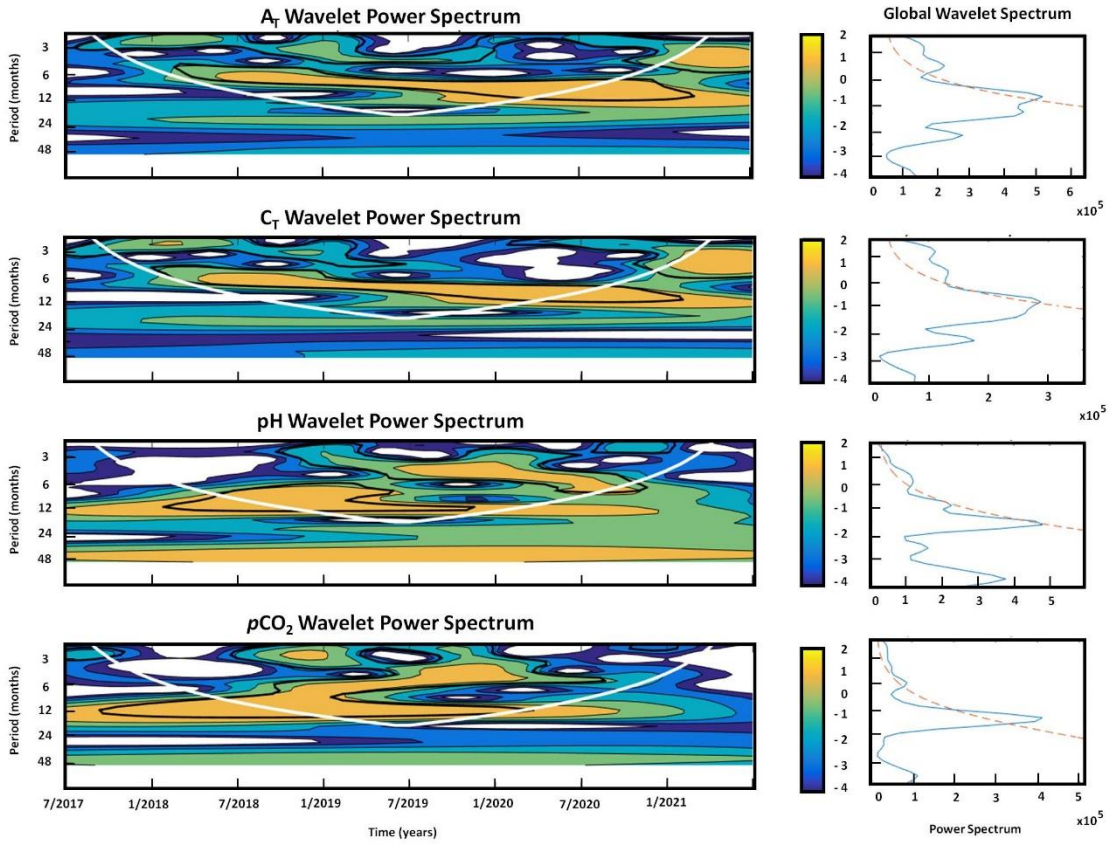

Figure 12. Global (right panels) and wavelet power spectra (left panels) of the **(a)** total alkalinity (A_T), **(b)** total dissolved inorganic carbon (C_T), **(c)** pH and **(d)** partial pressure of CO_2 (pCO_2) at BrOA #1 (pier-fixed station), considering the Morlet function as a mother wavelet. In the left panels, the area bounded by the white line indicates the region of the cone of influence, where the variance is reduced, and the solid black lines denote the regions with a significance level higher than 95%. The yellow colors represent high energy, and the blue colors indicate low energy. The color bar shows the units of energy in $\log_2$ form. In the right panels, the 95% level of significance is marked by the red dashed lines, while the sum of energy for each period is represented by the thin blue lines.

4.4.2 Drivers of the variability in carbonate system parameters

The processes of dilution and concentration of salts were identified as the dominant mechanisms responsible for changing the carbonate system parameters of the surface waters in the lower zone of the PLE (Fig. 13). The dilution process refers primarily to the freshwater input from rivers that reach the study area, while the salt concentration process refers to higher concentrations of salts in the system through saline intrusion that are not directly related to the

process of changing the state of the water (e.g., evaporation), although we cannot complete discard this combined influence. During periods of high seawater inflow in the estuary (marked by salinity values > 30), the surface concentration of salts prevailed (generally in autumn), whereas a dilution process was observed during periods of high freshwater discharge that were marked by salinity values < 20 (winter/spring; Fig. 13). Significant positive correlations were verified between salinity and both A_T and C_T in the studied area (Fig. 14a and 14b). As noted in Figure 6, the A_T and C_T concentrations deviated slightly from the theoretical mixing line of riverine and salty waters from the adjacent sea, thus implying that processes causing increasing C_T, such as CO_2 ingassing and organic matter respiration (Fig. 14c), also acted to change (although with less intensity) the behavior of the carbonate system in the waters of the PLE.

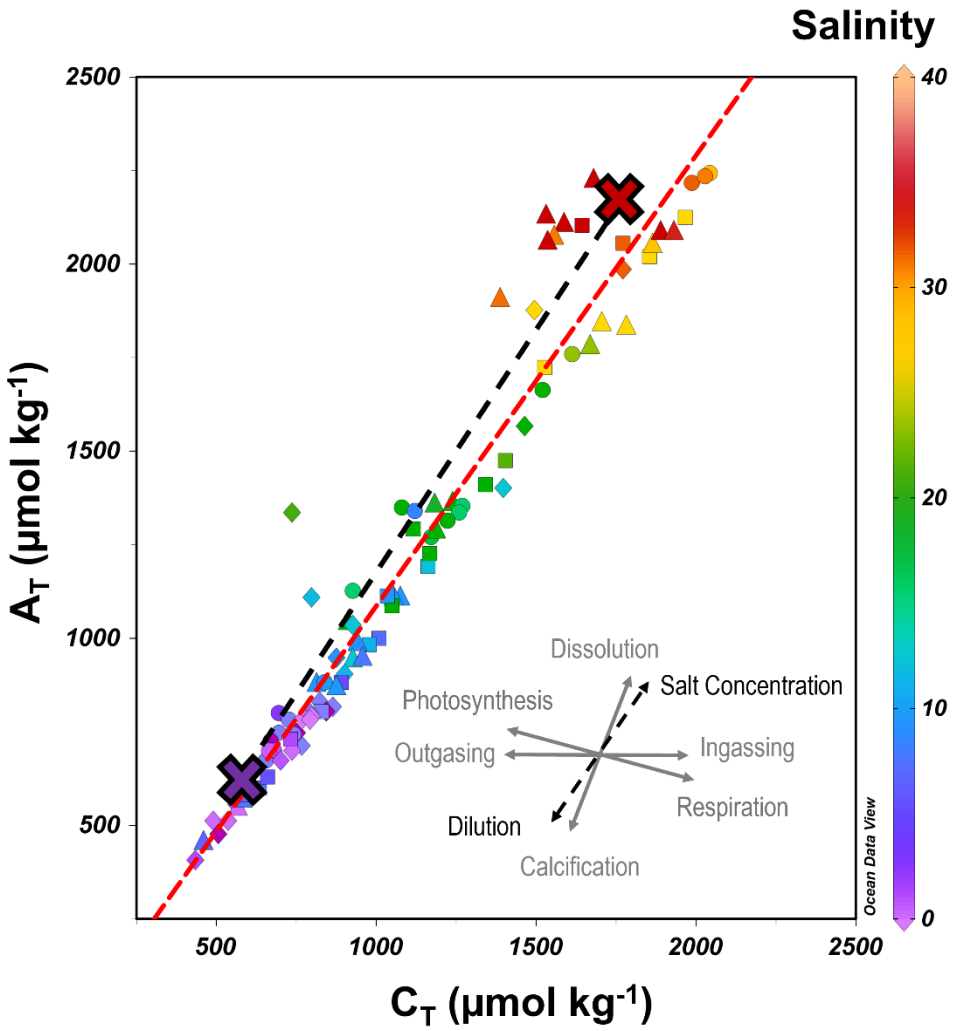

Figure 13. Total alkalinity (A_T; µmol kg^{-1}) and total dissolved inorganic carbon (C_T; µmol kg^{-1}) dispersion diagram. The A_T-C_T-salinity diagram considering the BrOA network dataset spanning between May 2017 and June 2021, with summer represented by dots, autumn by triangles, winter by squares and spring by diamonds. The inset arrows show the main processes (as indicated), adapted from Zeebe and Wolf Gladrow [2007], governing the variability in the carbonate system of the Patos Lagoon Estuary. The black dashed line depicts the theoretical conservative mixing line of riverine and ocean waters that indicate the effect of dilution and concentration of salt on changing the A_T-C_T concentrations. The purple and the red crosses represent the riverine and ocean waters endmembers. The red dashed line depicts the linear regression curve from the dataset.

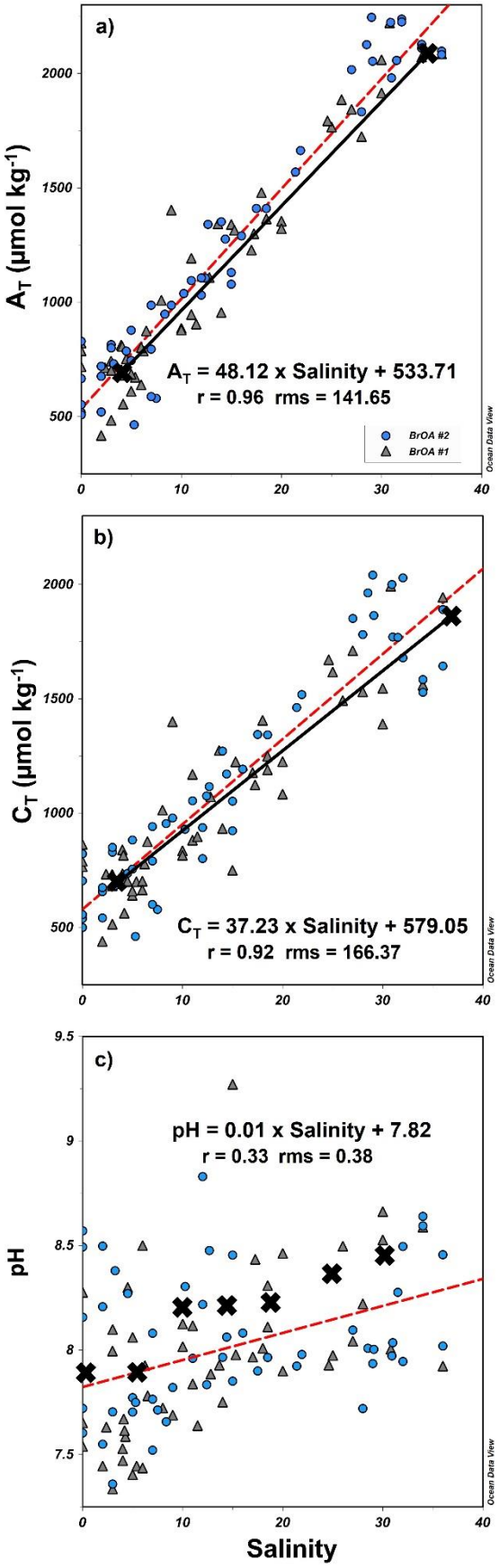

Figure 14. Total Plots of salinity versus **(a)** total alkalinity (A_T; µmol kg^{-1}), **(b)** total dissolved inorganic carbon (C_T; µmol kg^{-1}) and **(c)** pH at the total scale. The dataset considers the BrOA #1

(gray triangles) and BrOA #2 (blue dots) stations in the Patos Lagoon Estuary spanning from May 2017 to June 2021. The black crosses in (a) and (b) indicate the riverine and ocean endmembers and the black line represents the theoretical conservative mixing line. The black crosses in (c) indicate the averaged pH at each salinity range of 0-5, 6-10, 11-15, 16-20, 21-25, 26-30, and >31. The red dashed line represents the linear trend of the dataset.

4.5 Discussion

4.5.1 Comparison of the carbonate system parameters in the PLE with other environments around the world

The complex balance between freshwater outflows and seawater inflows leads to large variations in salinity, which significantly affect the physical and chemical properties of estuarine waters. Thus, the substantial variations in A_T and C_T concentrations observed in the lower zone of the PLE display a typical distribution pattern that has been observed in other estuarine environments around the world [e.g., Koné et al. 2009, Joesoef et al. 2017, Proum et al. 2018, Yao et al. 2020]. In fact, the A_T and C_T in the lower estuarine zone are variable over time and in subregions of the PLE, with monthly averages reaching maximum amplitudes of ~1,800 for the A_T and ~1,540 µmol kg^{-1} for the C_T in the lower estuarine zone (Fig. S2a and S2b). Furthermore, values of ~2,100 µmol kg^{-1} for the A_T and ~2,000 µmol kg^{-1} for the C_T were observed at the mouth of the PLE (i.e., BrOA #2). In addition, in shallow estuaries dominated by freshwater discharge, such as in the PLE, variations in the A_T from ~260 to ~1,600 µmol kg^{-1} (tropical lagoon systems) [Koné et al. 2009] and from ~600 to ~1,300 µmol kg^{-1} (temperate estuary) [Evans et al. 2013) have been reported. Moreover, a wide spatial range of C_T has been identified ($975 < C_T < 2{,}015$ µmol kg^{-1}) [Joesoef et al. 2017) in temperate estuaries dominated by the influence of tides and seawater intrusions. This result has also been observed for subtropical river-dominated

estuaries, where C_T values range from 450 µmol kg^{-1} to 2,100 µmol kg^{-1} [Jiang et al. 2008]. Conversely, estuaries with distinct hydrodynamics and lower variations in salinity (15.3 < salinity < 36.5) than those in the PLE have small ranges of A_T (2,418 < A_T < 3,054 µmol kg^{-1}), as identified in subtropical estuaries [Yao et al. 2020]. Hence, the range of both A_T and C_T in the PLE are consistent with the values recorded in estuaries worldwide with a high salinity amplitude. Thus, the ranges of the A_T and C_T found in the PLE (Fig. S2a and S2b) reflect the mixing of freshwater (low A_T and C_T values) and seawater (high A_T and C_T values) sources. The maximum observed values of A_T and C_T, which are comparatively higher than those in similar estuaries, are likely due to the presence of salty (> 36) Tropical Water and the composition of the shelf waters that intrude into the estuary [Möller et al. 2008, Carvalho-Borges et al. 2018].

The alkaline environment of the surface waters in the lower zone of the PLE is characterized by average pH values of 8.0 and supersaturated $CaCO_3$ conditions. However, ΩCa is only undersaturated during the high flood months, but ΩAr is more often undersaturated throughout the year (Fig. 9h). This sensitive property might be used to verify the relation between carbonate system parameters and estuary characteristics [Borges and Abril 2011]. Therefore, even the slightest variation observed in these parameters can be an indicator of a significant change in the state of the biogeochemical environment. Estuaries dominated by microtidal regimes, such as the PLE, were estimated to have pH values ranging from 5.8 to 8.3, as observed in the tropical estuarine system [Proum et al. 2018]. On the other hand, estuaries associated with hydrodynamics different from the PLE (e.g., ocean-dominated hydrodynamics), such as subtropical estuaries, have smaller pH amplitudes ranging from 8.0 to 8.3 [Yao

et al. 2020]. Although sampling was conducted with different periodicities, the values obtained in our region oscillate between 7 and 9.5 (Figure S2c). Therefore, similar to A_T and C_T, the pH values are associated with the mixing of freshwater discharge (low pH values) and inflowing seawater (high pH values). The minimum pH values observed here are likely due to the very high level of freshwater discharge [e.g., Möller et al. 2001].

The average pCO_2 observed for the surface waters of the PLE (380 µatm on average) has the same range as that in the shallow subtropical estuaries (~230 to ~1,500 µatm) [e.g., Yao et al. 2020]. Even compared to other estuaries worldwide, its maximum value of ~1,400 µatm is still lower than that of ~10,000 µatm observed in other regions [e.g., Borges et al. 2005, Borges et al. 2006, Jiang et al. 2008, Guo et al. 2009, Cai 2011, Jeffrey et al. 2018]. This can be likely associated with the swing behavior of the PLE between the ocean-dominated and riverine-dominated biogeochemical conditions that each prevail during half year. Hence, the geomorphological characteristics of this large, choked lagoon coupled with the strong influence of seawater, especially due to wind action that helps to modulate the periods of flooding in the estuary, play important roles in modulating the carbonate system dynamics of the PLE.

4.5.2 The seasonal variability in the carbonate system parameters

Most carbonate system parameters in the PLE exhibit a well-marked seasonal pattern (Fig. 9) influenced by temperature and freshwater discharges that modulate the thermal and nonthermal effects on the pCO_2 variations. The seasonal pattern of freshwater discharge into the lagoon is typical of middle

latitudes and is marked by a high level of discharge in winter and early spring followed by low to moderate levels of discharge during summer and autumn [Vaz et al. 2006]. The local hydrology influences the temporal variability in the carbonate system parameters in the PLE. This influence is mainly reflected in the distribution of salinity, which is characterized by the balance of the dominance of the waters from the main rivers and the adjacent ocean. The highest A_T values in summer and the lowest values in spring, as well as low pCO_2 in summer and the higher values observed between winter and spring, are also related to the hydrological pattern, suggesting two scenarios: the region swings between ocean-dominated estuarine biogeochemical conditions during the summer and autumn and riverine-dominated biogeochemical conditions during the winter and spring. The former behavior is marked by higher salinity, higher A_T and C_T concentrations, water that is more alkaline (higher pH), a lower water pCO_2 and higher $CaCO_3$ saturation than the periods of riverine-dominated functioning, when the opposing behaviors of the carbonate system parameters occur (Fig. 15).

Changes observed in the carbonate system parameters in different periods (Figs. 9, 10, 11 and S2) followed the increase/decrease in freshwater discharge in the PLE. Therefore, the shifts in freshwater discharge drive the quarterly and semiannual variability in carbonate system parameters. In fact, this pattern is also evidenced by the finding that dilution/concentration are the main processes controlling the surface carbonate system in the lower zone of the PLE (Fig. 13). The large amplitude and variation in A_T, which varies over seasonal and intraseasonal periods in the PLE, may be related to high mean freshwater discharge from the main rivers at both stations. Since A_T is a weighted sum of different dissolved constituents, the concentration increases and decreases

proportionally with salinity variations [Cossarini et al. 2015]. Freshwater discharge can alter A_T based on the dilution and evaporation balance [Fry et al. 2015], as we observed in the PLE, where the seawater inlet and outlet exert noticeable influence. Although freshwater discharge data were not available for the entire studied period, we associate the lowest salinity values with river water discharge and the highest values with seawater input. The freshwater discharge exerts a distinct influence on the different parts of the lower zones of the PLE, as reflected in the carbonate system. The waters at sheltered areas within the inner PLE (BrOA #1) present a slightly longer water residence time than those at the mouth of the lower estuary (BrOA #2) [Möller et al. 2001, Lisboa 2015], leading to lower variability in the carbonate system parameters.

The carbonate system parameter values in early spring are also attributed to the increased input of continental organic matter from higher freshwater discharge that can undergo decomposition. Environments with more organic matter also favor an increase in phytoplankton and drift macroalgae blooms that occur in this season, causing a change in the values of the parameters of the carbonate system at the end of the spring period [Haraguchi et al. 2015, Lanari and Copertino 2017, Lanari et al. 2018]. Furthermore, the productivity in the waters of the PLE also act to further increase the organic matter respiration, which lead to changes in the pH. This can be observed because the pH and salinity distribution show that, during the majority of the time, the pH measured are lower than those pH values at averaged-salinity, which indicate the prevalence of organic matter respiration process [e.g., Carstensen and Duarte 2019]. Despite the higher temperatures in the summer that decrease CO_2 solubility (thermal effect), the seawater input with higher A_T and lower C_T

increases the residence time in the PLE, which may favor the development of phytoplankton cells and consequently lead to lower pCO_2 values [Odebrecht et al. 2015]. Furthermore, shallow estuaries are also influenced by other nonthermal processes that alter the surface water biogeochemistry (e.g., redox reactions at the sediment-water interface) [Crosswell et al. 2020]. Additionally, the shallow areas of the inner PLE respond faster to wind action [Moller et al. 2001, Lanari and Copertino 2017], which may cause resuspension of bottom fine sediments and organic matter, therefore increasing pCO_2 directly compared to the lower deeper estuary. This process also reduces benthic and water column photosynthesis due to the decreased light caused by turbidity. However, photosynthesis plays an important role in changing the carbonate system parameters between spring and summer, mainly by decreasing the pCO_2 levels.

Although the dilution and concentration of salts are the predominant processes, biogeochemical processes related to biological activity also interfere with levels of carbonate system parameters [Lee et al. 2006] and photosynthetic carbon fixation causes a net reduction in C_T and pCO_2 in water, leading to increases in A_T, pH, ΩCa and ΩAr. These properties are mainly observed in the shallow and inner station in the estuary (BrOA #1). Photosynthesis is linked to the phytoplankton composition, which is mainly dominated by diatoms in the PLE [Haraguchi et al. 2015]. Additionally, phytoplankton growth is largely light limited and affected by the retention time of water in the PLE [Odebrecht et al.,2015]. The high nutrient concentration [Niencheski and Windom 1994, Niencheski et al. 2006] mainly favors the growth of diatoms, which comprise the dominant phytoplankton group (more than 50%), followed by cyanobacteria, flagellates, dinoflagellates, and chlorophytes along the coastal offshore gradient [Islabão et

al. 2017]. However, recent studies report increasing trends in the growth of dinoflagellates and cyanobacteria due to shifts in salinity [e.g., Haraguchi et al. 2015, Islabão et al. 2017]. Furthermore, microphytoplanktonic diatoms tend to show a higher capacity for capturing CO_2 in water [e.g., Hopkinson et al. 2011] than nano and picophytoplanktonic species, which helps to balance the acidity and carbon concentration. Although diatoms are the dominant phytoplankton group in the PLE, the phytoplankton community composition varies seasonally and interannually [Haraguchi et al. 2015]. Further studies examining how the phytoplankton community composition alters the pCO_2 distribution in the surface waters of the PLE are being evaluated.

The high amplitude of C_T and its seasonal variations in the PLE may be related to the high concentration of organic matter [Borges and Abril 2011, Yao et al. 2020], which increases the carbon levels in the water. The surface waters of the lower PLE have high organic matter concentrations due to large continental inputs, abundant macrophyte communities and local anthropogenic sources [Baumgarten and Niencheski 2010]. C_T is strongly influenced by several estuarine processes since carbon is involved in several organic and inorganic processes, such as biological productivity, the oxidation/degradation of organic carbon and the dissolution and precipitation of calcite, in addition to CO_2 exchange with the atmosphere [Cai 2011, Samanta et al. 2015]. The carbon inputs and corresponding reactions contribute to the widespread supersaturation of CO_2, decreases in pH, ΩCa and ΩAr, an increase in pCO_2 levels (Fig. S2c) and prominent heterotrophy [e.g., Feely et al. 2009, Borges and Abril 2011, Cloern et al. 2014]. Therefore, the carbonate system variations at the mouth of the system are mainly driven by the balance between the input and output of freshwater,

which is mainly related to heterotrophic respiration and degradation of organic matter. This result was confirmed by the nonthermal effects prevailing throughout the year and becoming more accentuated during winter (BrOA#1) and early spring (BrOA#2). Finally, the surface water is supersaturated in $CaCO_3$ when a lower concentration of allochthonous organic matter is observed. However, low saturation states in relation to aragonite and calcite were observed in winter and spring, probably due to the freshwater dilution effect. These changes may exert some direct effects on organisms and environmental health, generally hampering calcification processes [Heinze et al. 2021].

In summary, the interaction between the thermal and nonthermal effects on pCO_2 was evidenced by T:NT<1 throughout the year. During summer and autumn, seawater inflow contributed to the prevalence of nonthermal factors, including vertical mixing, biological processes, and air–sea CO_2 exchange, influencing the C_T, which is directly related to pCO_2. During winter and spring, the high level of freshwater discharge contributed to deep mixing that causes pCO_2 to increase due to the upwelling of high-C_T waters and biological processes. Even with the biological C_T drawdown during spring, the pCO_2 was still higher than during summer and autumn. In general, these thermal and nonthermal effects on pCO_2 constantly overlap, hampering the interpretation of their individual effects on pCO_2 variations.

4.6 Concluding remarks

This study is the first to show the seasonal variability in the carbonate

chemistry of the surface waters of the lower PLE and how the interaction between well-known hydrological patterns affects the biogeochemical parameters. The dilution and concentration of salt processes drive variability in carbonate system parameters of the lower surface waters of the lower estuarine zone due to their contributions to nonthermal effects on estuarine waters. The seasonal cycle of the carbonate system parameters reflects the seawater dominance during summer and autumn, and the riverine dominance between winter and spring. Overall, the studied region is, on average, a naturally alkaline environment with saturated $CaCO_3$ conditions throughout the period analyzed. However, potential risks of undersaturation cannot be excluded, notably during riverine-dominated periods. The low pCO_2 (~394 μatm, on average) and the high pH values observed in the PLE reveal that this environment likely acts as a CO_2 ingassing region. However, when determining the magnitude of this process, the net water-air CO_2 exchange and the processes that drive pCO_2 in coastal environments are still a challenge to constrain. Additionally, ENSO events have a high influence on the interannual variability in the PLE [e.g., Odebrecht et al. 2017] and longer time series of the carbonate system properties in the region should be further evaluated (mainly the water pCO_2 that oscillates interannually). This analysis is relevant because the period analyzed here was generally characterized by neutral ENSO events, except the period of La Niña conditions between October 2020 and March 2021. Importantly, the lower estuarine zone of the PLE swings between biogeochemical conditions more related to riverine characteristics (winter and spring) for half the year and ocean characteristics that prevail during the other half (summer and autumn). Thus, any changes in the freshwater inflow in the PLE might completely alter the seasonal behavior of the CO_2-carbonate

system, which would affect the ecosystem services in the region. Notably, the natural and anthropogenic effects on the carbonate system parameters over time must be decoupled to overcome the limitation of determining the CO_2 fluxes in estuarine waters [e.g., Cai 2011; Yao and Hu 2017]. Thus, monitoring programs must continue to improve our understanding of carbonate system variability at low frequencies in the PLE. Despite the great impacts of human activity, the PLE seems to resist major changes in the carbonate system. This resiliency is an important feature and can help us to understand similar estuaries that are heavily influenced by human activity.

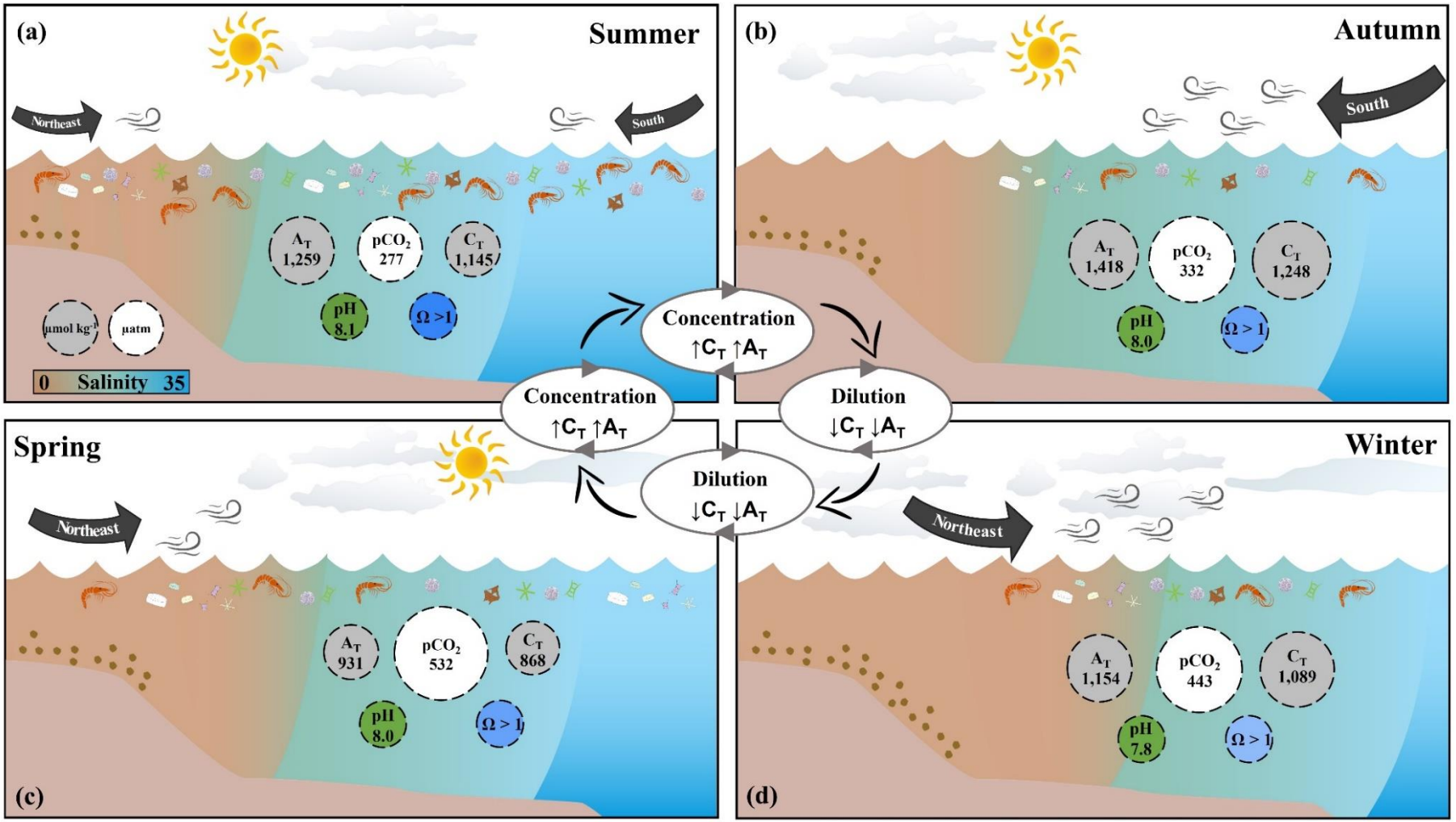

Figure 15. Summary of the main physical and biogeochemical processes controlling and changing the distribution of carbonate system parameters in the Patos Lagoon Estuary surface waters during **(a)** summer, **(b)** autumn, **(c)** spring, and **(d)** winter. The dominant biogeochemical processes between the seasons are

indicated by the ellipses in the center. The color shading from brown to blue represents the change from freshwater to seawater dominance. The basic pH condition is labeled in green, while acidic conditions are presented in yellow. The blue color of the carbonate calcium saturation state (Ω) indicates supersaturation (Ω > 1). The dominant winds of each station are represented by arrows. The average values of each carbonate system parameter (total alkalinity - A_T, total dissolved inorganic carbon - C_T, pH, and partial pressure of CO_2 - pCO_2) are represented for each season, as indicated by the values in the circle and the units in (a).

Capítulo V: Fluxos líquidos de CO_2 no Estuário da Lagoa dos Patos

O segundo manuscrito investiga os fluxos líquidos de CO_2 na parte sul do ELP no período de maio de 2017 a junho de 2021. Nesse contexto, este trabalho fornece a variabilidade sazonal dos fluxos de CO_2 e as principais fontes de carbono na região de estudo. De autoria de Cíntia Albuquerque, Rodrigo Kerr, Thiago Monteiro, Eunice da Costa Machado, Andréa da Consolação de Oliveira Carvalho e Carlos Rafael Borges Mendes, intitulado "***Water-air exchanges in the lower estuary of the Patos Lagoon: seasonal variability, drivers, and sources of CO_2***", foi submetido no periódico *"**Biogeochemistry**"* em fevereiro de 2022 e encontra-se em revisão. Cada autor teve uma participação importante na confecção desse manuscrito. A análise dos dados e as principais interpretações deste estudo foi feita por mim, como parte da minha tese de doutorado. Rodrigo Kerr liderou as atividades da rede BrOA na Lagoa dos Patos, propôs o estudo e fez a supervisão da condução do planejamento, da coleta e análise dos dados. Thiago Monteiro, Eunice Machado. e Andréa Carvalho

contribuíram como especialistas em sistemas carbonato e biogeoquímica de estuários. Carlos Rafael Mendes contribuiu como especialista em ecologia do fitoplâncton. Todos os autores contribuíram para a interpretação dos resultados e da redação final do manuscrito submetido ao periódico.

Abstract

We investigated the primary drivers of changes in the partial pressure of carbon dioxide (pCO_2) together with the seasonal and interannual variability in the water-air net carbon dioxide flux (FCO_2) in the lower estuarine zone surface waters of Patos Lagoon, the largest choked lagoon worldwide. Sampling occurred monthly during May 2017-June 2021 at the estuary's inner inlet and mouth, which are contrasting hydrodynamic zones in the Patos Lagoon Estuary (PLE). The water pCO_2 was mainly controlled by seasonal changes in total alkalinity and total dissolved inorganic carbon. The lower zone experienced periods of CO_2 ingassing (austral summer/autumn) and CO_2 outgassing (austral winter/spring). During summer/autumn, both protected and sea-exposed areas uptake an average of –15 mmol m^{-2} d^{-1} CO_2, whereas during winter/spring, CO_2 emissions prevail, reaching an average of 22 mmol m^{-2} d^{-1} at the inner estuary. Additionally, while much of the CO_2 absorbed in summer/autumn is released to the atmosphere in the inner estuarine zone, the summer/autumn CO_2 uptake in the estuary mouth is 4-fold higher than the winter/spring CO_2 released. Unlike most estuarine systems, the PLE acted as a net CO_2 sink of –2 mmol m^{-2} d^{-1} during the period investigated. The balance between CO_2 uptake and emissions in the PLE was modulated by the combination of wind speed, freshwater discharge, water temperature, and outflow/inflow currents. Furthermore, phytoplankton

blooms and strong wind-induced vertical mixing lead to highly variable CO_2 exchanges. The highest estuarine CO_2 concentration by autochthonous production indicates heterotrophy in estuarine waters. Part of this carbon produced in the estuary is exported to the coast, as evidenced by the high CO_2 concentration in the estuary mouth. Therefore, the lower estuarine zone resists increased CO_2 concentrations and has overcome regional anthropogenic emissions. The regional FCO_2 range and complex PLE biogeochemistry dynamics need ongoing investigation to improve knowledge of regional CO_2 exchanges and elucidate the role of large estuaries and coastal bays in the global carbon budget.

5.1 Introduction

Estuaries are known to be large sources of carbon dioxide (CO_2) to the atmosphere [e.g., Cai 2011, Bauer et al. 2013, Evans et al. 2013, Dinauer and Mucci 2017, Yao & Hu 2017, Yao et al. 2020], with the surface water partial pressure of CO_2 (pCO_2) ranging from 350 to 10,000 µatm and the water-air CO_2 net flux (FCO_2) ranging from –5 to 80 mol C m^{-2} $year^{-1}$ [Cai 2011]. This CO_2 outgassing behavior is attributed to intense carbon fixation and respiration in estuarine waters, owing to the higher primary production and leading to high rates of organic matter decomposition. The high amounts and fast cycling of autochthone and allochthone inputs of organic matter are degraded by microbial action, which causes supersaturation of CO_2 in estuarine surface waters [Sunda and Cai 2012]. The carbon inputs and their reactions support prominent heterotrophy and contribute to the widespread supersaturation of CO_2, decreasing pH [e.g., Feely et al. 2010, Borges and Abril 2011, Cloern et al. 2014]. The changes in estuarine pCO_2 regulate the water-air CO_2 gradients that

determine the direction of CO_2 exchanges [Sarma et al. 2001]. In addition, estuaries are commonly neglected in global FCO_2 inventories, and estuarine processes are not factored into the global carbon budget [e.g., Cotovicz et al. 2020]. Furthermore, estuaries are highly productive regions where natural biogeochemical reaction rates are elevated; thus, understanding CO_2 dynamics in these environments is essential [Sarma et al. 2001].

Patos Lagoon (Fig. 16) is the largest choked lagoon in the world [Kjerfve 1986], and it is connected to the sea by a narrow channel [Castelão and Möller 2003, Marques and Möller 2008, Marques et al. 2009] in extreme southern Brazil (~32°S). The hydrodynamics of the Patos Lagoon Estuary (PLE) are dominated by wind at time scales associated with the passage of frontal systems and the strength of freshwater discharge in the microtidal region [Möller et al. 2001]. The seawater intrusions are greater during the autumn due to the more frequent passage of frontal systems. In this case, southerly winds combined with low freshwater input allow flooding and salinization of the water. Northeastern winds occur at the end of winter and during spring, with periods of high freshwater discharge that favor ebb flow. The north and south quadrant winds form vertical salinity structures that can range from a salt wedge to a well-mixed gradient [Möller et al. 2001, Möller and Fernandes 2010]. The complex balance between freshwater outflow and oceanic inflow leads to large variations in salinity, which significantly affects physical [e.g., Möller et al. 2001], chemical [e.g., Niencheski et al. 2006, Albuquerque et al. under review] and biological properties [e.g., Haraguchi et al. 2015]. Although the PLE is a well-studied environment in terms of estuarine hydrodynamics [e.g., Möller et al. 2001, Möller and Fernandes 2010], biology and physiology of dominant estuarine species, and ecosystem ecology [e.g., Haraguchi et al. 2015, Abreu and Odebrecht 2016, Mendes et al. 2016,

Islabão et al. 2017, Odebrecht et al. 2017], very little is known about estuarine carbon biogeochemistry [Albuquerque et al. under review]. Recently, the first assessment of the estuarine carbonate system in the region indicated that the surface waters in the lower zone of the PLE have natural alkaline conditions, with an average pCO_2 of ~380 μatm and a supersaturated calcium carbonate environment with respect to both calcite and aragonite [Albuquerque et al. under review]. Additionally, the predominant estuarine processes governing changes in the carbonate system in the region were dilution and concentration of salts due to freshwater input and seawater intrusions, respectively. Notwithstanding its socioeconomic and environmental significance [Odebrecht et al. 2017], only a few studies have assessed the chemical changes in estuarine waters in this complex environment [e.g., Niencheski et al. 2006, Baumgarten and Niencheski 2010, Wallner-Kersanach et al. 2016].

Studies on water-air CO_2 exchanges in estuarine regions are mostly located along the European, Asian, Indian, and eastern North American coasts [e.g., Bauer et al. 2013, Evans et al. 2013], while knowledge of CO_2 coastal dynamics in the Southern Hemisphere remains limited. Few studies have addressed the water-air CO_2 exchange systems that border the Brazilian coast [e.g., Noriega et al. 2013, Noriega and Araujo 2014, Cotovicz et al. 2015, Cotovicz et al. 2020, Abril et al. 2021], where highly diversified environments in terms of CO_2 saturation with the atmosphere were found. As a larger body of water in the Southern Hemisphere, a better understanding of the regional behavior of the CO_2 fluxes in the PLE is mandatory for its inclusion in a global CO_2 analysis. Therefore, in this study, we present the first overview of the behavior of the water-air CO_2 exchanges in the lower estuarine zone of the Patos Lagoon (Fig. 16) by investigating the pCO_2 drivers, sources of CO_2 in the region,

and the temporal variability in the water-air CO_2 fluxes in this environment. This assessment of the intrinsic variability in the CO_2 system in the PLE represents the first step toward understanding both anthropogenic and climatic impacts that may affect the carbon dynamics in the region.

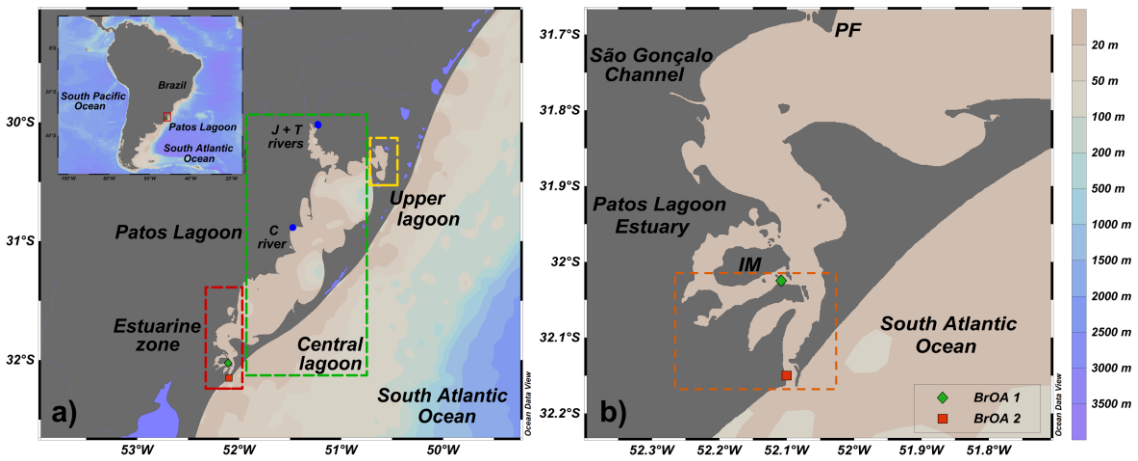

Figure 16. Map of the study region: Patos Lagoon. **(a)** Location of Patos Lagoon and geomorphological divisions for the estuarine zone (red rectangle), central lagoon (green rectangle) and upper lagoon (yellow rectangle). The inset in (a) shows a South American map with the location of Patos Lagoon (red rectangle). Blue dots indicate the regions of freshwater discharge from the Jacuí and Taquari (J + T) and Camaquã (C) Rivers. **(b)** Location of the pier-fixed monitoring BrOA #1 (green diamond) and #2 (red square) stations in the Patos Lagoon Estuary with the southern region highlighted (orange rectangle). Marinheiros Island (IM) and Ponta da Feitoria (PF) are indicated.

5.2 Data and Methods

5.2.1 Database from the Brazilian monitoring programs

The databases of the Brazilian Long-Term Ecological Research (BR-LTER) [Odebrecht and Abreu 2019, Lemos et al. 2021] (dataset available at https://doi.org/10.15468/xmlvxm) and the Brazilian Ocean Acidification Network (BrOA Network) [Kerr et al. 2016] (dataset available by request at https://carbonteam.furg.br/2-uncategorised/47-monitoramento) were compiled for the study of a four-year monthly time series (May 2017-June 2021) in two zones of the PLE. The pier-fixed station BrOA #1 is in the inner mesomixohaline region, while BrOA #2 is in a more exposed area of the lower euhaline region.

The stations are marked by differences in water salinity and hydrodynamics. The physical, biological, and chemical parameters were sampled by BR-LTER and included surface water (~1 m) temperature, salinity, chlorophyll-a (Chl-*a*) and dissolved nutrients (i.e., nitrate, nitrite, silicic acid, and phosphate). The surface water (~1 m) total alkalinity (A_T), total dissolved inorganic carbon (C_T) and pH were sampled by the BrOA Network monitoring program. For more details about the datasets and sampling methodology, the reader is referred to Albuquerque et al. [under review] and Lemos et al. [2021].

5.2.2 Sampling and determination of physical, chemical, and biogeochemical properties

Surface water temperature and salinity were measured *in situ* by a digital thermometer (± 1°C) and portable refractometer (± 1), respectively. The water sample was collected, and the salinity was further verified in the laboratory by a conductivity meter. Water for A_T analysis was sampled in 500 mL borosilicate glass bottles and fixed with 100 µL of a supersaturated mercury chloride solution to prevent biological activity, following the procedure described by Dickson et al. [2007]. The samples were refrigerated to prevent evaporation, and A_T was measured by potentiometric titration in a closed cell [Dickson et al. 2007] with an automated titrator (Metrohm® Titrando 808) and a combined glass-reference electrode (Metrohm® 6.0262.100) at a controlled temperature of 25 ± 0.1°C sustained by a thermostatic bath (Tamson® TLC 15). The analytical precision of the A_T analyses was ± 4.0 µmol kg^{-1} (ranging from 2.3 < A_T < 5.0 µmol kg^{-1} considering the analyzed sample batches). Water for pH analysis was sampled in 125 mL borosilicate amber flasks, and the pH was potentiometrically

determined before two hours after sampling. We used a Metrohm® 913 or 914 pH meter coupled with a glass-reference electrode cell and a temperature sensor. The uncertainty for pH was ≤ 0.05 pH NBS units. The total scale was chosen and further used for pH at *in situ* temperature.

The pCO_2 and other CO_2-carbonate variables not directly measured were estimated through the software CO_2Sys v.2.1 developed by Lewis et al. [1998] and modified by Pierrot et al. [2006]. Surface water temperature, salinity, A_T, pH, silicic acid, and phosphate concentrations were used as input parameters. Since the study was performed in an estuarine environment with a broad salinity range, we applied the following set of constants: the K_1 and K_2 dissociation constants of Millero et al. [2006], such as those used in PLE [Albuquerque et al. under review] and other estuary and coastal environments [Liu et al. 2017, Carstensen et al. 2018, Chen et al. 2020); and the sulfate and borate constants of Dickson [1990] and Uppström [1974], respectively. The pCO_2 uncertainty was determined to be ±46 µatm according to Orr et al. [2018]. A more detailed description of the sampling procedure and laboratory analysis of A_T and pH and reconstruction of pCO_2 is fully described in Albuquerque et al. [under review].

5.2.3 Drivers of partial pressure of CO_2 (pCO_2)

The pCO_2 drivers were calculated based on the seasonal differences in parameters and their corresponding partial derivatives. The differences in pCO_2 were separated into contributions representing the roles of differences in temperature (Temp), salinity (Sal), A_T, and C_T. The relative contributions of the drivers changing pCO_2 (i.e., ΔpCO_2^{drv}) were assessed by converting their relative changes into pCO_2 units (µatm) following Lenton et al. [2012] and Eq. 32:

$$\Delta pCO_2^{drv} = (\partial pCO_2/\partial Temp)\ \Delta Temp + (\partial pCO_2/\partial Sal)\ \Delta Sal + (\partial pCO_2/\partial A_T)\ \Delta A_T + (\partial pCO_2/\partial C_T)\ \Delta C_T \quad (32)$$

where ΔTemp, ΔSal, ΔA_T and ΔC_T are the respective differences in the water surface property averages between each season and the previous season in the lower zone of the PLE, considering the sampling period from May 2017 to June 2021. The partial derivatives (δ) were calculated using Eqs. 33-35 [see details in Sarmiento and Gruber 2006], and the term involving temperature was calculated using Eq.36 [Takahashi et al. 2014]:

$$\partial pCO_2/\partial C_T = (pCO_2/\partial C_T)\ \text{Fator Revelle} \quad (33)$$

$$\partial pCO_2/\partial A_T = (pCO_2/\partial A_T)\ \text{Fator de Alcalinidade} \quad (34)$$

$$\partial pCO_2/\partial Sal \approx (pCO_2/\partial Sal) \quad (35)$$

$$\partial pCO_2/\partial Temp\ \Delta Temp \approx 2pCO_2\ \{Exp\ [0.0423\ (\Delta Temp/2)] - 1\} \quad (36)$$

where the Revelle and Alkalinity factors are 14.2 and –26.5, respectively.

5.2.4 Water-air CO_2 net flux

The water-air FCO_2 were obtained by Eq. 37:

$$FCO_2 = K_t\ K_s\ (\Delta pCO_2) \quad (37)$$

where K_t is the coefficient for CO_2 transfer velocity as a function of wind speed (U), K_s is the solubility coefficient of CO_2 calculated as a function of both temperature and salinity [Weiss 1974], and ΔpCO_2 is the difference between surface water pCO_2 and atmospheric pCO_2 (pCO_2^{air}). CO_2 is taken up by estuarine water when the FCO_2 value is negative (ingassing), while it is released to the atmosphere when the FCO_2 value is positive (outgassing).

The pCO_2^{air} was calculated following Eq. 38:

$$pCO_2^{atm} = xCO_2^{ar} [pAr - (1.5/101.325) - pH_2O) \quad (38)$$

where xCO_2^{air} (ppm) is the mole fraction of atmospheric CO_2 in dry air, obtained from the Mauna Loa Observatory (NOAA ESRL Global Monitoring Laboratory, 2019) [Thoning et al. 2021], with data 6 months before the corresponding period due to the atmospheric response between the Northern and Southern Hemispheres [Millero 2013]. pAir is the barometric pressure from the Rio Grande city (Brazil) meteorologic station, and pH_2O (atm) is the water vapor pressure calculated using salinity and temperature [Weiss and Price 1980].

The main challenge in calculating FCO_2 in estuarine waters is the determination of K_t due to its complex hydrodynamics and varied geomorphology [e.g., Dinauer and Mucci 2017, Yao et al. 2020]. Several different predictive relationships between wind speed and gas transfer velocity of CO_2 have been proposed based on laboratory and field studies [e.g., Jiang et al. 2008, Raymond and Cole 2001, Takahashi et al. 2009]. Here, the gas transfer velocity K_t was parameterized using wind speed and the equation from Jiang et al. [2008], which was derived from Raymond and Cole [2001]. The parametrization of Jiang et al.

[2008] is mostly used in estuarine environments [e.g., Evans et al. 2013, Van Dam et al. 2018, Yao et al. 2020]. The following equation is the K_t equation (Eq. 39) of Jiang et al. [2008]:

$$K_t = [(0{,}314\ U_{10}^2) - (0{,}436\ U_{10} + 3{,}99)]\ (Sc/600)^{-0{,}5} \quad (39)$$

where U is the wind speed at 10 m height and Sc is the Schmidt number of CO_2 at *in situ* temperature [Wanninkhof 2014]. Average monthly wind speed data were available from the 8th Meteorology District of the National Institute of Meteorology (8th DISME/INMET) for Rio Grande do Sul State.

The average standard error of the calculated FCO_2 was ± 0.34 mmol m^{-2} d^{-1}. We recalculated K_t from the equation of Raymond and Cole [2001] to verify the sensitivity of FCO_2 based on the equations used. The average differences between the estimations derived from the original application used Jiang et al. [2008] and the Raymond and Cole [2001] approach were –0.3 ± 0.8 mmol m^{-2} d^{-1}.

5.2.5 CO_2 estuarine concentration estimates

We followed the approach described in Jiang et al. [2008] to determine the C_T change caused by river–ocean mixing, using C_{Tmr} (Eq. 40) to estimate the riverine water input and C_{Tmix} (Eq. 41) to estimate ocean mixing at each pier-fixed station (i):

$$C_{Tmr} = (S_i/S_{oc})\, C_{Toc} + [(1 - S_i)/S_{oc}]\, C_{Tr} \quad (40)$$

$$C_{Tmix} = [(S_{oc} - S_i)\, C_{Tr} + (S_i - S_r)\, C_{Toc}]/S_{oc} - S_r \quad (41)$$

where C_{Tr}, S_r, C_{Toc} and S_{oc} are the C_T and salinity river and ocean end-members, respectively, and S_i is the salinity at station *i*.

As there was no continuous sampling during the study period at the mouth of the river or at a fixed point in the ocean, the average values of C_{Tr}, S_r, C_{Toc} and S_{oc} representing the river and ocean most pure conditions were determined from the station closest to the river outlet (BrOA #1; salinity < 5) and from the nearest ocean station (BrOA #2; salinity < 32), respectively. Thus, the C_T and salinity river and ocean end-members were S_r = 2.57, C_{Tr} = 703.37 μmol kg^{-1}, S_{oc} = 31.36, and C_{Toc} = 1648.38 μmol kg^{-1}.

When there is no river influence, the C_T at station *i* can be calculated as follows:

$$C_{Tmo} = (S_i/S_{oc})\, C_{Toc} \quad (42)$$

where C_{Tmo} is C_T due to water mixing; C_{Toc} and S_{oc} are C_T and salinity at the ocean end-member, respectively; and S_i is the salinity at station *i*.

Then, produced/consumed C_T due to estuarine-biogeochemical processes (C_T^{est}) can be calculated as follows:

$$C_T^{est} = C_{Ti} - C_{Tm} \quad (43)$$

where C_{Ti} is C_T at station *i* and C_{Tm} is C_T due the mixing of river and ocean and can be calculated from Eqs. 40-42. Following the same approach, A_{Tm} and A_T^{est} can be estimated by simply replacing C_T with A_T. For A_T end-members, averages were also defined. A_{Tr} and A_{Toc} were 699.47 and 2087.04 μmol kg^{-1}, respectively.

Finally, the CO_2 estuarine concentration was calculated through the software CO_2Sys v.2.1 [Lewis et al. 1998, Pierrot et al. 2006] using C_T, A_T, salinity, and temperature as input parameters. We used $[CO_2]_{ocean}$, $[CO_2]_{river}$, and $[CO_2]_{est}$ to represent ocean-borne $[CO_2]$, river-borne $[CO_2]$, and estuarine-produced $[CO_2]$, respectively. Aqueous CO_2 ($[CO_2]$) does not mix conservatively, so $[CO_2]_{ocean}$ is the aqueous CO_2 concentration of the ocean end-member if these were diluted by freshwater with zero C_T, calculated by C_{Tmo} and A_{Tmo} (Eq. 43). $[CO_2]_{river}$ is the difference between $[CO_2]$ due to mixing and $[CO_2]_{ocean}$ [Jiang et al. 2008].

$$[CO_2]_{river} = [CO_2]_m - [CO_2]_{ocean} \quad (44)$$

$$[CO_2]_{est} = [CO_2]_i - [CO_2]_m \quad (45)$$

where $[CO_2]_m$ is $[CO_2]$ if conservative mixing occurred between river and ocean end-members, calculated using C_{Tmr} or C_{Tmix} and A_{Tmr} or A_{Tmix}; $[CO_2]_{ocean}$ is the aqueous CO_2 concentration of the ocean; and $[CO_2]_i$ is the aqueous CO_2 concentration at station *i*. The $[CO_2]$ is consumed when the $[CO_2]$ value is

negative, while the [CO_2] is produced in the estuary once the [CO_2] value is positive. When [CO_2] is calculated from C_T and A_T, the annual average temperature of 21.03°C was used since the dissolved [CO_2] is subject to changes in water temperature.

5.3 Results

5.3.1 Drivers on seasonal changes in the partial pressure of CO_2

A_T and C_T had the dominant effect on changes in pCO_2, while salinity and temperature had a minor influence on surface pCO_2 (Fig. 17). In summer, there was a considerable decrease in pCO_2, driven mainly by an increase in A_T. In autumn, winter and spring, there was an increase in pCO_2; however, its driver was different in each season. The increase in pCO_2 was partially counteracted by the temperature drawdown in autumn. In winter and spring, C_T and A_T had opposite effects on pCO_2 compared with summer and autumn. In winter, the decrease in A_T led to an increase in pCO_2. On the other hand, although C_T decreased considerably, pCO_2 increased in spring.

5.3.2 Seasonal and interannual variability in water-air CO_2 net flux

The seasonal cycle of water-air CO_2 net fluxes showed a similar variability pattern in the areas investigated but with different amplitudes at stations BrOA #1 and #2 (Fig. 17a and 17b). At the inner inlet station (BrOA #1), the seasonal amplitude of CO_2 exchanges varied from –38 to 54 mmol m^{-2} d^{-1} and was higher than that found at the mouth of the estuary (BrOA #2), which ranged from –29 to 21 mmol m^{-2} d^{-1}. In addition, although the net CO_2 ingassing during

summer/autumn seasons are very close to each other in both areas (average of ~ –16 ± 23 and ~ –18 ± 28 mmol m^{-2} d^{-1}), the same is not true for the behavior of the CO_2 exchange during winter/spring seasons. The winter/spring net CO_2 outgassing is 10-fold higher in the inner inlet zone (average of 22 ± 40 mmol m^{-2} d^{-1}) than that found near the more sea-exposed zone (average of 2 ± 31 mmol m^{-2} d^{-1}). In general, the net CO_2 outgassing was highest in spring (October and November) at the BrOA #1 station, although this behavior was also observed during winter. The lower estuarine zone of the Patos Lagoon acts as net CO_2 ingassing during half the year, from December to May, while a behavior of water-air CO_2 quasi-equilibrium is observed from June to September in the mouth of the estuary (Fig. 17a and 17b).

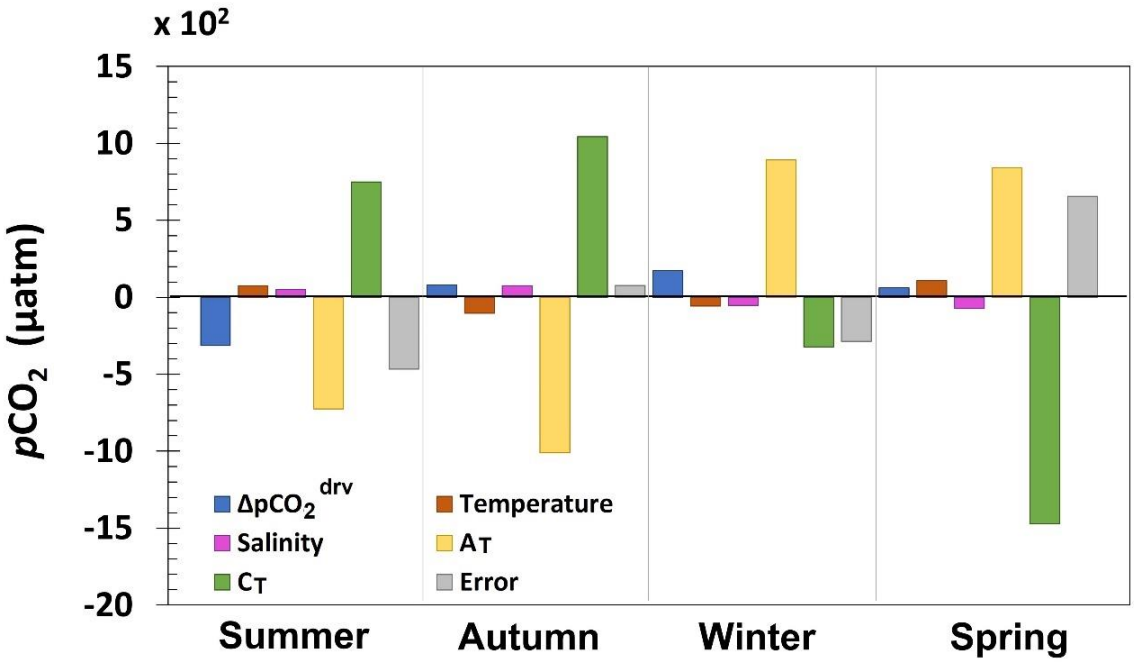

Figure 17. Effects of surface water temperature, salinity, total alkalinity (A_T) and total dissolved inorganic carbon (C_T) on the partial pressure of CO_2 (pCO_2) for each season for the stations located in the lower zone of the Patos Lagoon Estuary region. The variation in each parameter is calculated as the difference between the values of each parameter and their respective averages in previous seasons. The unit of all drivers is the same as that for pCO_2 (µatm), and their magnitudes represent their influence on pCO_2^{sw} changes. The error bars (gray) show the difference between the sum of all drivers and the actual variation in pCO_2 (ΔpCO_2^{drv}), indicating the extent to which the decomposition of pCO_2 into its drivers differs from ΔpCO_2^{drv}. More details are given in the methods section.

Despite the high monthly variability and the marked seasonal cycle of the CO_2 exchanges observed in the PLE (Figs. 18 and 19), during the 4-year period analyzed, the inner inlet zone behaved as net CO_2 outgassing to the atmosphere (2.9 ± 41.4 mmol m^{-2} d^{-1}), in contrast to the behavior as an estuarine net CO_2 sink zone (-7.2 ± 33.3 mmol m^{-2} d^{-1}) observed in the area close to the ocean. Thus, the net behavior during the entire period revealed that the lower zone of the PLE behaved as an area of CO_2 uptake (-2.1 ± 27.2 mmol m^{-2} d^{-1}; Fig. 19).

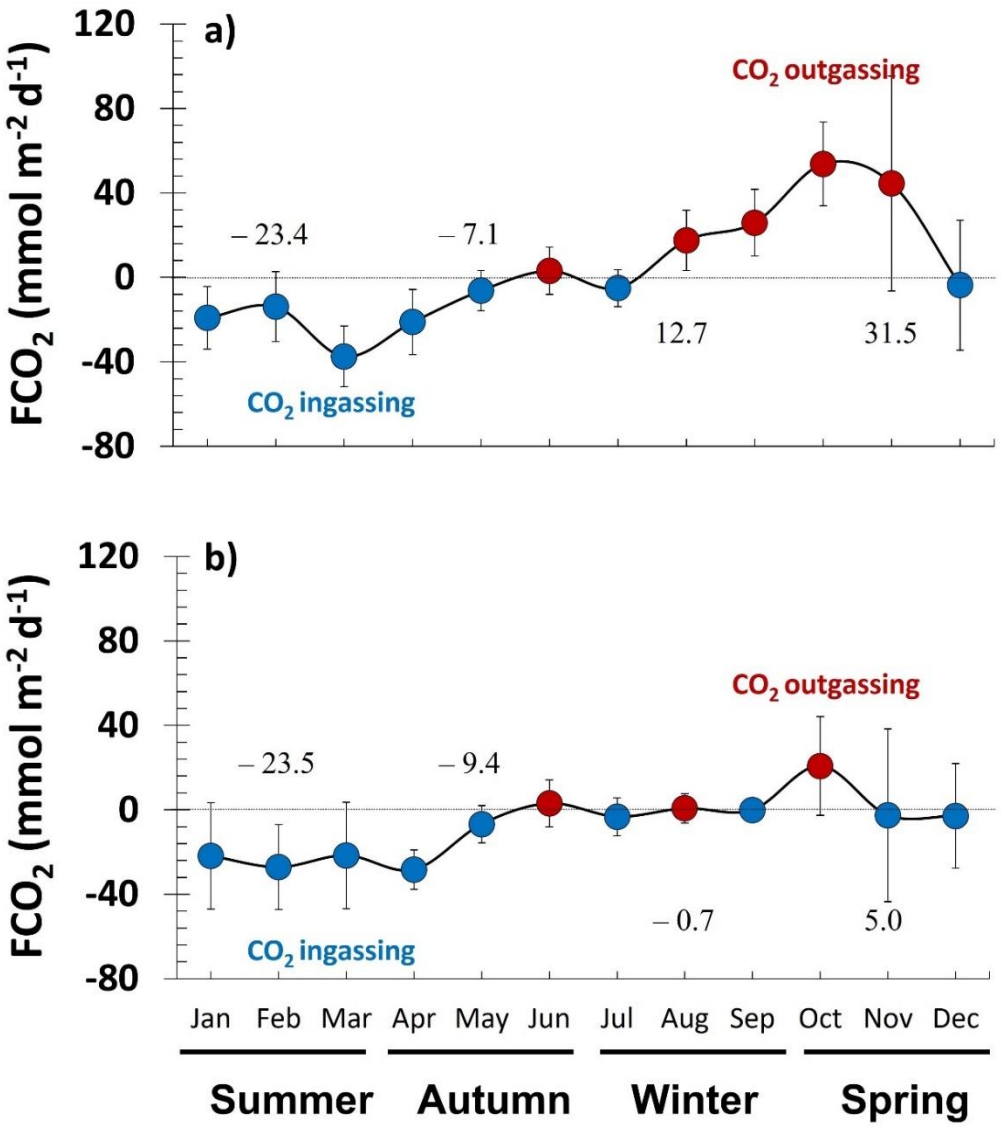

Figure 18. Seasonal cycle of surface water-air CO_2 net flux (FCO_2) of the lower zone of the Patos Lagoon Estuary obtained from May 2017 to June 2021 at the **(a)** pier-fixed station BrOA #1 (inner inlet) and **(b)** BrOA #2 (sea-exposed area). The error bars indicate the standard error of each month. The values indicate the average FCO_2 for each season. Blue dots indicate months of CO_2 ingassing, while red dots indicate months of CO_2 outgassing.

In 2019, there was intense CO_2 uptake (–23.9 ± 33.8 mmol m^{-2} d^{-1}) by the PLE surface waters, while in 2018, the region often released CO_2 (7.5 ± 41.3 mmol m^{-2} d^{-1}) to the atmosphere. The CO_2 outgassing was high in 2017. However, we did not evaluate the summer data when most of the CO_2 was absorbed. For 2021, we did not consider the winter/spring season, when CO_2 emissions are higher (Fig. 19). According to our analysis, the water-air net CO_2 fluxes evolve at periods of 3 and 6 months and one year, mainly at the BrOA #1 station (Fig. S4).

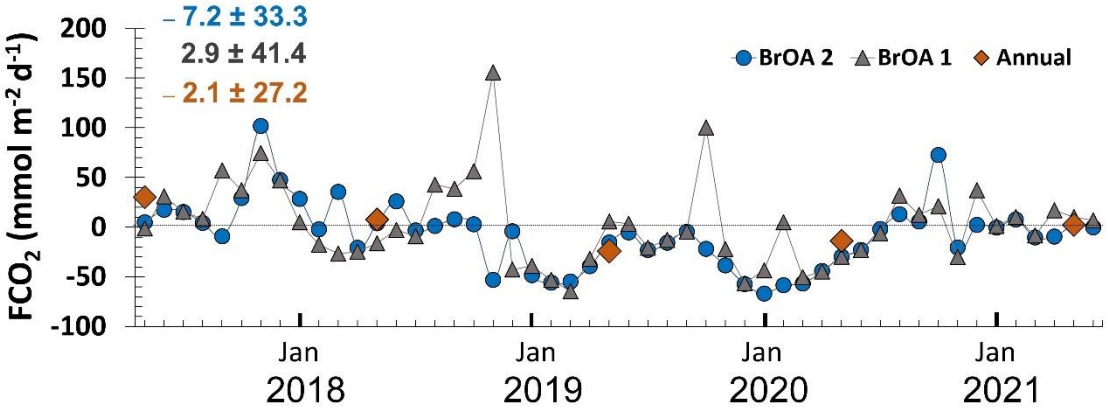

Figure 19. Monthly and interannual variability in water-air surface CO_2 net flux (FCO_2) for the BrOA #1 (gray triangles) and BrOA #2 (blue dots) stations at the Patos Lagoon Estuary from May 2017 to June 2021. The orange diamonds depict the annual averages (note that 2017 and 2021 do not consider all the seasons). The FCO_2 annual average and standard deviation for each estuarine station (color indicated by the legend) and joined regions (orange) are indicated in the top left.

5.3.3 River-borne, ocean-borne, and estuarine-generated CO_2

The seasonality of CO_2 concentrations is relatively different in each region analyzed. At the inner inlet station, the seasonal cycle of the CO_2 estuarine is marked and varies from –17 to 39 µmol kg^{-1}, while at the mouth of the estuary, the CO_2 estuarine varies from –9 to 31 µmol kg^{-1} (Fig. 20a and 20b). Despite the difference in estuarine, ocean and river CO_2 concentrations, the same variation was observed at both the inner inlet and estuarine mouth stations. The CO_2

concentrations averaged 1.8 ± 0.4 µmol kg^{-1} for the ocean, 2.2 ± 0.5 µmol kg^{-1} for the river and 5.2 ± 3.2 µmol kg^{-1} for all lower zones of the estuary during the summer/autumn seasons, while in the winter/spring seasons, the CO_2 estuarine concentration was more than 2-fold higher (average of ~ 13 ± 4.5 µmol kg^{-1}) than that in other seasons. Thus, the lower estuarine zone of the Patos Lagoon acts as a region of production of estuarine CO_2, mainly during months of high freshwater discharge into the lagoon (i.e., end of winter and spring; Figs. 20 and S5), with great magnitudes of CO_2 in the more protected embayment and less hydrodynamic zones. Regarding river-borne CO_2, the behavior of the PLE was different from that observed for estuarine CO_2. The river-borne CO_2 was higher in periods of high freshwater discharge, while in months where the freshwater discharge was low, the input of CO_2 with marine sources was intense.

Despite the small difference, the inner inlet zone produced more CO_2 (11.8 ± 12.6 µmol kg^{-1}) than the exposed area (9.1 ± 10.0 µmol kg^{-1}). At the end of 2018, there was a decrease in CO_2 estuarine production and an increase in CO_2 estuarine consumption in the region, with more CO_2 estuarine consumption at the mouth of the estuary (Fig. 20b) than in the sheltered area. From July 2019, the ocean-borne CO_2 increased at both stations.

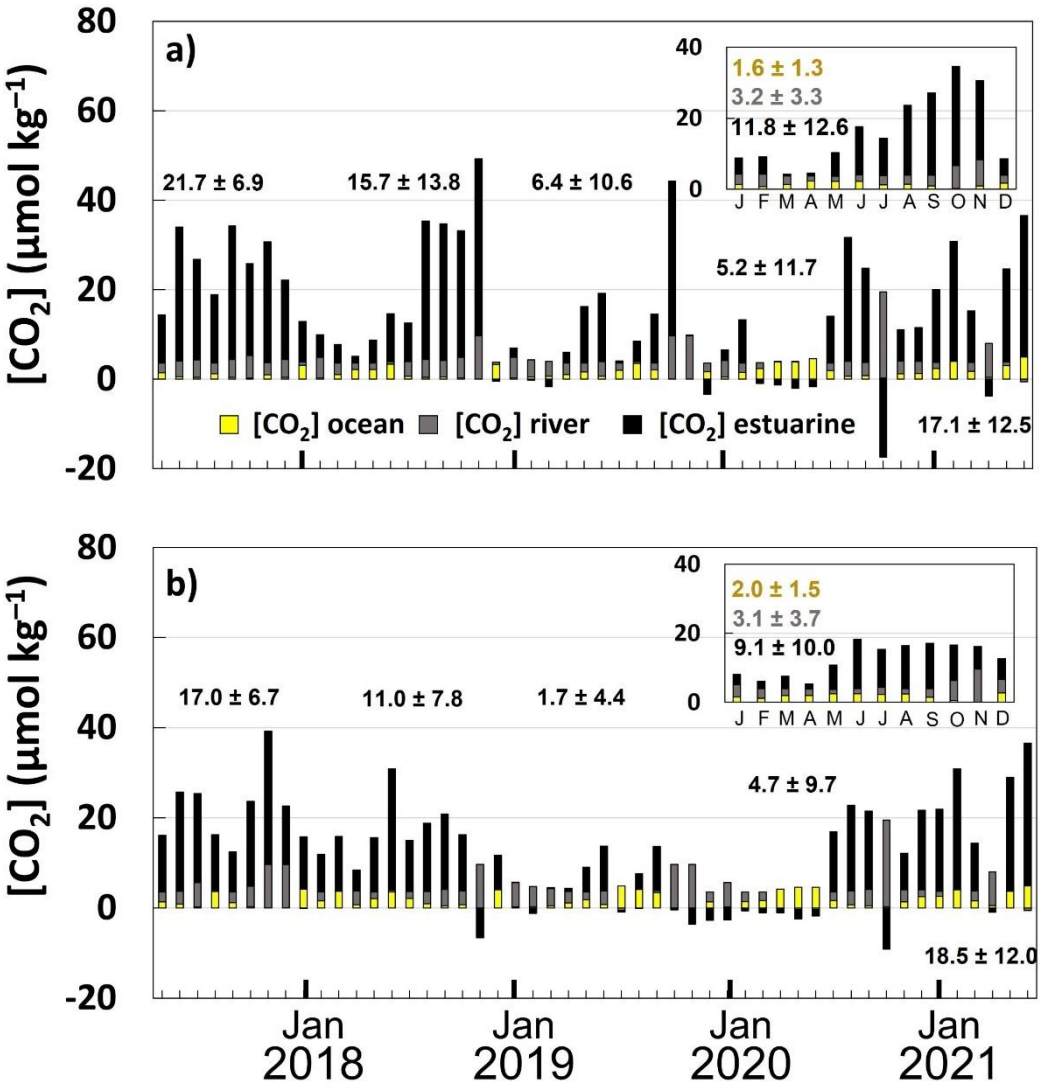

Figure 20. Monthly variability in aqueous surface CO_2 concentration ($[CO_2]_{ocean}$; yellow bars, $[CO_2]_{river}$; gray bars, and $[CO_2]_{estuarine}$; black bars) for the stations located in the lower zone of the Patos Lagoon Estuary from May 2017 to June 2021 in the **(a)** BrOA #1 and **(b)** BrOA #2 pier-fixed stations with annual average and standard deviation for CO_2 estuarine concentration. The seasonal cycle is inserted in the top right with the average and standard deviation for each CO_2 concentration.

5.4 Discussion

5.4.1 Seasonal drivers of pCO_2

The A_T and C_T variations were the main causes of changes in pCO_2 variability. The concentration of salts and dilution are the main processes

identified in the pCO_2 variation, indicated by increases (summer/autumn) and decreases (winter/spring) in A_T and C_T (Fig. 17). The lower estuarine zone of the Patos Lagoon shows a high amplitude of A_T (479 to 2,245 µmol kg^{-1}) and C_T (500 to 2,040 µmol kg^{-1}) [Albuquerque et al. under review], related to periods of increased (winter/spring) freshwater discharge and seawater inflows (summer/autumn). Furthermore, the PLE is a region with high organic matter concentrations due to large continental inputs, abundant macrophyte communities and local anthropogenic sources [Baumgarten and Niencheski 2010] that lead to heterotrophy and macroalgal blooms in spring, which directly influence the carbon concentration [Haraguchi et al. 2015, Lanari and Copertino 2017, Lanari et al. 2018]. Another factor is the hydrodynamic processes that lead to large variations in salinity [Haraguchi et al. 2015]. These features aid in the final behavior of A_T, C_T and salinity and indirectly affect the pCO_2 variation.

The estimated deviations of the analysis (Fig. 17) are an indication that some estuarine processes were not yet accounted for in the pCO_2 changes, such as the influence of phytoplankton biomass [e.g., Lee et al. 2006, Cai 2011] and the property changes related to groundwater input [e.g., Sadat-Noori et al. 2016, Jeffrey et al. 2018], which configures a current limitation and a challenge for further studies. The higher freshwater discharge in late winter and during spring brings a higher concentration of organic matter, supporting phytoplankton blooms in the PLE [Albuquerque et al. under review]. The deviations observed in summer and spring are probably due to photosynthesis rates [Albuquerque et al. under review], which leads to a decrease in pCO_2 levels. Groundwater may be enriched in dissolved carbon species; therefore, groundwater input affects the carbon concentration in water [Sadat-Noori et al. 2016], increasing the pCO_2 concentration. Although the approach used in this study is mostly used to infer

the main variables and processes affecting the pCO_2 distribution for oceanic waters [e.g., Takahashi et al. 2014, Moreau et al. 2017, Monteiro et al. 2020], it is also a useful approach in estuarine systems that have periods of waters with high salinity signals. However, as previously indicated, further investigation of coupled estuarine-biogeochemical processes must be performed to reduce uncertainties, mainly during freshwater dominance periods in the estuarine system.

5.4.2 Water-air CO_2 fluxes and CO_2 concentrations

Estuarine systems are significant sources of CO_2 to the atmosphere with recognized relevance for regional and global carbon budgets [e.g., Guo et al. 2009, Gupta et al. 2009, Jeffrey et al. 2018, Joesoef et al. 2015], and estuarine lower zones realize approximately 23 mmol m^{-2} d^{-1} [Chen et al. 2013]. The magnitude of the CO_2 exchanges in the lower estuarine zone of the PLE is variable, with values ranging from –66 to 155 mmol m^{-2} d^{-1} and a net CO_2 ingassing average of –2 mmol m^{-2} d^{-1} for the 4-year period investigated here (Fig. 19; Table 3). The variations observed in the lower zone of the PLE display a typical distribution pattern seen in other estuarine environments (Table 3), mainly in shallow estuaries dominated by freshwater discharge, such as the PLE [e.g., Evans et al. 2013, Koné et al. 2009] (Table 3). Moreover, the same range of water-air CO_2 exchanges observed in the subtropical PLE can be found in other tropical estuarine environments in Brazil [e.g., Cotovicz et al. 2020, Noriega and Araujo 2014], shifting between periods of CO_2 ingassing and CO_2 outgassing to the atmosphere over the year.

Table 3. Comparison between the range of water-air CO_2 flux (FCO_2) from previous estuarine studies around the world and the current study. The studies are organized first by country and second by climate.

Reference	Estuary location	Country	Climate	Type	Period	Water-air FCO_2 (range in mmol m^{-2} d^{-1})
This study	Lower zone of PLE South Brazil	Brazil	Subtropical	Freshwater discharge dominated	May 2017 to June 2021	−66 to 155
Cotovicz et al. 2020	Paraíba do Sul River Southwestern Brazil	Brazil	Tropical	Freshwater discharge dominated	February 2017 October 2017 March 2018	−37.8 to 216.1
Noriega and Araujo 2014	North and Northeast Brazilian estuaries	Brazil	Tropical and semiarid	Various	July 2012 to June 2013	2.4 to 175.2
Chen et al. 2020	Chesapeake Bay	USA	Subtropical	Partially mixed and microtidal	March to December 2016 February 2019	−11.2 to 92.4
Yao and Hu 2017	Mission-Aransas	USA	Subtropical semiarid	Freshwater discharge dominated	May 2014 to April 2015	−13.5 to 380.3
Ho et al. 2014	Shark River	USA	Tropical	Mangrove	November 2010 November 2011	20 to 118
Evans et al. 2013	Columbia River	USA	Temperate	Freshwater discharge dominated	August 2007 November 2007 April 2008 June 2008 September 2008	−53.0 to 193.2
Joesoef et al. 2015	Delaware	USA	Temperate	Freshwater discharge dominated	June 2013 August 2013 October 2013 November 2013 March 2014 July 2014 August to September 2014	−21.0 to 129.1

					October to November 2014 December 2014	
Crosswell et al. 2012	Neuse River	USA	Temperate	Macrotidal	June 2009 to July2010	−38 to 271
Dinauer and Mucci 2017	St. Lawrence	Canada	Temperate	Freshwater discharge dominated	July 2003 June 2006 May 2007 July 2007 June 2009 July 2009 July 2010 May 2011 June 2013 May 2016	−21.9 to 28.4
Koné et al. 2009	Lagoon's system	Ivory Coast	Tropical	Microtidal	June to July 2006 September 2006 November to December 2006 March 2007	−20.0 to 186.2
Gupta et al. 2009	Cochin	India	Tropical	Microtidal	February 2005 April 2005 September 2005	64 to 274
Guo et al. 2009	Pearl River	China	Subtropical	Freshwater discharge dominated	November 2002 February 2004 January 2005 August 2005 April 2007	−25.8 to 907.7
Oliveira et al. 2017	Tagus	Portugal	Temperate	Tide dominated	1999 to 2007	16.6 to 347.1
Borges et al. 2004	Scheldt	Netherlands	Temperate	Macrotidal	November 2002 April 2003	31 to 2,189
Bozec et al. 2012	Loire	France	Temperate	Tide dominated	April 2009 July 2009	−9 to 140

Flecha et al. 2015	Guadalquivir	Spain	Mediterranean	Mesotidal	October 2009 February to March 2010 November 2007 to August 2009	−0.7 to 83.9
Maher and Eyre 2012	Hastings River	Australia	Temperate	Wave dominated	June 2006	−8.7 to 25.3
	Camden Haven	Australia	Temperate	Wave dominated	October 2006 February 2007 April 2007	−16.5 to 12
	Wallis Lake	Australia	Temperate	Wave dominated		−30.4 to 26.2

Significant seasonal variation in the water-air CO_2 fluxes between summer/autumn and winter/spring was observed in the lower zone of the PLE. The results presented here demonstrate that the region experienced periods of both CO_2 ingassing (between December and May) and CO_2 outgassing (between June and November), mainly in protected areas along the estuary (Fig. 19b). CO_2 exchanges are modulated by winds [Wanninkhof 2014], different hydrodynamic conditions and/or extreme events [Sims et al. 2021]. The higher the wind speed is, the greater the influence on the gas exchange between the surface water and the atmosphere; thus, wind speed can play a crucial role in estuarine CO_2 fluxes [e.g., Yao et al. 2020] by exchanging momentum with the atmosphere. In addition, a shallower environment responds faster to wind action [Moller et al. 2001, Lanari and Copertino 2017], which seems to favor fast air-water gas exchange [Yao et al. 2020] and increased CO_2 gradient magnitudes. The water-air CO_2 fluxes in the lower zone of the PLE follow the seasonal pattern of freshwater discharge, which is what occurred with the variability in the carbonate system parameters [Albuquerque et al. under review]. In late winter and spring, the freshwater discharge is higher [Marques 2012], and consequently, the entry of organic matter promoting significant heterotrophy in relation to CO_2 is also higher, which is what occurs in the tropical coastal systems in northern and northeastern Brazil [Noriega and Araújo 2014]. In the same period, the higher wind speed (~ 4.0 m/s; Fig. S5) leads to higher gas transfer velocity in this period with respect to that of summer and autumn. The inner inlet station receives more influence from the freshwater discharge and has a high residence time, leading to an increase in CO_2, while the sea-exposed station is close to the ocean and directly influenced by seawater dynamics and outflow/inflow currents [Möller et

al. 2001, Lisboa 2015]. Thereafter, CO_2 outgassing in the inner inlet zone should be mainly related to heterotrophic respiration and degradation of organic matter generated on a larger scale by the influence of freshwater discharge, even though this area is also influenced by resuspension of fine bottom sediments [Moller et al. 2001, Lanari and Copertino 2017].

The phytoplanktonic community composition exerts a fundamental role in CO_2 uptake via photosynthesis. In the PLE, diatoms are the dominant phytoplankton group, followed by cyanobacteria, flagellates, dinoflagellates, and chlorophytes along the coastal offshore gradient [Islabão et al. 2017]. Microphytoplanktonic diatoms tend to show a higher capacity for capturing CO_2 in water [e.g., Hopkinson et al. 2011] than nano- and picoplanktonic species, which helps to balance the carbon concentration. The production of CO_2 was lower in the more sea-exposed area than in the inner inlet station, suggesting that the abundance of diatoms in the region closest to the coast is higher due to local hydrodynamics, mainly at the end of winter and spring. Moreover, in spring (October and November), the blooms caused by biological activity combined with vertical mixing due to the higher wind intensity lead to highly variable water-air CO_2 fluxes in the lower zone of the PLE (Fig. 19). Despite the different tide regimes, these seasonal conditions are similar to those previously observed in the macrotidal Neuse River estuary [Crosswell et al. 2012] and microtidal Aby Lagoon [Koné et al. 2009]. The water temperature influences the CO_2 fluxes because water-air CO_2 exchanges depend on the gas transfer velocity, which is further induced by temperature that changes the solubility of gas in water [Wanninkhof 2014]. The higher summer temperatures combined with the CO_2-unsaturated waters from the ocean turn the region into a CO_2 sink in summer and

autumn. In general, freshwater input, wind and water temperature are important in the exchange of CO_2; nevertheless, residence time and phytoplanktonic composition also modulate the CO_2 dynamics in different areas of the lower zone of the PLE over the seasons.

The production or consumption of CO_2 is an indicator of estuarine-biogeochemical processes [Yao et al. 2020] and plays a crucial role in determining the water-air CO_2 fluxes of the lower zone of the PLE. Most of the CO_2 released into the atmosphere is produced in the PLE itself. The high freshwater discharge between the end of winter and spring carries organic matter [Niencheski and Windom 1994, Niencheski et al. 2006] that favors photosynthetic respiration and degradation of organic carbon. These processes intensify the production of carbon for the estuary. Although the source is the river, heterotrophy occurs in the estuary because there is more time for the decomposition of organic matter. During this same period, CO_2 inputs from the river are also significant. These two CO_2 sources contribute to CO_2 supersaturation and outgassing to the atmosphere. Therefore, the observed seasonal pattern of CO_2 fluxes and different CO_2 sources suggest that heterotrophy controls the metabolic status of the estuarine waters, mainly in the inner areas of the PLE. In addition, the produced carbon is exported to the coast, which contributes to the high concentration of CO_2 in the mouth of the estuary. This region is a channel with high hydrodynamics [Möller et al. 2001], which allows faster currents and more intense water exchanges. Thus, this area prevents the surface water from CO_2 supersaturation by releasing the gas into the atmosphere.

The interannual variability in estuarine properties and processes in the

PLE is influenced by El Niño-Southern Oscillation (ENSO) events [e.g., Odebrecht et al. 2017, Albuquerque et al. under review]. The warm phase of ENSO, El Niño, is characterized by abnormal heating of surface waters in the tropical Pacific Ocean. ENSO affects the regional and global climate, changing the wind patterns worldwide and thus affecting the rainfall patterns in tropical and midlatitude regions [e.g., Cai et al. 2020]. Between May 2017 and June 2021, two ENSO events were identified. These events included one El Niño event (in 2017/2018; ENSO warm phase) [INPE 2021] and one La Niña event (in 2020/2021; ENSO cold phase) [INPE 2021]. Under El Niño conditions, freshwater discharge is above the average level (~1770 m^3 s^{-1}), and the opposite is true under La Niña conditions [Vaz et al. 2006, Seeliger and Odebrecht 2010]. The decreased water-air CO_2 fluxes from the beginning of monitoring, the increased CO_2 exchanges in the last two years (Fig. 18) and the composition of CO_2 (Fig. 20) are likely associated with the change from moderate El Niño (2017–2018) to the beginning of La Niña conditions (2019–2020). However, since the time series is relatively short, with some years (2017 and 2021) having missing months, further discussion on this matter is inhibited. Future research focusing on longer time series is still needed to better characterize the role of climate mode teleconnections with changes in the water-air CO_2 exchanges in the PLE.

Finally, it is worth mentioning that at the end of 2018 (October to December) and between November 2019 and January 2020, there was a dredging event in the port access channel located in the estuary [Mirlean et al. 2020]. These dredging activities resuspend the sediment, allowing nutrients and carbon to return to the water column and producing some impacts (e.g., water chemical alteration, mud deposition, and changes in the benthos composition),

and a monitoring program should always be considered to evaluate their environmental consequences [Torres and Philomena 2013, Mirlean et al. 2020]. The environmental impacts associated with the dredging process and spoil disposal can be characterized by direct effects on organisms and habitats and indirect effects attributed to alterations in water quality. Thus, in addition to likely ENSO effects on the region, the behavior of the studied area as a CO_2 ingassing zone (Fig. 19) and the increase in estuarine CO_2 consumption from that period (Fig. 20) onward may also be influenced by changes in the water properties and water-sediment processes caused by dredging, despite the controversial about the causes and consequences of mud deposition events along the coast [Calliari et al. 2022, Mirlean et al. 2020, 2021, Garcia et al. 2021].

5.5 Conclusion

Overall, the estuarine ecosystem of the Patos Lagoon behaved as summer/autumn CO_2 ingassing and winter/autumn CO_2 outgassing to the atmosphere. The combined effect of wind speed, continental freshwater discharge, inflow/outflow currents, water temperature, biological activity, and water residence time is responsible for the modulation of the CO_2 exchange in the PLE. However, comparing the different areas of the PLE lower zone, we noticed non-similar forcings acting on the variation in the CO_2 concentration. The water-air CO_2 flux variations at the mouth of the estuary were mainly driven by the balance between the seawater dynamics and freshwater discharge input/output, which influences the scenario of a CO_2 sink. In the inner estuary, heterotrophic respiration and degradation of organic matter contributed to CO_2

outgassing to the atmosphere between the end of winter and spring. Autochthonous production was responsible for the highest concentration of CO_2, indicating heterotrophy in the estuarine surface water. Part of the carbon produced is exported to the coast, contributing to a high concentration of CO_2 in the mouth of the estuary. Therefore, this study shows that the lower zone of the PLE is resilient to high CO_2 concentrations and has been able to overcome anthropogenic emissions in the region. Hence, long-term monitoring programs must continue to improve the understanding of CO_2 exchange variability and help shed light on the role played by the PLE on the global carbon budget.

Capítulo VI: Síntese da Discussão e Conclusões

Aqui serão destacados os principais pontos das discussões e das conclusões dos artigos científicos apresentados nos Capítulos IV e V. Primeiramente, os artigos serão abordados em conjunto, e por fim, teremos um fechamento geral concluindo a Tese através da verificação da hipótese formulada e das considerações finais.

6.1 Caracterização e variabilidade sazonal do sistema carbonato e dos fluxos líquidos de CO_2

A primeira caracterização do sistema carbonato nas águas superficiais na parte sul do ELP foi feita durante o período de maio de 2017 a junho de 2021. As altas variações nas concentrações de A_T e C_T observadas na zona inferior do ELP exibiram um padrão de distribuição típico, que tem sido observado em outros ambientes estuarinos ao redor do mundo, principalmente os que também

apresentaram uma elevada amplitude na salinidade. Essas variações encontradas refletem a mistura da água doce proveniente dos rios (que apresentam baixas concentrações de A_T e C_T) e da água salgada do oceano adjacente (que possuem altos valores de A_T e C_T). Os valores máximos observados dessas duas variáveis, que são comparativamente mais altos do que os descritos na literatura em estuários semelhantes, estão provavelmente ligados à presença da Água Tropical (que é considerada uma água salgada com valores de salinidade acima de 36) na composição da mistura ocênica com as águas da plataforma, que adentram o estuário em determinados períodos do ano.

A região estudada é, em média, um ambiente naturalmente alcalino (com 8,0 de média de pH) e apresentou condições saturadas de $CaCO_3$ durante todo o período analisado, sendo assim caracterizada por uma pCO_2 superficial relativamente baixa (~ 394 µatm, em média) e de variação semelhante a outros estuários subtropicais rasos relatados em estudos. Mesmo em comparação com estuários ao redor do mundo, o valor máximo de pCO_2 de ~1400 µatm ainda é inferior ao de ~10000 µatm observado em outras regiões. Assim, concluiu-se que as características geomorfológicas da lagoa, juntamente com a forte influência da água do mar e a descarga de água fluvial desempenham um papel importante na concentração dos parâmetros do sistema carbonato e na regulação da distribuição espaço-temporal.

A maioria dos parâmetros do sistema carbonato e os fluxos líquidos de CO_2 na interface água-ar no ELP exibiram um padrão sazonal bem-marcado. Grande parte da variação encontrada nos quatro parâmetros e na troca de CO_2

entre a água e o ar está relacionada a hidrologia local. O padrão sazonal de descarga de água doce na lagoa é típico de médias latitudes, o que significa alta descarga no inverno e no início da primavera, seguida de descarga baixa a moderada durante o verão e outono. Esse padrão se refletiu principalmente na distribuição da salinidade na região, que é caracterizada pelo equilíbrio da dominância das águas dos principais rios e do oceano adjacente. De fato, isso é evidenciado pela diluição/concentração de sais como os principais processos biogeoquímicos que controlaram a flutuação da A_T, do C_T, do pH e da pCO_2 durante esses períodos nas águas superficiais e nos resultados apresentados, que demonstraram que a região passou por períodos tanto de gaseificação de CO_2 (absorção pelo estuário entre dezembro e maio) quanto de desgaseificação de CO_2 (emissão para atmosfera entre junho e novembro), principalmente nas áreas protegidas mais rasas ao longo do estuário. Além disso, verificou-se que que as alterações da A_T e do C_T foram as principais causas das mudanças na variabilidade da pCO_2. Os desvios estimados encontrados nos parâmetros controladores da pCO_2 indicaram que outros processos estuarinos estejam atuando e ainda não foram contabilizados nas mudanças de pCO_2, tais como: (i) a influência da biomassa fitoplanctônica e da vegetação submersa, (ii) os processos biogequímicos associados às trocas e fluxos na interface água-sedimento, (iii) e as mudanças de propriedade relacionados à entrada de água subterrânea no ambiente, o que configura uma limitação atual desse método e um desafio para estudos futuros.

Em resumo, a interação entre os efeitos térmicos e não-térmicos na pCO_2 foi evidenciada por T:NT<1 ao longo do ano. Durante o verão e o outono, a entrada de água do mar contribuiu para a prevalência de fatores não-térmicos,

incluindo mistura vertical, processos biológicos e troca de CO_2 mar-ar, influenciando o C_T. Durante o inverno e a primavera, o alto nível de descarga de água doce contribuiu para a mistura profunda que faz com que a pCO_2 aumente devido à ressurgência de águas de alto C_T e processos biológicos. Mesmo com o rebaixamento biológico do C_T durante a primavera, a pCO_2 ainda foi maior do que durante o verão e o outono. Em geral, esses efeitos térmicos e não térmicos na pCO_2 se sobrepõem constantemente, dificultando a interpretação de seus efeitos individuais nas variações da pCO_2.

Outro fator atuante, principalmente na primavera, foi o aumento da decomposição da matéria orgânica devido às florações de fitoplâncton e macroalgas à deriva que ocorrem nesse período. A fixação fotossintética de carbono causa uma redução líquida de C_T e pCO_2, levando aos aumentos da A_T, do pH, do ΩCa e do ΩAr. A fotossíntese e a captação de CO_2 estão ligadas à composição da comunidade fitoplanctônica, sendo esta principalmente dominada por diatomáceas no ELP. Este grupo fitoplanctônico tende a apresentar maior capacidade de captura de CO_2 na água do que as espécies nano e picoplanctônicas, o que ajuda a equilibrar a acidez e a concentração de carbono. Logo, a maior absorção de carbono esteve, possivelmente, ligada ao grupo fitoplanctônico principal que habita a região. A produção de CO_2 foi menor na área mais exposta ao mar do que na estação interna, sugerindo que é maior a abundância de diatomáceas na região mais próxima da costa devido à hidrodinâmica local, principalmente no final do inverno e primavera. Além disso, na primavera (entre os meses de outubro e novembro), as florações causadas pela atividade biológica combinadas com a mistura vertical, devido à maior intensidade do vento, resultam em fluxos de CO_2 na interface água-ar altamente

variáveis na zona inferior do ELP. No entanto, estudos recentes relataram tendências crescentes no crescimento de dinoflagelados e cianobactérias devido a mudanças na salinidade no ELP, o que poderia vir a afetar a distribuição dos parâmetros do sistema carbonato e o ciclo do carbono no corpo lagunar.

A descarga de água doce teve uma influência distinta nas diferentes partes das zonas mais baixas do ELP, como é refletido e nitidamente observado no sistema carbonato e nos fluxos de CO_2 na interface água-ar no inverno e na primavera. As áreas abrigadas e mais rasas no interior do ELP (BrOA #1) possuem um tempo de residência da água maior do que a desembocadura do baixo estuário (BrOA #2), levando a uma menor variabilidade tanto nos parâmetros do sistema carbonato quanto nos fluxos de CO_2. Processos que alteram a biogeoquímica das águas superficiais, como reações na interface sedimento-água, tal como a ressuspensão de sedimentos finos e da matéria orgânica no fundo e a maior instabilidade da camada superficial da água causados pela ação dos ventos também foram fatores que interferiram na variabilidade de uma forma mais intensa nas áreas mais rasas do ELP. Ademais, notou-se que as temperaturas mais altas do verão combinadas com as águas insaturadas de CO_2 do oceano transformam a região em um sumidouro de CO_2 no verão e no outono. Ao serem analisados todos esses fatores, infere-se que, em geral, a entrada de água doce e o vento são importantes na troca água-ar de CO_2; no entanto, o tempo de residência e a composição fitoplanctônica também modulam a dinâmica do CO_2 em diferentes áreas da zona inferior do ELP ao longo das estações. Portanto, enquanto as variações dos parâmetros do sistema carbonato e dos fluxos de CO_2 na boca do estuário foram impulsionadas principalmente pela dinâmica da água do mar e as correntes de saída/influxo, no

interior do estuário, elas estavam relacionadas, principalmente, à respiração heterotrófica e à degradação da matéria orgânica.

A maior parte do CO_2 emitido para a atmosfera foi produzida no próprio ELP durante o período estudado. A alta vazão de água doce entre o final do inverno e a primavera repleta de matéria orgânica favoreceu os processos biológicos que intensificaram a produção de carbono para o estuário. Tanto o CO_2 produzido no estuário quanto o CO_2 vindo das águas fluviais contribuiram para a supersaturação e liberação de CO_2 para a atmosfera no baixo ELP durante os períodos de emissão de CO_2 para a atmosfera. Portanto, o padrão sazonal observado de fluxos de CO_2 e as diferentes fontes de CO_2 sugerem que a heterotrofia controla o estado metabólico das águas estuarinas, principalmente nas áreas internas do ELP.

A variabilidade interanual também foi observada nos parâmetros do sistema carbonato e nos fluxos de CO_2 no baixo ELP, e estão possivelmente associadas às teleconexões do modo climático conhecido como El Niño-Oscilação Sul (ENSO). A diminuição tanto da pCO_2 quanto dos fluxos de CO_2 na interface água-ar desde o início do monitoramento, o aumento das trocas de CO_2 nos últimos dois anos e a composição do CO_2 podem estar relacionados às mudanças ocasionados por um evento de El Niño moderado e o início das condições de La Niña que afetavam a região. No entanto, como a série temporal é relativamente curta, conclusões aprofundadas sobre esse assunto ainda não podem ser feitas. Ainda assim, algumas mudanças observadas a partir de dezembro de 2018 na troca de CO_2 entre a água e o ar podem estar relacionadas também aos eventos de dragagem, que ocorreram no canal de acesso ao porto localizado no estuário, apesar da controvérsia sobre as causas e consequências

dos eventos de deposição de lama ao longo da costa. Os impactos ambientais gerados pelo processo de dragagem e a disposição de rejeitos podem ser caracterizados por efeitos diretos sobre organismos e habitats e efeitos indiretos atribuídos às alterações na qualidade da água, como foi observado na área estudada pela gaseificação de CO_2 e pelo aumento do consumo de CO_2 estuarino a partir desse período. Por isso, são necessários mais estudos com foco em séries temporais mais longas (e modelos biogeoquímicos) para melhor caracterizar o papel das teleconexões do modo climático e dos eventos de dragagem com mudanças nos níveis da pCO_2 e da capacidade de tamponamento do ELP.

6.2 Considerações finais e direcionamentos futuros

Em relação à hipótese apresentada e testada no desenvolvimento desta Tese de Doutorado, i.e., "*O estuário da Lagoa dos Patos é uma fonte de CO_2 para a atmosfera durante todas as estações do ano e contribui com emissões significativas para as estimativas do balanço global de carbono.*", podemos concluir que ela foi refutada, pois o estuário funcionou como uma zona emissora de CO_2 para a atmosfera durante apenas o final do inverno e parte da primavera e não contribui significativamente para as estimativas do balanço global do carbono, uma vez que sua contribuição é de apenas 0,11% de um total de 0,1 Pg C ano^{-1} [Chen et al. 2013, Laruelle et al. 2013].

Em suma, as águas superficiais do baixo ELP são naturalmente alcalinas, saturadas em $CaCO_3$ e apresentam baixos valores de pCO_2. A diluição e a

concentração de sais foram as principais condicionantes da variação dos parâmetros do sistema carbonato ao longo das estações refletidos através do balanço da descarga de água doce e entrada de água do oceano adjacente. A entrada de água doce influencia fortemente e nota-se que nos períodos de enchente (verão/outono) o processo dominante é a concentração de sais, enquanto nos períodos de vazante (inverno/primavera), a diluição tem maior destaque. Entretanto, foi observado que regiões mais rasas e menos dinâmicas sofrem uma interferência maior da respiração e da degradação da matéria orgânica.

Os baixos valores encontrados da pCO_2 são reproduzidos nas condições de absorção de CO_2 (verão/outono) da atmosfera e emissão de CO_2 (inverno/primavera) para a atmosfera. A área mais interna apresentou um aumento na concentração de CO_2 durante o inverno e a primavera e relacionamos esse aumento, principalmente, à respiração heterotrófica e à degradação da matéria orgânica gerada em maior escala pela influência da descarga de água doce. Logo, esse equilíbrio no desempenho entre sumidouro e fonte de CO_2 do ELP foi modulado pela combinação da velocidade do vento, da vazão de água doce e das correntes de saída/entrada da água do mar, sendo a proliferação de fitoplâncton e a forte mistura vertical induzida pelo vento forçantes pontuais no ELP que levaram às trocas de CO_2 altamente variáveis nas diferentes regiões.

Ao contrário da maioria dos sistemas estuarinos, o ELP atuou, no geral, como um sumidouro líquido de –2 mmol m^{-2} d^{-1} de CO_2 durante o período investigado. Todavia, durante os períodos de supersaturação de CO_2, foi identificado que as principais fontes de carbono são advindas dos rios e

produzidas no próprio estuário. A maior concentração estuarina de CO_2 por produção autóctone indicou a heterotrofia em águas estuarinas e concluiu-se que parte desse carbono produzido no estuário é exportado para o litoral, evidenciado pela alta concentração de CO_2 na foz do estuário.

Apesar do grande impacto causado pela atividade humana, o ELP parece resistir a grandes mudanças no sistema carbonato. Portanto, este estudo ressalta que a zona inferior do ELP tem se caracterizado resistente as altas concentrações de CO_2 e sido capaz de superar as emissões antrópicas na região. Essa resiliência é uma característica importante e pode nos ajudar a entender estuários semelhantes fortemente influenciados pela atividade humana.

Novas investigações e estudos ainda são necessários para elucidar o papel do ELP no ciclo global do carbono. Há ainda muitas incógnitas e a falta de conhecimento de longo termo do funcionamento do ecossistema de cada estuário acarretam maiores desafios para o pleno entendimento. Por isso, o caminho é longo e tanto programas de monitoramento de longo prazo quanto a criação de modelos biogeoquímicos devem continuar em execução para melhorar o entendimento da variabilidade dos processos biogeoquímicos e das trocas de CO_2 em um ecossistema tão complexo quanto os ambientes estuarinos.

ANEXO I

Este anexo contém as seguintes figuras mencionadas no Capítulo IV: Fig. S1 e Fig. S2.

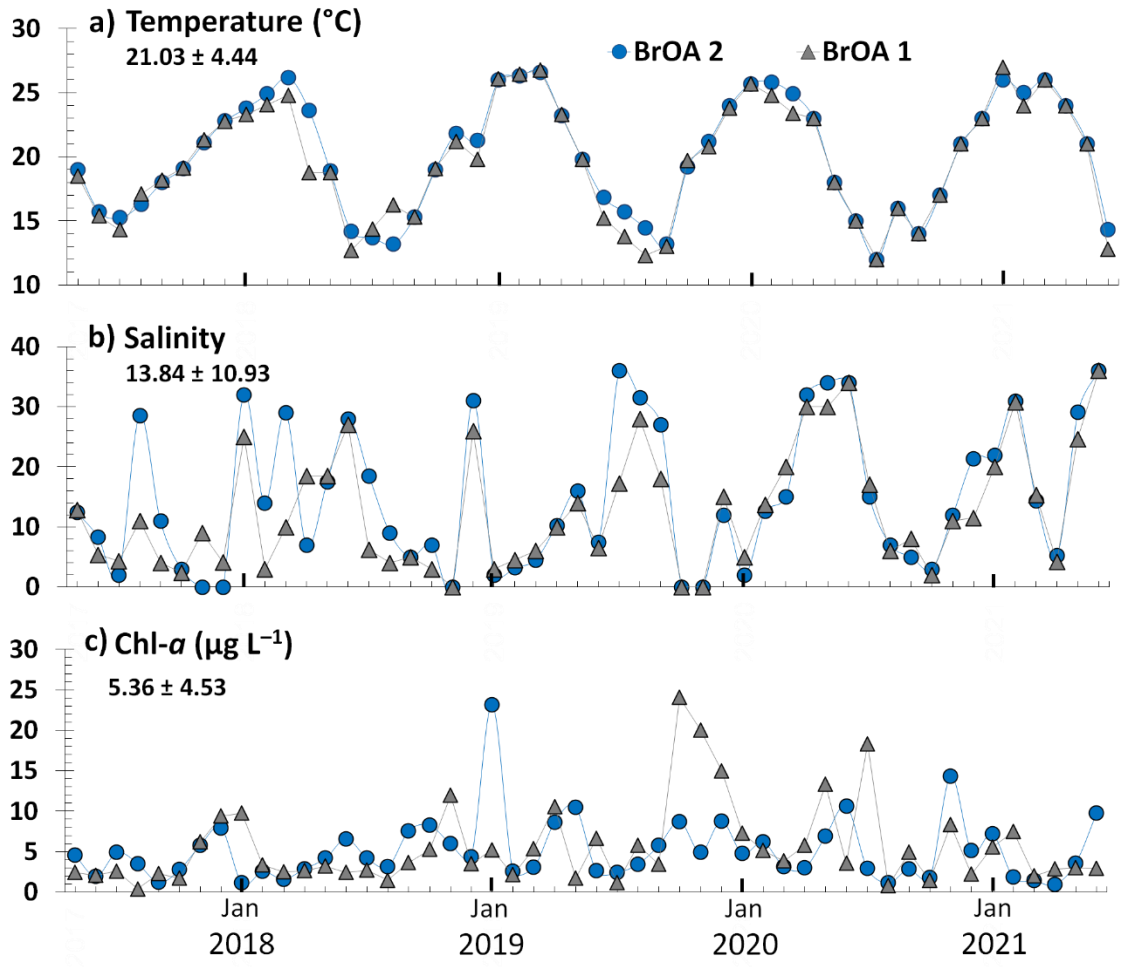

Figure S1. Monthly variability of surface water properties for the stations located in the BrOA #1 (gray line and dots) and BrOA #2 (blue line and dots) Patos Lagoon Estuary regions from May 2017 to June 2021. The annual average and standard deviation are indicated in the top left panels for water surface **(a)** temperature (°C), **(b)** salinity and **(c)** chlorophyll-*a* (Chl-*a*; µg L^{-1}).

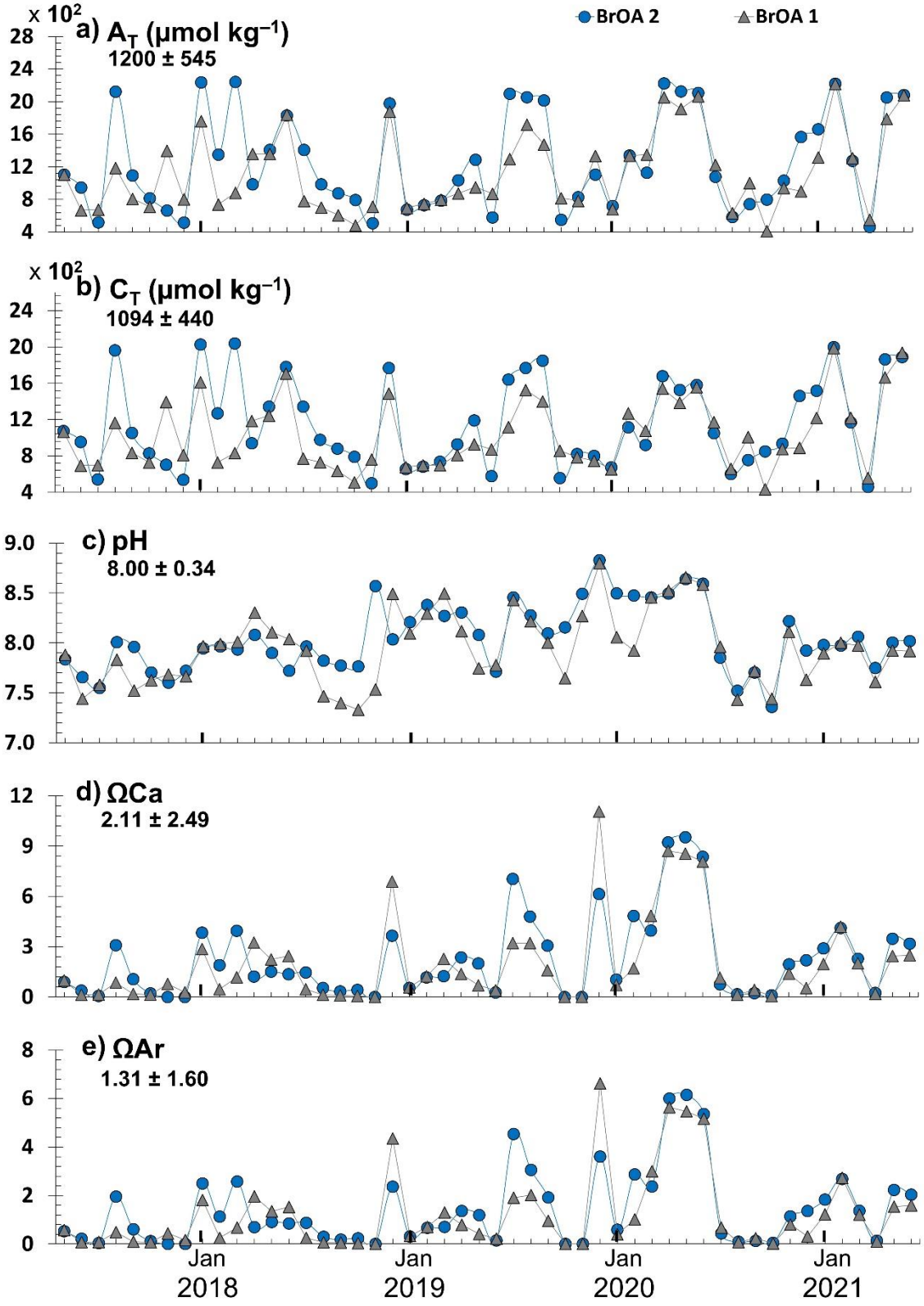

Figure S2. Monthly variability of surface water properties for the stations located in the BrOA #1 (gray line and dots) and BrOA #2 (blue line and dots) Patos Lagoon Estuary regions from May 2017 to June 2021. The annual average and standard deviation are indicated in the top left panels for water surface **(a)** total alkalinity (A_T; µmol kg^{-1}), **(b)** total dissolved inorganic carbon (C_T; µmol kg^{-1}), **(c)** pH at the total scale, **(d)** saturation state of calcite (ΩCa) and **(e)** saturation state of aragonite (ΩAr).

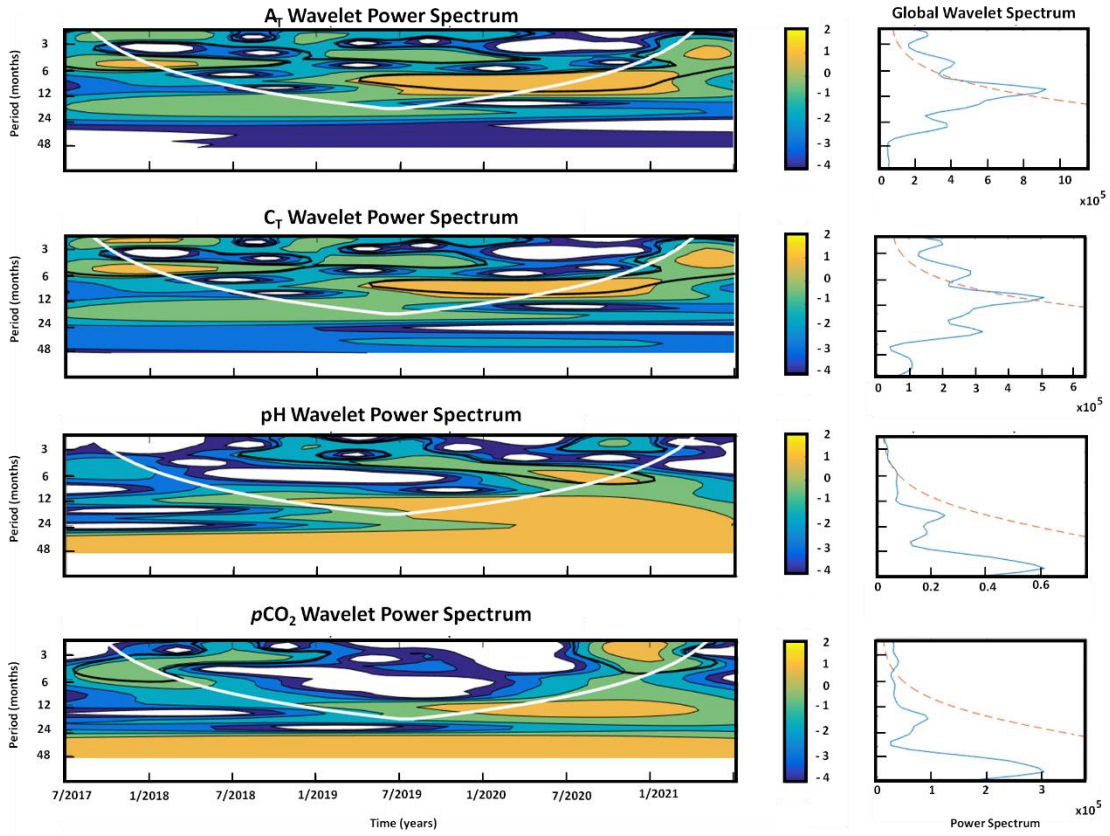

Figure S3. Global (right panels) and wavelet power spectra (left panels) of the **(a)** total alkalinity (A_T), **(b)** total dissolved inorganic carbon (C_T), **(c)** pH and **(d)** partial pressure of CO_2 (pCO_2) in BrOA #2 (pier-fixed station), considering the Morlet function as a mother wavelet. In the left panels, the area bounded by the white line indicates the region of the cone of influence, where the variance is reduced, and the solid black lines denote the regions with a significance level higher than 95%. The yellow colors represent high energy, and the blue colors indicate low energy. The color bar shows the units of energy in $\log_2$ form. In the right panels, the 95% level of significance is marked by the red dashed lines, while the sum of energy for each period is represented by the thin blue lines.

ANEXO II

Este anexo contém as figuras: Fig. S3 e Fig. S4 mencionadas no Capítulo V.

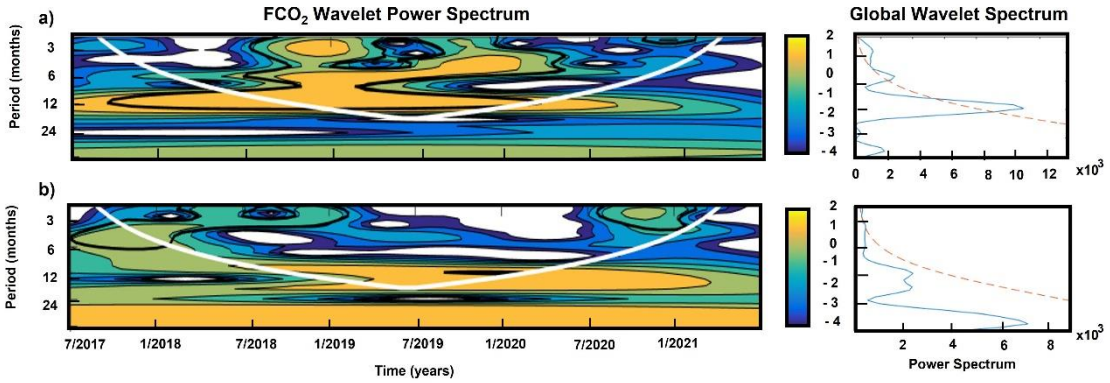

Figure S4. Wavelet spectrum of the CO_2 net flux (FCO_2) in the (a) BrOA #1 (pier-fixed station) and (b) BrOA #2 (pier-fixed station), considering the Morlet function as a mother wavelet. In the left, the area bounded by the white line indicates the region of the cone of influence, where the variance is reduced, and the solid black lines denote the regions with a significance level higher than 95%. The yellow colors represent high energy, and the blue colors indicate low energy. The color bar shows the units of energy in $\log_2$ form. In the right, the cone of influence is represented by the red dashed line and the sum of energy for each period is in the blue line.

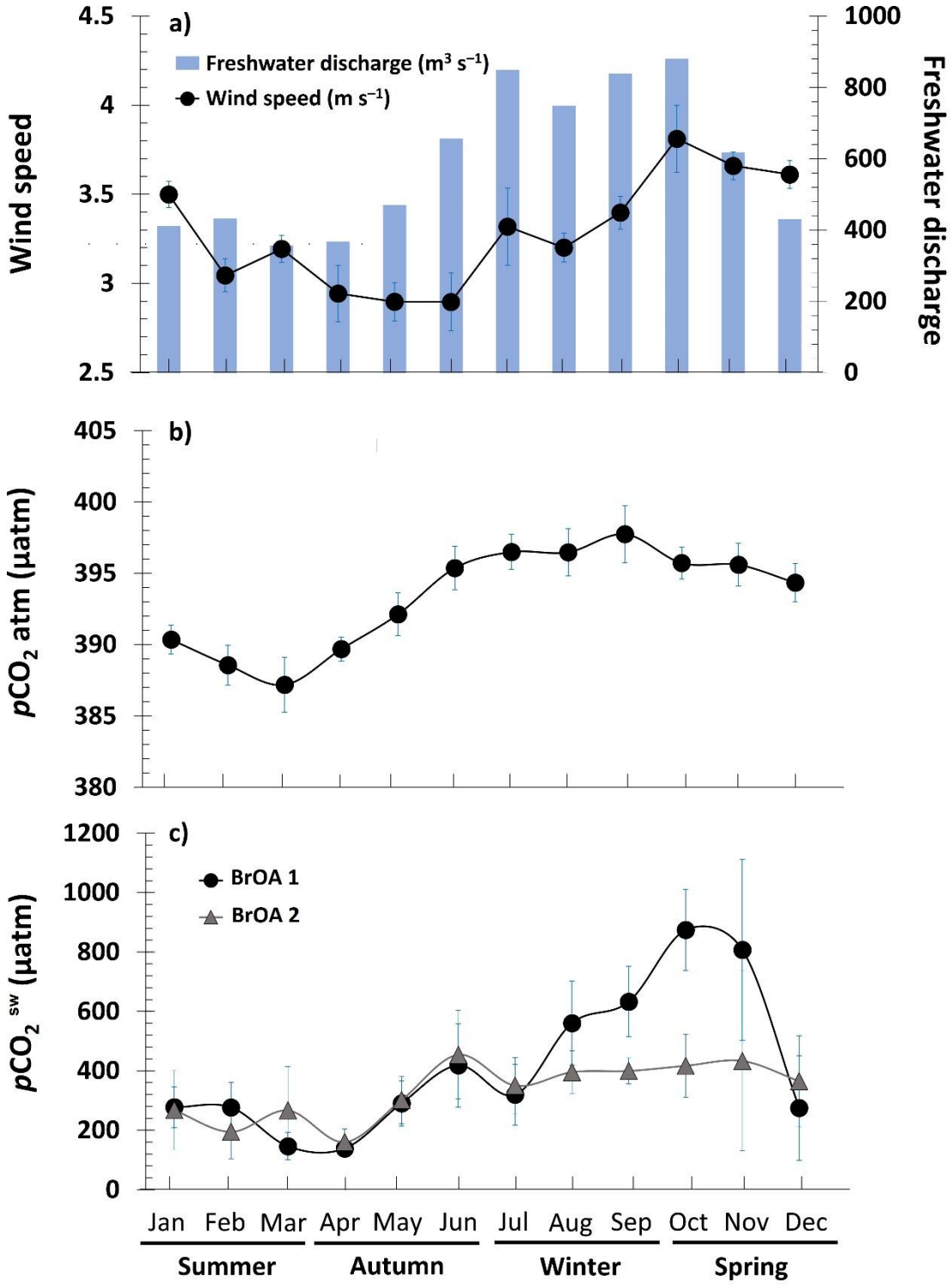

Figure S5. Seasonal cycle of (a) wind speed and riverine freshwater discharge ($m^3 s^{-1}$; blue bars), (b) partial pressure of CO_2 (pCO_2) of atmosphere and (c) partial pressure of CO_2 (pCO_2) of surface water for the stations located in the BrOA #1 (black line and dots) and BrOA #2 (gray line and triangles) of the lower zone of the Patos Lagoon Estuary obtained from May 2017 to June 2021. The errorbars indicated the standard error of each month.

Capítulo VII: Referências Bibliográficas

Abreu PC, Marangoni J, Odebrecht C (2016) So close, so far: differences in long-term chlorophyll a variability in three nearby estuarine-coastal stations. Marine Biology Research. https://doi.org/10.1080/17451000.2016.1189081

Abreu PC, Odebrecht C, Niencheski LF (2010) Nutrientes dissolvidos. In: Seeliger U, Odebrecht C (Eds.) O Estuário da Lagoa dos Patos: Um século de transformações. Rio Grande, FURG, Pp: 43–48

Abril G, Libardoni BG, Brandini N et al. (2021) Thermodynamic uptake of atmospheric CO_2 in the oligotrofic and semiarid São Francisco estuary (NE Brazil). Marine Chemistry. https://doi.org/10.1016/j.marchem.2021.103983

Albuquerque C, Kerr R, Monteiro T et al. (Under review) Seasonal and interannual in the carbonate system parameters of the Patos Lagoon Estuary.

Bauer JE, Cai WJ, Raymond PA et al. (2013) The Changing Carbon Cycle of the Coastal Ocean. Nature. 504:61–70, https://doi.org/10.1038/nature12857

Baumgarten MGZ, Niencheski LFH (2010) A coluna sedimentar como reservatório e fonte de nutrientes em enseadas estuarinas. Tropical Oceanography Online. 38:88–104

Bible JM, Sanford E (2016) Local adaptation in an estuarine foundation species: implications for restoration. Biological Conservation. 193:95–102, https://doi.org/10.1016/j.biocon.2015.11.015

Borges AV, Abril G (2011) Carbon Dioxide and Methane Dynamics in Estuaries. Estuarine and Coastal Science. 5:119–161, https://doi.org/10.1016/B978-0-12-374711-2.00504-0

Borges AV, Delille B, Frankignoulle M (2005) Budgeting sinks and sources of CO_2 in the coastal ocean: Diversity of ecosystems counts. Geophysical research letters. 32, https://doi.org/10.1029/2005GL023053

Borges AV, Delille B, Schiettecatte L et al. (2004) Gas transfer velocities of CO_2 in theree European estuaries (Randers Fjord, Scheldt, and Thames). Limnology and Oceanography. 49:1630–1641

Borges AV, Djenidi S, Lacroix G et al. (2003) Atmospheric CO_2 flux from mangrove surrounding waters. Geophysical Research Letter. 30, https://doi.org/10.1029/2003gl017143

Borges AV, Gypens N (2011) Carbonate chemistry in the coastal zone responds more strongly to eutrophication than to ocean acidification. Limnology and Oceanography. 55:346–353, https://doi.org/10.4319/lo.2010.55.1.0346

Borges AV, Schiettecatte L-S, Abril G et al. (2006) Carbon dioxide in European coastal waters. Estuarine, Coastal and Shelf Science. 70:375–387, https://doi.org/10.1016/j.ecss.2006.05.046

Bozec Y, Cariou T, Macé E et al. (2012) Seasonal dynamics of air-sea CO_2 fluxes in the inner and outer Loire estuary 9NW Europe). Estuarine, Coastal and Shelf Science. https://doi.org/10.1016/j.ecss.2011.05.015

Cai W (2011) Estuarine and coastal ocean carbon paradox: CO_2 sinks or sites of terrestrial carbon incineration? Annual Review of Marine Science. 3:123–145, https://doi.org/10.1146/annurev-marine-120709-142723

Cai W, Wang Y (1998) The chemistry, fluxes and sources of carbon dioxide in the estuarine waters of the Satilla and Altamaha Rivers, Georgia. Limnology and Oceanography. 43:657–668, https://doi.org/10.4319/lo.1998.43.4.0657

Cai W, Xu Y-Y, Feely RA et al. (2020a) Controls on surface water carbonate chemistry along North American ocean margins. Nature Communications 11. 2691, https://doi.org/10.1038/s41467-020-16530-z

Cai W, McPhaden MJ, Grimm AM et al. (2020) Climate impacts of the El Niño-Southern Oscillation on the South America. Nature Reviews Earth & Environment. 1:215–230, https://doi.org/10.1038/s43017-020-0040-3

Carstensen J, Duarte CM (2019) Drivers of pH Variability in Coastal Ecosystems. Environmental Science and Technology. 53 (8): 4020–4029, https://doi.org/10.1021/acs.est.8b03655

Carstensen J, Chierici M, Gustafsson BG, Gustafsson, E (2018) Long-term and seasonal trends in estuarine and coastal carbonate systems. Global Biogeochemical Cycles. 32:497–513, https://doi.org/10.1002/2017GB005781

Carter BR, Frolicher TL, Dunne JP et al. (2016) When can ocean acidification impacts be detected from decadal alkalinity measurements? Global Biogeochemical Cycles. 30: 595–612, https://doi.org/10.1002/2015GB005308

Castelão RM, Möller OO (2003) Sobre a circulação tridimensional forçada por ventos na Lagoa dos Patos. Atlântica, 25:91–106

Chen C-TA, Borges AV (2009) Reconciling opposing views on carbon cycling in the coastal ocean: Continental shelves as sinks and near-shore ecosystems as source of atmospheric CO_2. Deep-sea Research II. 56:578–590, https://doi.org/10.1016/j.dsr2.2009.01.001

Chen B, Cai W, Brodeur JR et al. (2020) Seasonal and spatial variability in surface pCO_2 and air-water CO_2 flux in the Chesapeake Bay. Limnology and Oceanography. 65:3046–3065, https://doi.org/10.1002/lno.11573

Chen C-TA, Huang T-H, Chen, Y-C et al (2013) Air-sea exchanges of CO_2 in the world's coastal seas. Biogeosciences. 10:6509–6544, https://doi.org/10.5194/bg-10-6509-2013

Ciais P, Sabine C, Bala G (2013) P. Carbon and Other Biogeochemical Cycles. In: Stocker TF, Qin D, Plattner GK et al. (Eds.) Climate Change 2013: The Physical Science Basis. Cambridge e New York, Cambridge University Press, Pp. 467–544

Cloern JE, Foster SQ, Kleekner AE (2014) Phytoplankton primary production in the world's estuarine coastal ecosystems. Biogeosciences. 11:2477–2501

Cossarini G, Lazzari P, Solidoro C (2015) Spatiotemporal variability of alkalinity in the Mediterranean. Biogeosciences. 12:1647–1658, https://doi.org/10.5194/bg-12-1647-2015

Cotovicz LC, Knoppers BA, Brandini N, et al. (2015) A strong CO_2 sink enhanced by eutrophication in a tropical coastal embayment (Guanabara Bay, Rio de Janeiro, Brazil). Biogeosciences. https://doi.org/10.5194/bg-12-6125-2015

Cotovicz LC, Vidal LO, Rezende CE et al. (2020) Carbon dioxide sources and sinks in the delta of the Paraíba do Sul River (Southeastern Brazil) modulated by carbonate thermodynamics, gas exchange and ecosystem metabolism during estuarine mixing. Marine Chemistry. 226 (103869), https://doi.org/10.1016/j.marchem.2020.103869

Crosswell JR, Wetz MS, Hales B, Paerl HW (2012) Air-water CO_2 fluxes in the microtidal Neuse River estuary, North Carolina. Journal of Geophysical Research. 125, https://doi.org/10.1029/2012JC007925

Delaney P (1965) Fisiografia e geologia de fisiologia da planície costeira do Rio Grande do Sul. Publicação Especial da Escola de Geologia de Porto Alegre. 6:1-105

Dickson AG (1981) An exact definition of total alkalinity and a procedure for the estimation of alkalinity and total inorganic carbon from titration data. Deep-Sea Research Part A. Oceanogr. Res. Papers 28 (6): 609-623

Dickson AG (2010) The carbon dioxide system in seawater: equilibrium chemistry and measurements U. Riebesell, V.J. Fabry, L. Hansson, J.-P. Gattuso (Eds.) Guide to Best Practices for Ocean Acidification Research and Data Reporting, Publications Office of the European Union Luxembourg

Dickson AG (1990) Thermodynamics of the dissociation of boric acid in synthetic seawater from 273.15 to 318.15 K. Deep-Sea Res. 37:755–766

Dickson AG, Afghan JD, Anderson GC (2003) Reference materials for oceanic CO_2 analysis: a method for the certification of total alkalinity. Marine Chemistry. 80:185–197

Dickson AG, Sabine CL, Christian JR (2007) Guide to Best Practices for Ocean CO_2 Measurements. North Pacific Marine Science Organization, Sidney

Dinauer A, Mucci A (2017) Spatial variability in surfasse-water pCO_2 and gas exchange in the world's largest semi-enclosed estuarine system: St. Lawence Estuary (Canada). Biogeoscience. https://doi.org/10.5194/bg-14-3221-2017

Doney SC, Fabry VJ, Feely RA, Kleypas JA (2009) Ocean acidification: the other CO2 problem. Annual Review of Marine Science. 1: 169–192, https://doi.org/10.1146/annurev.marine.010908.163834

Doney SC, Busch DS, Cooley SR, Kroeker KJ (2020) The impacts of ocean acidification on marine ecosystems and reliant human communities. Annual Review of Environment and Resources. 45:11.1–11.30, https://doi.org/10.1146/annurev-environ-012320-083019

Emerson SR, Hedges JI (2008) Chemical Oceanography and the Marine Carbon Cycle. Cambridge University Press. Cambridge

Evans W, Hales B, Strutton PG (2013) pCO_2 distributions and air-water CO_2 fluxes in the Columbia River estuary. Estuarine, coastal and shelf science. 117:260–272

Feely RA, Doney SC, Cooley SR (2010) Ocean acidification: Present conditions and future changes in a high CO_2 world. Oceanogr. 22:36–47

Flecha S, Huertas IE, Navarro G, et al. (2015) Air–Water CO_2 Fluxes in a Highly Heterotrophic Estuary. Estuaries and Coasts. https://doi.org/10.1007/s12237-014-9923-1

Gupta GVM, Thottathil SD, Balachandran KK et al. (2009) CO_2 supersaturation and net heterotrophy in a tropical estuary (Cochin, India): influence of anthropogenic effect. Ecossystem. https://doi.org/10.1007/s10021-009-9280-2

Friedlingstein P, Jones MW, O'Sullivan M et al. (2021) Global Carbon Project 2021. Earth System Science [preprint]. https://doi.org/10.5194/essd-2021-386

Fry CH, Tyrell T, Hain MP et al. (2015) Analysis of global surface ocean alkalinity to determine controlling processes. Marine Chemistry. 174:46–57

Gallego MA, Timmermann A, Friedrich T, Zee RE (2018) Drivers of future seasonal cycle changes in oceanic pCO_2. Biogesciences. 15:5315–5327, https://doi.org/10.5194/bg-15-5315-2018

Giannini F, Mendes CRB, Garcia CAE et al. (2021) Phytoplankton community and the fluorescence-derived photo-physiological parameters in the South Atlantic Ocean. Journal of Marine Systems. 218 103538, https://doi.org/10.1016/j.jmarsys.2021.103538

Gieskes JM (1969) Effect of temperature on the pH of seawater. Limnology and Oceanography. 14:679-685, https://doi.org/10.4319/lo.1969.14.5.0679

Gilman DL, Fuglister FJ, Mitchell Jr JM (1963) On the power spectrum of "red noise". J. Atmos. Sci. 20:182–184

GML (2022) https://gml.noaa.gov/ccgg/trends/mlo.html, acessado em 17 de fevereiro de 2022

Grimm AM, Ferraz SET (1998) Sudeste do Brasil: uma região de transição no impacto de eventos extremos da Oscilação Sul. Parte I: El Niño. In: Congresso Brasileiro de Meteorologia, Brasília, Anais. Brasília: SBMET

Guo X, Dai M, Zhai W et al. (2009) CO_2 flux and seasonal variability in a large subtropical estuarine system, the Pearl River Estuary, China. Journal of Geophysical Research. https://doi.org/10.1029/2008JG000905

Haraguchi L, Carstensen J, Abreu PC, Odebrecht C (2015) Long-term changes of the phytoplankton community and biomass in the subtropical shallow Patos Lagoon Estuary. Estuarine, Coastal and Shelf Science. 162:76–87

Hatje V, Da Costa, MF, Da Cunha LC (2013) Oceanografia Química: unindo conhecimentos em prol dos oceanos e da sociedade. Química nova. 36:1497–1508

Heinze C, Blenckner T, Martins H et al. (2021) The quiet crossing of ocean tipping points. PNAS. 118, https://doi.org/10.1073/pnas.2008478118.

Ho DT, Ferrón S, Engel VC et al. (2014) Air-water gas exchange and CO2 flux in a mangrove-dominated estuary, Geophysical Research Letter. https://doi.org/10.1002/2013GL058785

Hopkinson BM, Dupont CL, Allen AE, Morel FMM (2011) Efficiency of the CO_2-concentrating mechanism of diatoms. Proceeding of the National Academy of Sciences of the United States of America. 10:3830–3837, https://doi.org/10.1073/pnas.1018062108

IBGE (2022) https://www.ibge.gov.br/pt/inicio.html, acessado em 7 de Fevereiro de 2022

INPE (2021) http://enos.cptec.inpe.br/, acessado em 17 de Agosto de 2021

IPCC (2007) Climate Change 2007: The Physical Science Basis. Cambridge University Press, Cambridge, United Kingdom and New York, NY, USA

Islabão CA, Mendes CRB, Detoni AMS, Odebrecht C (2017) Phytoplankton community structure in relation to hydrographic features along a coast–to–offshore transect on the SW Atlantic continental shelf. Continental shelf research. 151:30–39, https://doi.org/10.1016/j.csr.2017.10.003

Jeffrey LC, Maher DT, Santos IR et al. (2018) The spatial and temporal drivers of pCO_2, pCH_4 and gas transfer velocity within a subtropical estuary. Estuarine, Coastal and Shelf Science. 208, 83–95, https://doi.org/10.1016/j.ecss.2018.04.022

Jiang LQ, Cai W, Wang Y (2008) A comparative study of carbon dioxide degassing in river- and marine dominated estuaries. Limnology and Oceanography. 53:2603–15, https://doi.org/10.4319/lo.2008.53.6.2603

Joesoef A, Huang W-J, Gao Y, Cai, W-J (2015) Air-water fluxes and sources of carbon dioxide in Delaware Estuary: spatial and seasonal variability. Biogeosciences. https://doi.org/10.5194/bg-12-6085-2015

Joesoef A, Kirchman DL, Sommerfield CK, Cai W (2017) Seasonal variability of the inorganic carbon system in a large coastal plain estuary. Biogeosciences. 14:4949–4963, https://doi.org/10.5194/bg-14-4949-2017

Joos F, Spahni R (2008) Rates of change in natural and anthropogenic radiative forcing over the past 20,000 years. Proceedings of the National Academy of Sciences of the United States of America. 105: 1425–1430. https://doi.org/ 10.1073/pnas.0707386105

Kerr R, Da Cunha LC, Kikuchi RKP et al (2016) The Western South Atlantic Ocean in a high-CO_2 world: current measurement capabilities and perspectives. Environmental Management. 57:740–752, https://doi.org/10.1007/s00267-015-0630-x

Khoo KH, Ramette RW, Culberson CH, Bates RG (1977) Determination of hydrogen ion concentrations in seawater from 5 to 40°C: standard potentials at salinities from 20 to 45. Anal. Chem. 49: 29–34

Kjerfve B (1986) Comparative Oceanography of Coastal Lagoons. In: Wolfe DA (Ed.) Estuarine Variability. London, Academic Press, Pp: 63–81.

Koné YJM, Abril G, Kouadio KN et al (2009) Seasonal variability of carbon dioxide in the rivers and lagoons of ivory coast (West Africa). Estuaries and Coasts. 32:246–260, https://doi.org/10.1007/s12237-008-9121-0.

Körtzinger A, Send U, Lampitt RS, Hartman S, Wallace DWR, Karstensen J et al. (2008) The seasonal pCO_2 cycle at 49°N/16.5°W in the northeastern Atlantic Ocean and what it tells us about biological productivity. Journal Physical Research. https://10.1029/ 2007j c0043 47

Lanari M, Copertino M (2017) Drift macroalgae in the Patos Lagoon Estuary (southern Brazil): effects of climate, hydrology and wind action on the onset and magnitude of blooms. Marine Biology Research (online). 13:36–47, https://doi.org/10.1080/17451000.2016.1225957

Lanari M, Copertino M, Cooling LA, Bom FC (2018) The impact of short-term depositions of macroalgal blooms on widgeon-grass meadows in a river-dominated estuary. Harmful algae. 78:36–46, https://doi.org/10.1016/j.hal.2018.07.006

Laruelle GG, Dürr HH, Lauerwald R et al. (2013) Global multi-scale segmentation of continental and coastal waters from the watersheds to the continental margins. Hydrology Earth System Science. 17: 2029–2051, https://doi.org/10.5194/hess-17-2029-2013

Le Quéré C, Andrew, RM, Friedlingstein P et al. (2018) Global Carbon budget 2018. Earth System Science Data. 10:2141–2194, https://doi.org/10.5194/essd-10-2141-2018

Lee K, Kim T-W, Byrne RH et al. (2010) The universal ratio of boron to chlorinity for the North Pacific and North Atlantic oceans. Geochimica et Cosmochimica Acta. 74:1801–1811, https://doi.org/10.1016/j.gca.2009.12.027

Lee K, Tong LT, Millero FJ et al (2006) Global relationships of total alkalinity with salinity and temperature in surface waters of the world's oceans. Geophysical Research Letters. 74:1801–1811, https://doi.org/10.1029/2006GL027207

Lemos VM, Lanari M, Copertino M et al (2021) Patos Lagoon Estuary and adjacent marine coastal biodiversity long-term data. Earth System Science Data Discuss. [preprint]. https://doi.org/10.5194/essd-2021-353

Lenton A, Metzl N, Takahashi T (2012) The observed evolution of oceanic pCO_2 and its drivers over the last two decades Global Biogeochemical Cycles. https://doi.org/10.1029/2011GB004095

Lewis E, Wallace D, Allison LJ (1998) Program developed for CO_2 system calculations. Carbon Dioxide Information Analysis Center, USA

Libes SM (2009) Introduction to marine biogeochemistry. Academic Press

Lisboa PV (2015) Escalas temporais de transporte do estuário da Lagoa dos Patos, Rio Grande, RS. Master's thesis, University of Rio Grande, Rio Grande do Sul, Brasil, unpublished.

Liu Q, Charette MA, Breier CF (2017) Geochimica et Cosmochimica Acta. 203:422–439, https://doi.org/10.1016/j.gca.2017.01.041

Maher DT, Eyre BD (2012) Carbon budgets for three autotrophic Australian estuaries: Implications for global estimates of the coastal air-water CO_2 flux. Global biogeochemical cycles. 26, https://doi.org/10.1029/2011GB004075

Marques, WC (2012) The temporal variability of the freshwater discharge and water levels at the Patos Lagoon, Brazil. International Journal of Geosciences. https://doi.org/10.4236/ijg.2012.34076

Marques WC, Fernandes EH, Monteiro IO, Möller OO (2009) Numerical modeling of the Patos Lagoon coastal plume, Brazil. Continental Shelf Research. 29:556–571

Marques WC, Möller OO (2008) Variabilidade temporal em longo período da descarga fluvial e níveis de água da Lagoa dos Patos, Rio Grande do Sul, Brasil. Revista Brasileira de Recursos Hídricos. 13: 155–163

Marreto RN, Baumgarten MGZ, Wallner-Kersanach M (2017) Trophic quality of waters in the Patos Lagoon estuary: a comparison between its margins and the port channel located in Rio Grande, RS, Brazil. Acta Limnologica Brasiliensia. 29

Mendes CRB, Odebrecht C, Tavano VM, Abreu PC (2016) Pigment-based chemotaxonomy of phytoplankton in the Patos Lagoon estuary (Brazil) and adjacente coast. Marine Biology Research. https://doi.org/10.1080/17451000.2016.1189082

Millero FJ (2013) Chemical Oceanography. CRC Press.

Millero FJ, Graham TB, Huang F et al (2006) Dissociation Constants of Carbonic Acid in Seawater as a Function of Salinity and Temperature. Marine Chemistry. 100:80–94, https://doi.org/10.1016/j.marchem.2005.12.001

Mirlean N, Calliari L, Johannesson K (2020) Dredging in an estuary causes contamination by fluid mud on a tourist ocean beach. Evidence via REE ratios. Marine Pollution Bulletin. https://doi.org/10.1016/j.marpolbul.2020.111495

Möller, O.O. 1996. Hydrodynamique de la lagunes dos Patos. Mesures et Mode´lisation. DSc.

Dissertation, University Bordeaux I, Bordeaux, France

Möller OO, Castaing P, Salomon JC, Lazure P (2001) The Influence of Local and Non-Local Forcing Effects on the Subtidal Circulation of Patos Lagoon. Estuaries. 24:297–311

Möller OO, Castaing P, Fernandes EL, Lazure P (2007) Tidar frequency of a Southern Brazil coastal lagoon: choking and short period forced oscillations. Estuaries. 30:311–320

Möller OO, Fernandes EH (2010) Hidrologia e Hidrodinâmica. In: Seeliger U, Odebrecht C (Eds.) O Estuário da Lagoa dos Patos: Um século de transformações. Rio Grande, FURG, Pp: 17–30

Möller OO, Piola A, Freitas AC, Campos EJD (2008) The effects of river discharge and seasonal winds on the shelf off Southeastern South America. Continental Shelf Research. 28:1607–1624

Monteiro T, Kerr R, Orselli IBM, Lencina-Avila JM (2020) Towards an intensified summer CO2 sink behaviour in the Southern Ocean coastal regions. Progress in Oceanography. https://doi.org/10.1016/j.pocean.2020.102267

Moreau S, Penna AD, Llort J et al (2017) Eddy-induced carbon transport across the Antarctic circumpolar current. Global Biogeochemical Cycles. https://doi.org/10.1002/2017GB005669

Murrell MC, Lores EM (2004) Phytoplankton and zooplankton seasonal dynamics in a subtropical estuary: importance of cyanobacteria.Journal of Plankton Research. 26:371–382, https://doi.org/10.1093/plankt/fbh038

Niencheski LF, Baumgarten MGZ, Cabrera L, Juliano SK (2006) Patos Lagoon: indicators of organic pollution. Journal of Coastal Research. 39:1357–1359

Niencheski LF, Windom, HL (1994) Nutrient flux and budget in Patos Lagoon estuary. Science of the Total Environment. 149:53–60, https://doi.org/10.1016/0048-9697(94)90004-3

Noriega C, Araujo M (2014) Carbon dioxide emissions from estuaries of nothern and northeastern Brazil. Scientific Reports. https://doi.org/10.1038/srep06164

Noriega CED, Araujo M, Lefèvre N (2013) Spatial and temporal variability of the CO_2 fluxes in a tropical, highly urbanized estuary. Estuaries and coast. https://doi.org/10.1007/s12237-013-9608-1

Odebrecht C, Abreu PCOV (2019) Phytoplankton and water quality parameters in the Patos Lagoon estuary and adjacent marine coast. Sistema de Informação sobre a Biodiversidade Brasileira - SiBBr. Sampling event dataset https://doi.org/10.15468/xmlvxm accessed via GBIF.org on 2020-06-09

Odebrecht C, Abreu PC, Carstensen J (2015) Retention time generates short–term phytoplankton blooms in a shallow microtidal subtropical estuary. Estuarine, Coastal and Shelf Science. 162:35–44, https://doi.org/10.1016/j.ecss.2015.03.004

Odebrecht C, Secchi ER, Abreu PC, Muelbert JH, Uiblein F (2017) Biota of the Patos Lagoon estuary and adjacente marine coast: long-term changes induced by natural and human-related factors. Marine Biology Research. 13:3–8, https://doi.org/10.1080/17451000.2016.1258714

Oliveira AP, Cabeçadas G, Mateus MD (2017) Inorganic carbon distribution and CO_2 fluxes in a large European estuary (Tagus, Portugal). Scientific Reports. https://doi.org/10.1038/s41598-017-06758-z

Orr JC, Epitalon J, Dickson AG, Gattuso J (2018) Routine uncertainty propagation for the marine carbon dioxide system. Marine Chemistry. 207:84–107, https://doi.org/10.1016/j.marchem.2018.10.006

Pierrot D, Lewis E, Wallace DWR (2006) MS Excel Program Developed for CO_2 System

Calculations, ORNL/CDIAC-105a. Carbon Dioxide Information Analysis Center. Oak Ridge National Laboratory, U.S. Department of Energy, Oak Ridge, Tennessee. https://doi.org/10.3334/CDIAC/otg.CO2SYS_XLS_CDIAC105a

Proum S, Santos JH., Lim LH, Marshall DJ (2018) Tidal and seasonal variation in carbonate chemistry, pH and salinity for a mineral-acidified tropical estuarine system. Regional Studies in Marine Science.17, 17–27

Raymond PA, Cole JJ (2001) Gas exchange in rivers and estuaries: Choosing a gas transfer velocity. Estuaries. 24:312–317

Roobaert A, Laruelle GG, Landschützer P et al. (2019) The spatiotemporal dynamics of the sources and sinks of CO2 in the global coastal ocean. Global Biogeochemical Cycles. 33:1693–1714, https://doi.org/10.1029/2019GB006239

Sadat-Noori M, Maher DT, Santos IR (2016) Groundwater discharge as a source of dissolved carbon and greenhouse gases in a subtropical estuary. Estuaries and coasts. https://doi.org/10.1007/s12237-015-0042-4

Salt LA, Thomas H, Bozec Y et al. (2016) The internal consistency of the North Sea carbonate system. Journal of Marine Systems. 157:52–64, https://doi.org/10.1016/j.jmarsys.2015.11.008

Samanta, S., Dalai, T.K., Pattanaik, J., Rai, S.K. and Mazumdar, A. 2015. Dissolved inorganic carbon (DIC) and its $\delta^{13}C$ in the Ganga (Hooghly) River estuary, India: Evidence of DIC generation via organic carbon degradation and carbonate dissolution. Geochimica et Cosmochimica Acta. 165, 226–248, doi: 10.1016/j.gca.2015.05.040

Sarma VVSS, Kumar MD, Manerikar M (2001) Emission of carbono dioxide from a Tropical Estuarine System, Goa, India. Hydrology and Biogeochemical Cycles. https://doi.org/10.1029/2000GL006114

Sarmiento J, Gruber N (2006) Ocean Biogeochemical Dynamics Princeton Univ. Press, New Jersey

Seeliger U (2001) The Patos Lagoon Estuary, Brazil. In: Seeliger U., Kjerfve B. (Eds) Coastal Marine Ecosystems of Latin America. Ecological Studies (Analysis and Synthesis), vol 144. Berlin, Heidelberg, Springer

Seeliger U, Cordazzo C, Barcellos L (2004) Areias do Albardão: Um guia ecológico ilustrado do litoral no extremo sul do Brasil. Rio Grande, Ecoscientia

Seeliger U, Odebrecht C (2010) O Estuário da Lagoa dos Patos: Um Século de Transformações. Rio Grande, FURG

Seeliger U, Odebrecht C, Castello JP (1998) Os ecossistemas costeiro e marinho do extremo sul do Brasil. Rio Grande, Ecoscientia

Sims RP, Bedington M, Schuster U et al (2021) Tidal mixing of estuarine and coastal waters in the Western English Channel controls spatial and temporal variability in seawater CO_2, Biogeosciences Discuss. [preprint]. https://doi.org/10.5194/bg-2021-166

Strickland JDH, Parsons TR (1972) A Practical Hand Book of Seawater Analysis. Fisheries Research Board of Canada Bulletin 157, 2nd Edition

Sunda WG, Cai W (2012) Eutrophication induced CO_2–acidification of subsurface coastal waters: interactive of temperature, salinity and atmospheric pCO2. Environmental Science & Technollogy. 46:10651–10659, https://doi.org/10.1021/es300626f

Tagliani PRA, Landazuri H, Reis EG et al. (2003) Integrated coastal zone management in the Patos Lagoon estuary: perspectives in context of developing country. Ocean & Coastal. 46:807–

822

Takahashi T, Olafsson J, Goddard JG, Chipman DW, Sutherland SC (1993) Seasonal variation of CO_2 and nutrients in the high-latitude surface oceans: A comparative study. Global Biogeochemical Cycles. 7: 843– 878

Takahashi T, Sutherland SC, Seeney C, Poisson A, Metzl N, Tillbrook B, Nojiri Y (2002) Global sea-air CO_2 flux based on climatological surface oceano pCO_2, and biological and temperature effects. Deep Sea Research. 49: 1601–1622, https://10.1016/ S0967-0645(02) 00003-6

Takahashi T, Sutherland SC, Chipman DW (2014) Climatological distributions of pH, pCO_2, total CO_2, alkalinity, and $CaCO_3$ saturation in the global surface ocean, and temporal changes at selected locations Marine Chemistry. https://doi.org/10.1016/j.marchem.2014.06.004

Takahashi T, Sutherland SC, Wanninkhof R et al (2009) Climatological mean and decadal change in surface ocean pCO_2, and net sea-air CO_2 flux over the global oceans. Deep sea research part II: Topical studies in oceanography. https://doi.org/0.1016/j.dsr2.2008.12.009

Thoning KW, Crotwell AM, Mund JW (2021) Atmospheric carbon dioxide dry air mole fractions from continuous measurements at Mauna Loa, Hawaii, Barrow, Alaska, American Samoa and South Pole. 1973-2020, Version 2021-08-09 National Oceanic and Atmospheric Administration (NOAA), Global Monitoring Laboratory (GML), Boulder, Colorado, USA https://doi.org/10.15138/yaf1-bk21 FTP path: ftp://aftp.cmdl.noaa.gov/data/greenhouse_gases/co2/in-situ/surface/

Torres JR, Philomena LA (2013) Environmental Port Management: Conceptual Model Development and Use of Tools to Evaluate and Monitor Dredging Activities in the Port of Rio Grande, Brazil. African Journal of Environmental Economic and Management. 1:22–27
Torrence C, Compo GP (1998) A practical guide to wavelet analysis. Bull. Am. Meteorol. Soc. 79:61–78

Touratier F, Goyet C, Houpert L et al. (2016) Role of deep convection on anthropogenic CO_2 sequestration in the Gulf of Lions (northwestern Mediterranean Sea). Deep-Sea Research I. 113: 33–48, https://doi.org/10.1016/j.dsr.2016.04.003

Uppström LR (1974) Boron/chlorinity ratio of deep-sea water from the Pacific Ocean. Deep-Sea Res. 21:161–162

Van Dam BR, Crosswell JR, Paerl HW (2018) Flood-driven CO_2 emissions from adjacent North Carolina estuaries during Hurricane Joaquim (2015). Marine Chemistry. https://doi.org/10.1016/j.marchem.2018.10.001

Vargas CA, Contreras PY, Pérez CA, Sorbazo M, Saldías GS, Salisbury J (2016) Influences of riverine and upwelling waters on the coastal carbonate system off Central Chile and their ocean acidification implications.Journal of Geophysical Research. 121: 1468–1483, https://10.1002/2015JG003213

Vaz AC, Möller OO, Almeida TL (2006) Análise quantitativa da descarga dos rios afluentes da Lagoa dos Patos. Atlântica. 28:13–23

Vieillard AM, Newell SE, Trush S (2020) Recovering from Bias: A call for futher study of under-represented tropical and low-nutrient estuaries. JGR Biogeosciences. https://doi.org/10.1029/2020JG005766

Vinagre C, Narciso L, Pimentel M, Cabral HN, Costa MJ, Rosa R (2013) Contrasting impacts of climate change across seasons: effects of flatfish cohorts. Regional Environmental Change. 13: 853–859, https://10.1007/s10113-012-0376-4

Wallner-Kersanach M, Mirlean N, Baumgarten MGZ et al (2016) Temporal evolution of the contamination in the southern area of the Patos Lagoon estuary, RS, Brazil. Journal of Integrated Coastal Zone Management. https://doi.org/10.5894/rgci596

Wanninkhof R (2014) Relationship between wind speed and gas exchange over the ocean revisited. Limnology and oceanography. https://doi.org/10.4319/lom.2014.12.351

Weiss RF (1974) Carbon dioxide in water and seawater: the solubility of a non-ideal gas. Marine Chemistry. https://doi.org/10.1016/0304-4203(74)90015-2

Weiss RF, Price BA (1980) Nitrous oxide solubility in waterand seawater. Marine Chemistry. https://doi.org/10.1016/0304-4203(80)90024-9

Welschmeyer NA (1994) Fluorometric analysis of chlorophyll-a in the presence of chlorophyll-b and pheopigments, Limnol. Oceanogr. 39:1985–1992

Yao H, Hu X (2017) Responses of carbonate system and CO_2 flux to extended drought and intense flooding in a semiarid subtropical estuary. Limnology and Oceanography. 62, 112–130, https://doi.org/10.1002/lno.10646

Yao H, McCutcheon MR, Staryk CJ, Hu X (2020) Hydrologic controls on CO_2 chemistry and flux in subtropical lagoonal estuaries of the northwestern Gulf of Mexico. Limnology and Oceanography. 1–19, https://doi.org/10.1002/lno.11394

Zavialov PO, Pelevin VV, Belyaev NA, Izhitskiy AS et al. (2018) High resolution LiDAR measurements reveal fine internal structure and variability of sediment – carrying coastal plume. Estuarine, Coastal and Shelf Science. 205: 40–45, https://10.1016/j.ecss.2018.01.008

Zeebe RE (2012) History of seawater carbonate chemistry, atmospheric CO_2 and ocean acidification. The Annual Review of Earth and Planetary Sciences. 40:141–16

Zeebe RE, Wolf-Gladrow D (2007) CO_2 in Seawater: Equilibrium, Kinetics, Isotopes. Elsevier Oceanography Series 65

Zhai W, Dai M, Guo X (2007) Carbonate system and CO2 degassing fluxes in the inner estuary of Changjiang (Yangtze) River, China. Marine Chemistry. 107:342–356, https://doi.org/10.1016/j.marchem.2007.02.011